DEVELOPMENT OF AN INJECTABLE POLYMER-CALCIUM PHOSPHATE CEMENT COMPOSITES FOR BONE SUBSTITUTION

by

Öznur Demir Oğuz

B.S., in Biomedical Engineering, Yeditepe University, 2011

M.S., in Biomedical Engineering, Boğaziçi University, 2014

Submitted to the Institute of Biomedical Engineering

in partial fulfillment of the requirements

for the degree of

Doctor

of

Philosophy

Boğaziçi University

2020

ACKNOWLEDGEMENTS

First of all, I would like to express my sincere gratitude to my advisor Assoc. Prof. Dr. Duygu Ege for her endless support, patience, guidance and motivation throughout my Ph.D. study. During this time, she has not only supported me as a mentor but also as a friend.

It is my pleasure to thank to my thesis progress committee members, Assoc. Prof. Dr. Bora Garipcan and Assoc. Prof. Dr. Osman Bulut for their valuable help, insightful comments and contributions during my studies. I would also like to thank to my other thesis committee members, Assist. Prof. Dr Özgül Gök and Assist. Prof. Dr. Ayşe Sena Sarp for allocating their time on reviewing my thesis and giving valuable feedback.

In addition, I would like to thank to my colleagues and friends for their wonderful collaboration and support. Besides my work, I spent really good time in this institution and I will be leaving with so many good memories.

Finally, I would like to give my special thanks to my parents, my sister and my mother-in-law. I always felt their blessings on me during my thesis work. Above all, I owe my appreciation to my dear husband, Can, for always being by my side. You always have encouraged me to do my best in everything.

This study was supported by the Scientific and Research Council of Turkey (TUBITAK) with grand number 117M231 and Boğaziçi University Scientific Research Council (BAP) with grand number 12240.

ACADEMIC ETHICS AND INTEGRITY STATEMENT

I, Öznur Demir Oğuz, hereby certify that I am aware of the Academic Ethics and Integrity Policy issued by the Council of Higher Education (YÖK) and I fully acknowledge all the consequences due to its violation by plagiarism or any other way.

Name :

Signature:

Date:

ABSTRACT

DEVELOPMENT OF AN INJECTABLE POLYMER-CALCIUM PHOSPHATE CEMENT COMPOSITES FOR BONE SUBSTITUTION

Since the discovery of injectable calcium phosphate (CaP) cements, they are widely used to fill irregularly shaped bone defects. This created an alternative to more invasive methods such as use of autografts, allografts, xenografts and synthetic pre-shaped scaffolds. Hence, this thesis aimed to design an alternative injectable bone substitute (IBS) that can better accommodate CaP additives while preserving bone-like rheological properties and performance. In this thesis, an IBS was prepared by using methylcellulose (MC), gelatin and bioceramic powder mixture. Initially, three different powder to liquid (P/L) formulations were adjusted to investigate the chemical structure, rheological characteristics, handling, mechanical and in vitro degradation properties. Then, the effect of graphene oxide (GO) incorporation investigated by analyzing their physicochemical properties and in vitro responses. Results showed that the elastic modulus was increased up to 6.89 $\pm$ 2.25 MPa from 1.72 $\pm$ 0.76 MPa with the addition of 2 wt% GO on day 14. The extracted solution of the GO reinforced IBS was found to be biocompatible with bone marrow mesenchymal stem cells (BMMSCs). Finally, zoledronic acid (ZOL) was incorporated into IBS samples. Results showed that the presence of ZOL prolonged the setting time of the IBS samples. The mechanical properties decreased with ZOL addition and increased with the incorporation of GO which was found as 25.73 MPa. In in vitro cell studies, both the inhibitory effect of ZOL and GO loaded IBS on MCF-7 cells and proliferative effect on osteoblast cells were observed. In conclusion, the outcomes of this thesis indicated that prepared IBS may be promising candidates to fill bone defects and assist bone recovery for non-load bearing applications.

Keywords: Injectable Bone Substitute, Calcium Phosphate Cement, Methylcellulose, Graphene Oxide, Zoledronic Acid, Osteoporosis, MCF-7 cells.

ÖZET

KEMİK İKAMESİ İÇİN ENJEKTE EDİLEBİLİR POLİMER-KALSİYUM FOSFAT ÇİMENTO KOMPOZİTLERİNİN GELİŞTİRİLMESİ

Enjekte edilebilir kalsiyum fosfat (CaP) çimentolari geliştirildikten sonra düzensiz yapıya sahip kemik kusurları tedavisinde kullanılmaya başlandı. Bu otograft, allograft, zenograft ve önceden şekillendirilmiş sentetik iskele yapıları gibi invazif metotlara bir alternatif sağlamış oldu. Bundan dolayı, bu tezin amacı kemik benzeri reolojik özellikleri ve performansı korurken, CaP′a eklenecek yapıları daha iyi barındıracak alternatif bir enjekte edilebilir kemik ilavesi (IBS) dizayn etmektir. Bu tez çalışmasında, IBS farklı ağırlık oranlarında metilselüloz (MC), jelatin ve biyoseramik toz karışımı kullanarak hazırlanmıştır. İlk olarak, üç farklı toz/sıvı (P/L) formülasyonu hazırlanarak kimyasal yapı, reolojik karakteristikleri, kullanma, mekanik ve in vitro bozunma özellikleri araştırılmıştır. Sonrasında, grafen oksit (GO) ilavesinin fizyokimyasal özellikleri ile in vitro tepkisine etkisi analiz edilmiştir. Sonuçlara göre 14. günde ağırlıkça oranı % 2 GO ilaveli numunelerde elastik modülde 1.72 ± 0.76 MP değerinden 6.89 ± 2.25 MPa değerine artış görülmüştür. GO ile güçlendirilmiş IBS örneklerinin bekletilmesiyle elde edilen çözeltinin, kemik iliği mezenkimal kök hücreleri (BMMSC'ler) ile biyouyumlu olduğu bulunmuştur. Son bölümde, zoledronik asit (ZOL) IBS örneklerine ilave edilmiştir. Sonuçlara göre ZOL′ün varlığı IBS örneklerinin katılaşma süresini uzatmıştır. ZOL ilavesi ile elastisite modülü değeri azalmış, GO ilavesi ile artmıştır ve sonuç 25.73 MPa olarak bulunmuştur. In vitro hücre çalışmaları, ZOL ve GO içeren IBS örneklerinin hem MCF-7 hücrelerini inhibe ettiği hem de osteoblast hücrelerini çoğalttığı gözlenmiştir. Sonuç olarak, bu tezin bulguları hazırlanan IBS′in yük taşımayan kemik uygulamaları için kemik hasarlarını dolduracak ve kemik iyileşmesine yardım etme konusunda gelecek vadeden biyomalzemeler olduğunu göstermiştir.

Anahtar Sözcükler: Enjekte Edilebilir Kemik İkamesi, Kalsiyum Fosfat Çimentosu, Metilselüloz, Grafen Oksit, Zoledronik Asit, Osteoporoziz, MCF-7 hücreleri.

TABLE OF CONTENTS

LIST OF FIGURES

LIST OF TABLES

LIST OF SYMBOLS

$CaCO_3$	Calcium Carbonate
CO_2	Carbon Dioxide
CaO	Calcium oxide
$CaSO_4.2H_2O$	Calcium sulfate dihydrate
$CaHPO_4$	Monotite, Dicalcium phosphate anhydrous
$Ca_4(PO_4)_2$	Tetracalcium Phosphate
$C_6H_5Na_3O_7$	Sodium Citrate Tribasic Dihydrate
$Ca_2HPO_4.2H_2O$	Dicalcium Phosphate Dihydrate
cpc	centipoise
g	gram
Hz	hertz
kV	kilovolt
MPa	Mega Pascals
mA	milliamper
ml	milliliter
mM	millimolar
Mw	Molecular weight
°C	degree Celsius
μl	microliter

LIST OF ABBREVIATIONS

ANOVA	Analysis of Variance
BMMSC	Bone Marrow Mesenchymal Stem Cells
BP	Bisphosphonate
CaP	Calcium Phopsphate
CPC	Calcium Phosphate Cement
CSD	Calcium Sulfate Dihydrate
DCPD	Dicalcium phosphte dihydrate
DMA	Dynamic Mechanical Analysis
FACIT	Fibril-Associated Collagen with Tnterrupted Triple Helices
FPPS	Farnesyl Pyrophosphate Synthase
FTIR	Fourier Transform Infrared Spectroscopy
GGPPS	Geranylgeranyl Pyrophosphate Synthase
GO	Graphene Oxide
G′	Storage modulus
G″	Loss modulus
HA	Hydroxyapatite
HMDS	Hexamethyldisilazane
IBS	Injectable Bone Substitute
MC	Methylcellulose
P/L	powder to liquid
SC	Citric Acid
SEM	Scanning Electron Microscopy
TTCP	Tetracalcium phosphate
XRD	X-ray Diffraction
ZOL	Zoledronic Acid

1. INTRODUCTION

1.1 Motivation

In biomaterials field, the aim is to explore the underlying science behind the function, interaction of biomaterials and living tissue and designing advanced biomaterials [8]. Therefore, biomaterials area serves as an interface between materials, biology and health including tissue-biomaterial interaction, chemical, morphological and structural communication, signaling and biological responses, health risks, toxicology, biological safety, calcification, corrosion and degradation of biomaterials, devices and prosthetics [8, 9]. High bioactivity, the appropriate level of resorbability, and optimum mechanical strength are the key design parameters for biomaterials which are used for bone regeneration [10, 11, 12]. It is important to develop bioactive scaffolds, which promote the osteogenic differentiation and induce new bone formation, for regeneration of bone defects [12].

Traditional therapies for bone repair are carried out by implantation of bone grafts which requires the prior knowledge of the size and shape of the defect, the shaping of corresponding bone substitutes and then their implantation via surgery [13, 14]. It leads to the problem that scaffolds cannot fit exactly to the defect area [13, 15]. As a fundamental motivation of the presented work, the injectable material was prepared to repair non-load bearing bone defects over traditional therapies. Hence, this PhD research offers the minimally invasive alternative for possible bone regeneration applications.

The use of IBS is very promising due to elimination of the need for an open surgery, minimizing patient discomfort, the risk of infection, scar formation and the cost of treatment. It also provides the optimal defect filling, implant fixation and ease of handling [13, 14]. In order to achieve optimum levels of injectability of the produced composites, this research also focused on the introduction of natural crosslinks to the

polymer phase, incorporation of carbon-based reinforcing material as GO. Hence, a hybrid material system of natural polymers with calcium phosphate cement (CPC) was developed to mimic the highly mineralized collagen-based matrix of native bone. These composites CaPs, natural polymers, carbon-based reinforcing material) which were exploited in this study were mixed with different weight fractions of the natural polymer/CPC and carbon reinforcement phase in order to create mechanically compatible bone substitute formulations to the desired non-load bearing anatomic regions of the bone defects. This was another motivation of the presented work in terms of designing uniform, adjustable synthetic bone grafts. Biological safety and efficacy of these IBS was examined by conducting chemical, mechanical and in vitro analysis. Moreover, as the exploited natural polymers and CPCs are economically viable, this study shows potential to produce IBS end-products for the health sector.

We are also aware of that the osteoporosis is one the most commonly diagnosed bone disease [16]. Osteoporosis is not only coming from aging or metabolic bone disorders, but it may also be caused by bone metastases secondary to breast cancer. Bisphosphonates (BPs) are commercially used as an anti-osteoporotic drug. Besides, it is prescribed for patients with breast cancer to prevent the bone metastases. Its bioavailability is really low so that it requires an extended usage; however, their extended usage can cause some side effects like osteonecrosis of the jaw, atypical subtrochanteric femoral fractures, gastric ulcer, dysphagia and esophagitis [17, 18, 19, 20]. Local delivery of BPs to bone have been beneficial for prevention of the potential side effects [21, 22]. Here, we are also motivated to use prepared IBS samples as an alternative local bisphosphonate delivery with minimally invasive technique to treat osteoporosis. Therefore, the effect of bisphosphonate loading on physicochemical and in vitro properties of prepared IBS samples was evaluated.

1.2 Objectives and Outline of the Thesis

Research done by CaP and natural polymer combinations showed that this had extra advantages as IBS due to the inherent biocompatibility of natural polymers

[23, 24]. The combination of CPC and polymers also has the ability to tailor important parameters to develop novel IBS. These parameters can be listed as biocompatibility, bioactivity, osteoconductivity, osteoinductivity, injectability, viscosity, mechanic properties, toxicity, micro- and macro-porosity, working time, setting time and resorption rate. The designed IBS materials should exhibit good workability, have a suitable setting time with low or no heat output, have suitable mechanical properties, be non-toxic, be biocompatible, be osteoconductive, and they should integrate with bone over the time scale of bone ingrowth and remodeling [25]. Therefore, the main purpose of my Ph.D. research was to produce IBS of which the key parameters such as biodegradability, mechanical properties, setting temperature, setting time, viscosity, and injectability should be in balance within molecular composition of produced IBS.

In this study, MC and gelatin were added to CPC to improve their handling properties and mechanical strength, and also, BP was blended to increase osteoconductive properties of IBSs. Hence, to meet the requirement for orthopedic applications of non-load bearing bone, uniform non-toxic composites (CaPs, natural polymers, GO and BPs) were developed for different weight fractions of natural polymer/CPC, GO and BPs. Therefore, the main purpose of the study is to produce IBS to be used in the administration of bone defects, particularly for the non-load bearing region of bone tissue, and then to examine the handling and physicochemical properties, and in vitro response of intended IBS.

The main objectives of the thesis were presented below:

- Presenting the motivation and assessment of the literature related to this thesis

  The motivation behind this thesis work was presented in the Chapter 1. Related to these motivations, background information on bone tissue and bone remodeling was overviewed in Chapter 2. Also, systemic review on bone grafting and injectable bone substitutes were carried out in Chapter 2.

- Development and characterization of IBS which mimics both organic and inorganic components of bone by using MC/gelatin and CPCs combination

Within this principle objective, the weight fraction of MC to gelatin was optimized to obtain gelation at physiological body temperature. Also, citric acid (SC) as a gelling agent was used to reduce gelling time and optimize the handling properties of IBS. The P/L ratio was adjusted to optimize mechanical properties, injectability, degradability, setting time and temperature for adequate IBS formation. All these results are presented in Chapter 3 and 4.

- Evaluating the physicochemical and in vitro response of GO incorporation and its effects on handling properties of IBS

  In consideration of the preliminary work and Chapter 4, prepared IBS composite was reinforced with GO. Different formulations were examined for handling and mechanical properties, as well as their in vitro responses. These results are given in Chapter 5.

- Examination of the effect of BP incorporation, an anti-osteoporotic drug, by means of handling and mechanical properties.

  Briefly, low- and high- concentration of BP was loaded into IBS and the influence of BPs release on the in vitro responses of IBS was studied. The findings are introduced in Chapter 6.

2. BACKGROUND

2.1 Bone Structure and Biology

Bone is considered as a distinct organ formed by three essential components which are bone cells, bone minerals, and bone matrix. Its organic substrate composes of abundantly collagen type I (approximately 40 % of volume), its inorganic material is largely hydroxyapatite (HA) (approximately 45 % of volume) and the water composes the rest of the volume (approximately 15%) [26]. The organic part of the bone also consists of smaller amounts of type III and V collagen, fibril-associated collagen with interrupted triple helices (FACIT), growth factors, osteonectin, osteocalcin, and blood proteins. Crosslinking of collagen fibrils gives the strength of collagen fibrils. Most important properties are stiffness and strength of bone. The inorganic part of the bone also contains minor amounts of carbonate, potassium, magnesium, strontium, sodium, chloride and fluoride [27]. The inorganic part of bone produces its stiffness and rigidity. The hierarchical microstructure of bone matrix in Figure 2.1 shows that HA minerals are deposited orderly within type I collagen matrix [14]. Thus, this organic and inorganic combination makes the bone's mechanical properties particular in terms of stiffness and tensile strength.

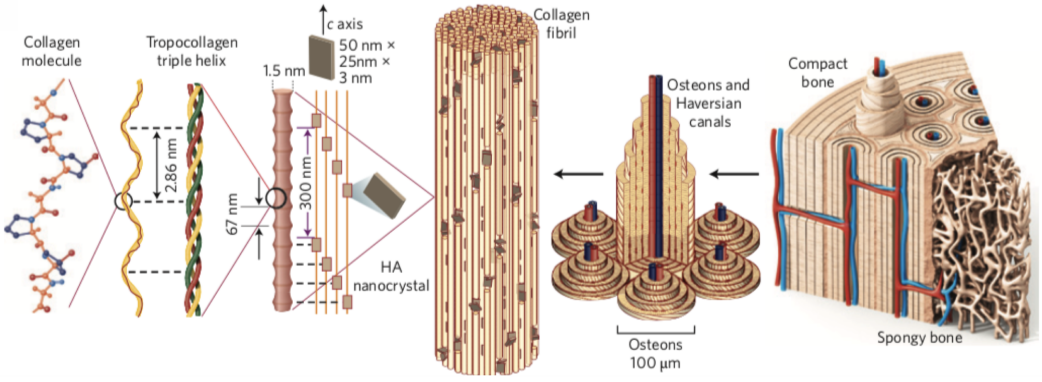

Figure 2.1 The hiearchical structure of bone tissue [1].

The hierarchical structure of bone shows that cortical (compact) and trabecular (cancellous) bone are two main parts [28]. The surface of the cortical bone is covered by the periosteum. This layer mostly consists of blood vessels and bone cells which are responsible for bone growth and repair as well [29]. Under periosteum, cortical bone shows itself with its compact and solid structure which shields the cancellous bone. Trabecular bone consists of a honeycomb-like system of trabecular plates and bars scattered in the bone marrow partition as seen in Figure 2.2. The cortical and trabecular bone tissue makes the macrostructure of bone, the microstructure of bone consists of Haversian systems, osteons, and single trabeculae [30]. When this microstructure of bone is magnified through nanostructure level, collagen fibrils are detected. At nanostructure scale, there are also CaP crystals and non-collagenous proteins which are located between the gaps of collagen fibrils [28].

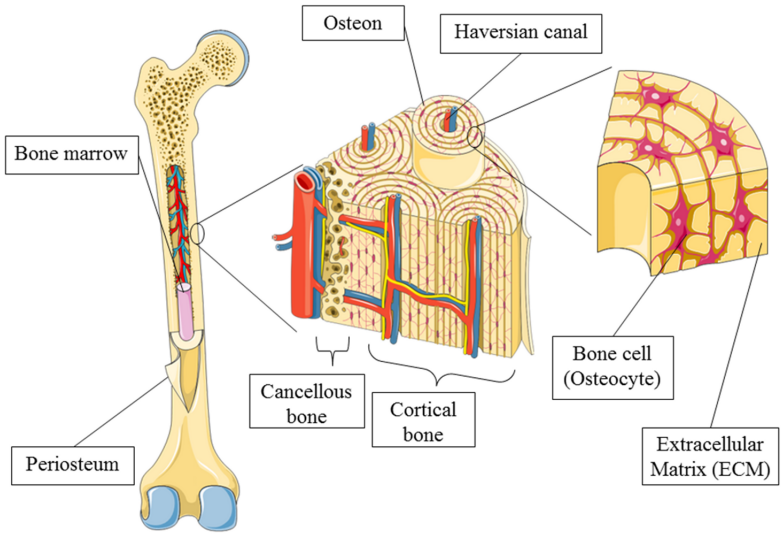

Figure 2.2 Schematic of bone structure [2].

The bone tissue comprises of four different cell types which are osteocytes, osteoblasts, bone-lining cells and osteoclasts [3]. They are either originated from hematopoietic stem cells or mesenchymal stem cells. Osteocytes are responsible for extracellular concentrations of calcium and phosphate. Also, they allow cell to cell interaction, ion and growth factor transportation with their extensions called canaliculi. When bone is exposed to mechanical stimuli, the osteocyte also acts as a controller of osteoblastic differentiation of mesenchymal precursors [31]. Osteoblasts are responsible

for bone formation and they participate in matrix development and calcification. The osteoblast cell is responsible for bone regeneration by producing and secreting osteoid, unmineralized bone, which converts into a mineralized bone matrix. The mesenchymal progenitors are induced of WNT-signaling to differentiate to osteoblasts [32]. These cells also regulate the formation and activation of osteoclasts. Osteoclasts are in charge of the bone resorption. They are able to break down the organic and inorganic matrix of bone. The osteoclast apposes to the bone surface with the assistance of integrin [33]. The zone between the osteoclast and the bone surface is the sealing zone. The integrin attaches to RGD (arginine, glycine, aspartic acid) in osteopontin. Thereafter the osteoclast becomes polarized and develops a ruffled border against the bone surface. A proton-pump then releases protons (H^+), reducing pH and resolving the HA crystals. The osteoclasts also release proteolytic enzymes that decompose matrix proteins [34].

2.2 Biology and Biomechanics of Bone Healing

Bone undergoes constant remodeling through lifetime due to its highly dynamic physiology [29]. The remodeling cycle occurs mainly in three phases which are resorption, reversal, and formation. Figure 2.3 shows the illustration of bone remodeling phases [3]. Bone formation requires osteogenic cells following a differentiation cascade of the osteogenic cells. The osteoclasts identify the location for resorption and start the process. During the resorption phase, most of the matrix proteins break down. The osteoclasts initiate activation of osteoblasts near the resorption lacuna. The osteoblasts relocate to the lacuna and start osteoid deposition to rebuild bone in the lacuna. This process may go on for several months [35].

Fracture healing is also a dynamic process which involves cell growth, differentiation factors, hormones, and extracellular matrix. Fracture healing as illustrated in Figure 2.4 results in three continuous steps which are called inflammatory stage, reparative stage, and remodeling stage [35, 36]. Shortly, in inflammation stage, also known as immediate reaction, bleeding occurs and vasodilation and leukocyte migration starts. During this process, hematoma formation begins between two separate

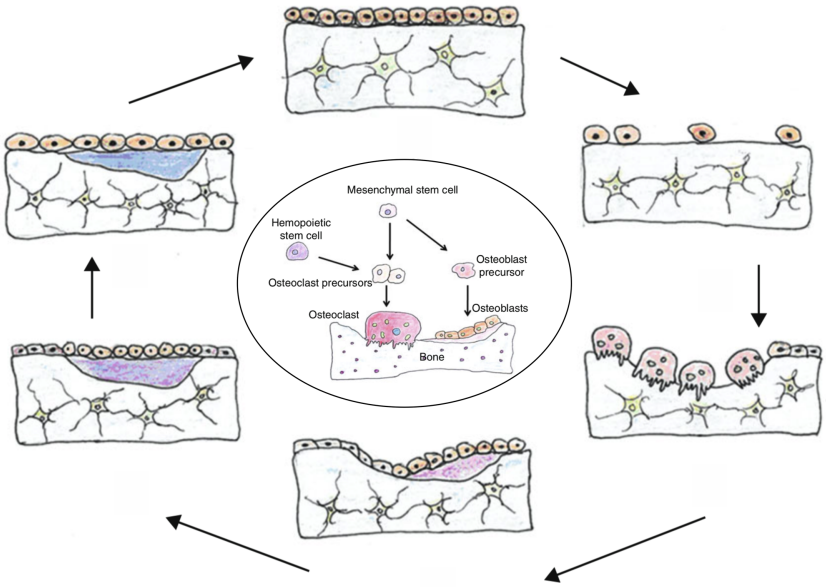

Figure 2.3 Remodeling cycle of bone [3].

edges of the fractured side in which cell migration occurs and bioactive agents exist. Angiogenesis and tissue granulation also occur in this stage. Intramembranous ossification, chondrogenesis, and endochondral ossification result in the reparative phase. Cell proliferation and differentiation and callus formation also take place in this phase. Following the callus formation, fractured bone is healed by mineralization. This newly formed bone tissue goes through remodeling phase. In this last stage of fracture healing, bone resorption and formation go on to give the bone its physical properties and function.

The repair and remodeling processes initially begin at the outer layer of the bone called periosteum as mentioned in Section 2.1. At periosteum, osteoprogenitors and osteocytes relocate through the defect site, producing a bony bridge to interfere fracture [35]. When this linking cannot be initiated by fracture remodeling, hypertropic non-union arises which requires the use of bone grafting.

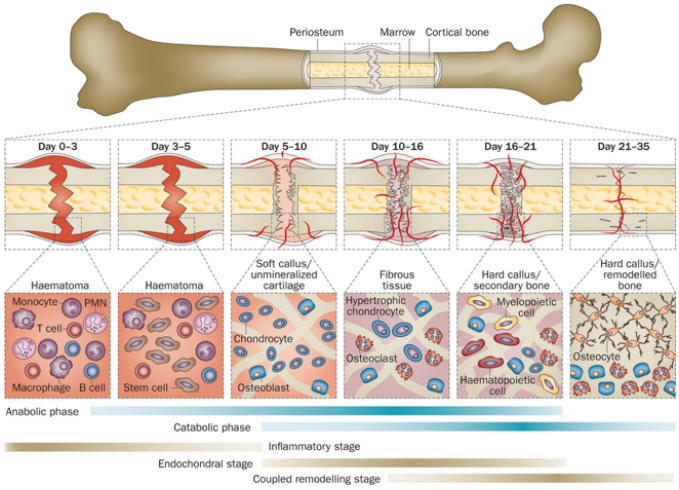

Figure 2.4 Schematic of fracture healing of bone [4].

2.3 Bone Grafting and Injectable Substitute Materials

Bone loss may occur due to trauma, tumors, osteoporosis, infection or some other diseases. The golden method for the treatment of bone loss to date is to use autologous bone grafts, however, they have drawbacks such as infections, reoperations, sensory loss, or insufficient amount [11, 12, 37, 38]. Allografts, which means to take bone from other humans, may be implanted to alternate an autologous bone graft. It seems as a practical method to heal bone loss, but it also has some risks like donor side morbidity, infections, or immunogenic responses. Another alternative of nature-derived bone graft is called xenografts, harvested from non-human mammals. They also have same limitations like auto- and allografts [14, 39]. Developing clinically relevant biomaterials for use in bone substitutes plays an important role in overcoming these restrictions. Currently, bone repair is mostly carried out with previously shaped bone substitutes and their implantation with a surgery. In spite of the sufficient outcome of these in vitro prepared bone substitutes, they may lead to additional bone loss, trauma for the surrounding tissue and also wide surgical wounds [14]. In order to utilize minimally invasive techniques, development of injectable substitutes for filling bone defects is a promising alternative to fill bone defects (Figure 2.5) [40, 5].

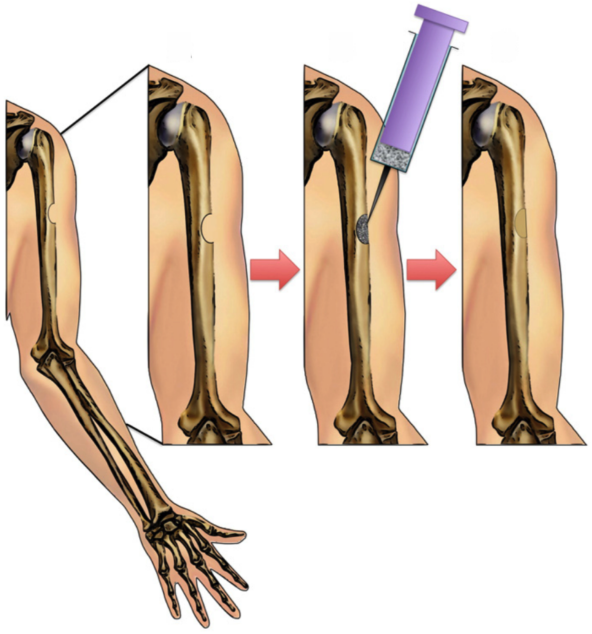

Figure 2.5 Schematic representation of how injectable bone substitutes are used [5].

2.4 Polymeric Injectable Bone Substitute Materials

As an IBS, various scaffold materials are studied and hydrogels are the most widely exploited candidate. Biocompatible, biodegradable, stimuli-responsive natural or synthetic polymers are crucial platforms for the therapeutic IBS applications [14, 41]. More specifically, natural polymers show better biocompatible properties comparing with synthetic polymers [42]. Most abundantly used natural biopolymers as an IBS can be listed as chitosan, alginic acid, hyaluronic acid, gelatin, collagen, agarose, matrigel, and cellulose derivatives [42]. Polymer-based IBS can also be classified as physical or chemical gel, depending on their gelling structure. While physical and hydrophilic association between polymer chains or particles are called as physical crosslinking, chemical crosslinking has covalently linked polymer chains in the structure [43]. Unsteady functional group, cytotoxic indicator, and inadequate coupling are the main limitations for chemical gelling systems [42, 43]. Thus, a thermo-sensitive polymer with slight chemical alterations may possess a promising alternative in the field of IBS. Most abundantly used natural polymers are hyaluronic acid and chitosan. They are generally combined together with thermo-sensitive polymers to supply thermo-

sensitivity. For example, hyaluronic acid is generally used with stimuli responsive polymers such as PNIPAAm [44], pluronic acid [45] and gelatin [46]. The addition of glycerophosphate to chitosan solution makes a thermo-sensitive gelling system. The chitosan- glycerophosphate system was studied to deliver insulin and revealed success as an injectable hydrogel delivery system [45]. There are also other successful studies with chitosan- glycerophosphate system for injectable drug delivery [46].

Cellulose is another alternative natural polymer which is also a renewable resource. By the incorporation of alkyl and methyl groups to the hydrophobic groups of cellulose, hydrophobic groups on cellulose turn the cellulose into a thermo-sensitive polymer [47, 48]. MC, one of the cellulose ether derivatives, has been widely exploited as drug delivery matrix, adhesives, and cosmetics. It is also a good candidate for IBS due to its adjustable thermo-responsive properties [47]. As Ghanaati et. al. [49] reviewed that while cellulose contributes to the mechanical properties for bone substitution, a modification of cellulose fiber called methylation augments the osteoconductivity. Studies revealed that the addition of cellulose in bone substitutes causes the slow resorption of the CPC so leads to longer implant lifetime [50]. The composites of β-tricalcium phosphate, HA and MC induced bone formation in defect model in rabbits [51]. There are no other studies that combine both calcium phosphate and MC in literature. However, researchers have studied on MC as an injectable hydrogel and drug delivery system for bone tissue repair [52, 53, 54]. Based on the studies done with cellulose, it can be emphasized that cellulose has a crucial potential for injectable delivery system due to its both hydrophilic and hydrophobic parts and ability of pairing with other polymers. Gelatin, collagen, agarose and matrigel are other natural polymers which are thermo-sensitive. Except matrigel, they show reverse thermo-responsive properties like forming a gel at lower temperature while being liquid at higher temperature [42]. Gelatin is known as a chemical derivative of collagen. It has certain biological characteristics comparable with collagen, like easy processability into microspheres, fine gelling behavior, controllable degradation characteristics, and plenty of functional groups for further functionalization and modification [55]. Due to these unique properties of gelatin, it is widely used for controlled delivery of drugs [56], biomolecules [57] and growth factors [58] for bone tissue repair and applications [59].

In addition, these properties make gelatin an ideal organic additive [60]. Due to the presence of its RGD groups, integration of gelatin to the polymeric hydrogel substitute supports cell-surface recognition, cell physiology and cellular affinity. As a result of this incorporation, gelatin guides stem cells through the biological pathway and improve the cell proliferation and differentiation to osteoblasts [61, 62]. Researchers developed MC-grafted-acrylamide/gelatin microspheres drug delivery system for the release of nifedipine. The study revealed that the crosslinking of MC and gelatin enhanced the nifedipine release profile [63]. In another study, biopolymer film of MC and gelatin was formed to test the antimicrobial activity [64]. The study result showed that films made by gelatin-methylcellulose blends had improved inhibition diameters compared to the other experimental groups types [64]. All of these findings indicate that thermo-responsive polymers have a great interest in the field of IBS.

2.5 Calcium Phosphate-Based Injectable Bone Substitutes

CPC are one-of-a-kind and clinically approved injectable bone graft ceramics with their unique properties such as self-setting ability, good injectability, easy moldability, increased reactivity and high feasibility in controlled drug delivery in bone regeneration since 1980′s [14, 65, 66, 67]. In situ self-setting of CPC is firstly developed by Chow et al. [68, 69]. Up to date, CPCs are used for numerous bone diseases treatment including tibial plateau fracture [70, 71], femoral neck fracture [72, 73], joint fixation [74, 75], maxillofacial and craniofacial repair [76, 77], alveolar bone grafting [78], restoring of bone defects [52] and many other applications. However, the CPCs have some drawbacks including their fast resorbability and weak mechanical properties. These properties should be improved in order to make them more applicable in practice. In literature, many application and methods are presented to hinder these drawbacks of CPCs such as adjusting rheological behavior [5, 79], using pore-making agents like acetic acid or citric acid [80], rapid setting by sodium phosphate addition [81], combination with poly(methyl methacrylate) for improving mechanical properties or adding monocrystalline HA for improved osteogenesis and vascularization [82, 83, 84, 85]. Moreover, there are other methods that have been found to enhance their bone repair-

ability by adding other components or elements. For instance, mineralization and cell proliferation could be obtained by combining calcium silicate with CPCs [86]. Similarly, doping CPCs with zinc, magnesium and fluoride ions also promote bone mineralization and improve mechanical strength [87, 88]. The addition of calcium sulfate to the CPC also supports to improve the drawbacks of CPC by improving handling properties and osteogenesis [14, 42, 88].

2.6 Calcium Phosphate-Polymer Based Injectable Bone Substitutes

CPCs also have the ability to harden in physiological temperature and then form HA which is the main component of the bone′s mineral phases [11]. However, they possess some problems as a biomaterial such as high resorbability, poor mechanical properties, and low degradability. Not only to overcome these drawbacks but also to mimic the highly mineralized collagen-based matrix of native bone, the combination of natural polymers with CPC is a practical approach. This combination has two advantages. While CPC serves to improve mechanical properties of the composition, it also enhances the osteoconductive properties of the polymer [25]. Combination of CPCs with PLA [89], acrylic acid [90] or hydroxypropyl methylcellulose [91] could enhance mechanical properties. Also, CaP and cellulose combination may lead the permeation of body fluid into this combination matrix through the micropores and this association enabled angiogenesis, cell migration, growth, and finally lead to a new bone formation [14]. Besides the important parameters of injectable polymeric materials, mechanical properties play a crucial role on the physical integrity of bone substitutes. For example, Debeaufort and Voilley [92] studied MC and polyethylene glycol film. Their mechanical results showed that tensile strength increased due to the incorporation of MC fibers [92]. Francis et al. [93] studied the mechanical properties of gelatin, crosslinked gelatin, gelatin/HA blend and gelatin/HA spin-spray. According to their findings, blending of gelatin showed higher tensile strength then the other form [92]. Baumann et al. [94] developed hydrogel by using MC and hyaluronan which has good injectability,

swelling, degradation, and diffusivity. In short, research done by CaPs and polymers combinations as injectable bone repair materials can help to eliminate their particular limitations and can help to improve key parameters mentioned above. Hence, the CaP-polymer based structures are still developing research directions.

2.7 Graphene Oxide as a Reinforcing Agent

GO, chemically oxidation form of graphite, has appealed great interest in bone tissue applications due to their extraordinary physical, electrical and chemical properties, large surface area and chemical purity [95]. Accordingly, the use of GO with CPC as a reinforcing agent is an efficient way to improve CPC′s mechanical properties, stability, handling properties, osteoconductivity, cell adhesion, proliferation and differentiation [95, 96, 97, 98]. To date, various studies showed that GO added bone scaffolds exhibits not only good physicochemical properties [96, 97, 99, 100, 101, 102] but also enhanced cellular activity both in vitro [103, 104, 105] and in vivo [98, 105, 106]. However, two common application problems are still existing while producing graphene composites. Structural damage could occur while sintering graphene with ceramics or uneven distribution of graphene could arise in the matrix due to the strong van der Waals force between graphene layers [107]. Therefore, its incorporation into polymer matrix is important to achieve homogenous and stable dispersion of GO in CPC.

2.8 Bisphosphonate for Bone Healing

One of the pharmaceutical treatments for osteoporosis is the systemic administration of BPs which efficiently leads to augmentation of bone density, inhibits bone loss, and minimizes the treat of bone fractures [108]. Increase of bone mineral density and reduction of bone resorption occur with BP incorporation, because they suppress osteoclast-mediated bone resorption [7]. Particularly, nitrogen-containing BPs have high efficacy to increase bone mineral density due to the interaction of nitrogen moiety

with crystal surface of the bone mineral. Figure 2.6 shows the chemical structure of BP that has two side chains, R_1 and R_2. While R1 defines its bindings to HA, R_2 shows its potency [7, 6]. BP is also classified as nitrogen containing and non-nitrogen containing BP depending on their R_2 chain. Their inhibition of osteoclast-mediated bone resorption mechanisms is also different regarding to their R_2 chain type. Figure 2.7 shows their mechanism of actions in molecular level. Non-nitrogen containing BPs suppress the mitochondrial adenine nucleotide translocase (ADP) and cause the osteoclast apoptosis by integration with non-hyrolyzable analogues of ATP (AppCp). On the other hand, nitrogen containing BPs have a different pathway to inhibit osteoclast activity. This pathway is called as mevalonate pathway which involves the prenylation [6]. Briefly, farnesyl pyrophosphate synthase (FPPS) is interrupted by nitrogen containing BPs. Nitrogen containing BPs also impede an enzyme called the geranylgeranyl pyrophosphate synthase (GGPPS) in mevalonate pathway. Intercellular localization and functions of osteoclasts prevented with this blockage in mevalonate pathway [7, 6]. In addition to that nitrogen containing BPs also have anti-tumor effect [7].

The regular administration of BPs is oral; however, this leads to less than 1 % absorption from gastro-intestinal tract [17]. Also, with their extended usage, BPs have side effects such as osteonecrosis of the jaw, atypical sub-trochanteric femoral fractures, gastric ulcer, dysphagia and esophagitis [17, 18, 19]. Therefore, local delivery of BPs to bone have been beneficial for prevention of the potential side effects [21, 22]. Among the types of BPs, ZOL has been extensively studied because of its high efficacy to increase bone mineral density and reduce bone resorption which occurs by osteoclast-mediated bone resorption inhibition [109, 110]. The IBS matrix system is allowed to load or to conjugate drug and biomolecules for treatment of bone defects. There is also a developing interest to produce a drug delivery system which is able to achieve controlled and localized treatment by using CPCs to the bone disease location. Drugs or biomolecules can be incorporated either in the powder or the liquid phase of the IBS matrix [21, 66]. Delivery of bisphosphonate within an injectable bone substitute matrix is mostly done by using CPC, polymer-based CPC, and/or a polymer matrix. Polymer-based CPC is used in order to investigate the direct impact of BP on the bone

(a)

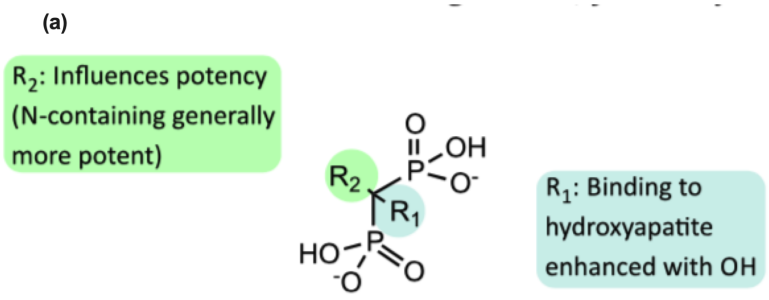

Generic bisphosphonate

(b)

Bisphosphonate	R_1	R_2	Entrance on US market
Etidronate	-OH	CH_3	1977
Clodronate	-Cl	Cl	*
Tiludronate	-H	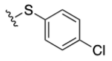	1997
Alendronate	-OH	NH_2	1995
Pamidronate	-OH	NH_2	1991
Ibandronate	-OH	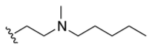	2003
Risedronate	-OH		1998
Zoledronate	-OH		2007

Figure 2.6 (a) Structure of bisphosphonate, (b) types of bisphosphonate [6].

healing process. Studies showed that incorporation of BPs to the IBS may alter the physicochemical properties of IBS such as hardening time, morphology, porosity and mechanical properties within acceptable limits [110, 111, 112, 113, 114, 115, 116, 117]. For example, addition of BPs marginally decreased mechanical properties of the BPs added IBS samples [111, 117, 118, 119, 120, 121]. Setting time of the samples increased with the incorporation of BPs to the structure [111, 117, 119, 120, 121]. In vitro results revealed the inhibitory effect of these IBS on osteoclasts and promotive effect on osteoblasts [109, 119, 120, 121, 122, 123, 124, 125]. Boanini et al. [121] compared the in vitro effect of ZOL and alendronate by HA nanocrystals. ZOL showed much more affinity than the alendronate for HA structure, however, they showed similar degree of osteoclast apoptosis. The affinity of ZOL to HA was explained with their good structural match [111]. In vivo studies of BP loaded CPC-based scaffolds also proved the increase of bone formation by incorporation of BP [37, 117, 118, 121, 126, 127, 128, 129]. Studies done by using polymers showed promising results with regards to their cohesive properties not only together with CPCs but also with BPs. The outcome

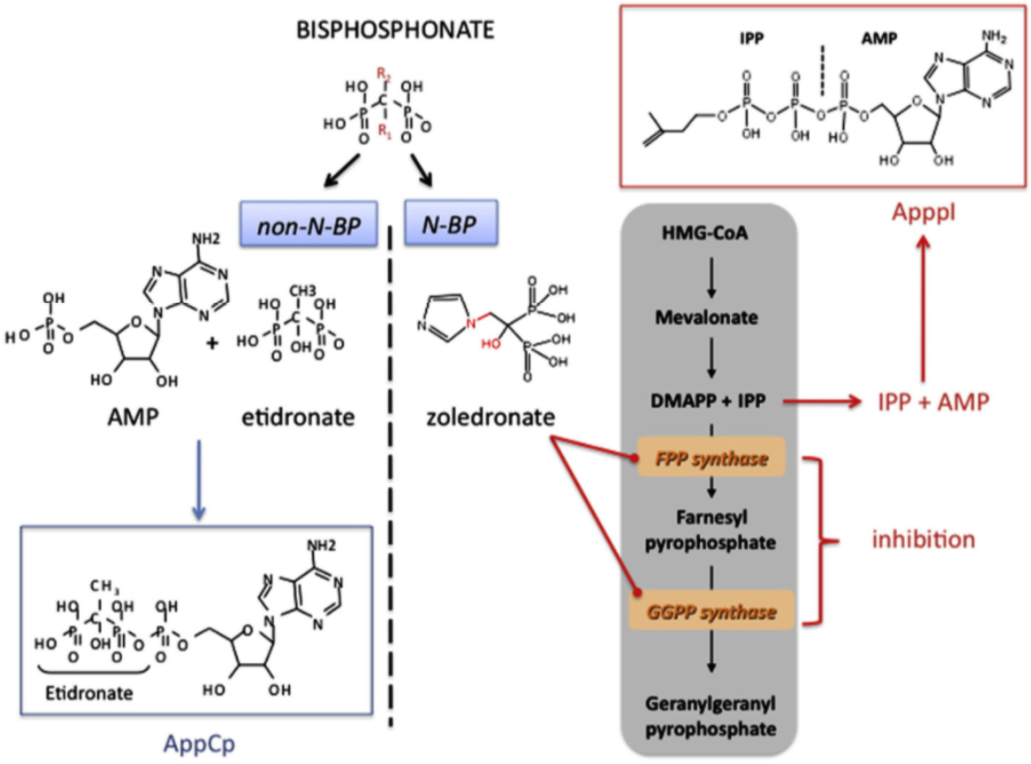

Figure 2.7 Molecular mechanisms of action of bisphosphonates [7].

of non-covalently bond matrix system would be another alternative for an effective localized delivery of BPs. Despite all these comprehensive studies, BP incorporation to the CPC together with the natural polymers is investigated further in order to enhance anti-tumor and anti-osteoporotic properties of the cement matrix as an IBS.

To conclude, an ideal IBS with the combination of polymers and CPC can be developed which stimulates new bone formation with adjustable setting time, suitable rheological properties for injection, ideal mechanical properties for the intervention site of the orthopedic applications. Also, GO can be incorporated as a reinforcing agent into IBS and BPs can be loaded to induce anti-osteoporosis and anti-cancer properties of the IBS.

3. PRELIMINARY STUDIES

In this thesis, IBS material was prepared by the gelation of liquid phase encapsulating powder phase. The liquid phase is composed of gelatin (from bovine skin, gel strength ~225 g Bloom, Type B), MC (viscosity 15 cps, Mw 14 kDa, DS 1.5-1.9)) and sodium citrate tribasic dihydrate (SC, $C_6H_5Na_3O_7$, Mw 294.10 g/mol, mp: >300 °C (lit.), pH 7.0-9.0 at 25 °C), and the powder phase is composed of tetracalcium phosphate $Ca_4(PO_4)_2$, TTCP), dicalcium phosphate dihydrate (DCPD, $Ca_2HPO_4.2H_2O$, Mw 172.09 g/mol, d:2.31 g/mL) and calcium sulfate dihydrate (CSD, $CaSO_4.2H_2O$, Mw 172.17 g/mol). While designing the IBS, the various parameters like hydrophilicity, stiffness and strength, porosity/permeability, biodegradability and biocompatibility should be kept in balance [15, 25]. In order to sustain this balance, some of the parameters were used as given in the literature including preparation of powder phase mixture, dissolving the polymers and the treatment of GO as well. As a result of manipulation of independent parameters, the desired physiological properties were obtained by optimization of the weight fraction of MC to gelatin, SC concentration, cohesion/stability of prepared IBS samples at 37 °C in phosphate buffer saline (PBS) solution. Therefore, as a preliminary work, gelation temperature and time measurements were carried out by using test tube inversion technique [130] to optimize the weight fraction of MC to gelatin and SC concentration. To sum up, the aim of this preliminary work is to decide the MC, gelatin and SC concentrations as a liquid component while adjusting the gelation temperature closed to body temperature (36.5-37.5 °C) and also record the gelation time of liquid component at 37 °C. The detailed experimental procedures and the findings were presented in this Chapter.

3.1 Experimental Procedure

3.1.1 Preparation of Powder Component Mixture

Powder mixture was prepared by mixing TTCP, DCPD and CSD. TTCP was synthesized with solid state reaction by heating an equi-molar mixture of monetite ($CaHPO_4$, Mw 136.06 g/mol), calcium carbonate ($CaCO_3$, Mw 100.09 g/mol, d: 2.93 g $\leq$ 30 μm particle size) at 1500 °C for 6 h, using a 5 °C/min heating rate and 10 °C/min cooling rate. The heated mixture was ground in a mortar and then sieved. Then phase purity of the synthesized TTCP crystals was analyzed by using X-ray diffraction (XRD) (Rigaku D/MAX-Ultima+/PC, Austin, TX, USA) and Fourier transform infrared structure (FTIR) (Perkin Elmer, Waltham, MA, USA) [131] before preparing the powder component. Powder component was prepared by mixing an equi-molar mixture of DCPD and TTCP powder and then this CPC mixture was added to the CSD in a 4 to 1 mass ratio [131].

3.1.2 Preparation of Liquid Component Mixture

Decired amount of MC powder was dissolved in distilled water at 90 °C. Then, to obtain clear MC solution, dispersed MC powder at 90°C was stored at refrigerator overnight [132]. Gelatin solution was also prepared in distilled water at 50 °C and used at room temperature [133]. After preparation of MC and gelatin solution, they were blended by adding various MC and gelatin concentration to obtain the proper ratio for adjustment of gelling temperature at 37 °C. The desired amount of SC solution was also prepared by dissolving in distilled water at room temperature.

3.1.3 Preperation of Injectable Bone Substitutes

Different percentage of bioceramic powder mixture were blended with different concentrations of liquid phase mixture in order to form IBS samples.

3.1.4 Gelation Temperature and Time Measurements

To optimize the gelation time and temperature, gelatin concentration was kept constant at 5 (w/v)% and 2.5 (w/v)%; then MC concentration was varied between 1.5 (w/v) to 16.0 (w/v) %. In the same time hydrogel containing SC (1.0, 2.0, 3.0 and 5.0 (w/v) %) was also prepared with the MC (1.5 (w/v) % w/v to 10 (w/v) %) and 2.5 (w/v)% gelatin solution. Prepared hydrogel samples were placed in a glass test tube. After that, test tubes were placed at water bath and temperature was increased with 1 °C/min heating rate starting from room temperature to 60 °C. With 5 min intervals, test tubes were tilted and the gelation temperature was recorded for every sample. The gelation temperature was recorded at which the samples stopped flows after inversion of the test tubes. For the gelation time measurement, temperature of water bath was kept constant at 37 °C. Then samples within test tubes were placed at water bath and allowed to equilibrate at 37 °C. Test tubes were tilted in every minute to check the gelation status and time passed was recorded [130]. The gelation temperature of SC incorporated hydrogel was also measured by using a rheometer (Anton Paar, MCR302, Graz, Austria) at 2 °C/min heating rate, 5 Pa shear stress and 10 rad/s angular frequency. Gelation time of SC incorporated hydrogel was measured at 37 °C, 5 Pa shear stress and 10 rad/s angular frequency.

3.2 Findings of the preliminary Experiments

3.2.1 Analysis of Synthesized TTCP

TTCP powder was synthesized as described in Section 3.1.1 and Figure 3.1 shows the XRD analysis of the synthesized powder. The relevant Miller Indices of TTCP, HA and monetite are also presented. According to XRD graph, TTCP and hydroxyapatite peaks were detected since the powder was furnace-cooled [131, 134, 135, 136]. A trace amount of monetite and calcium oxide (CaO) were also found from the XRD analysis. The matched peaks with JCPDS file No. 25-1137, No. 09-0432 and No. 09-0080 is

given in Figure A.1.

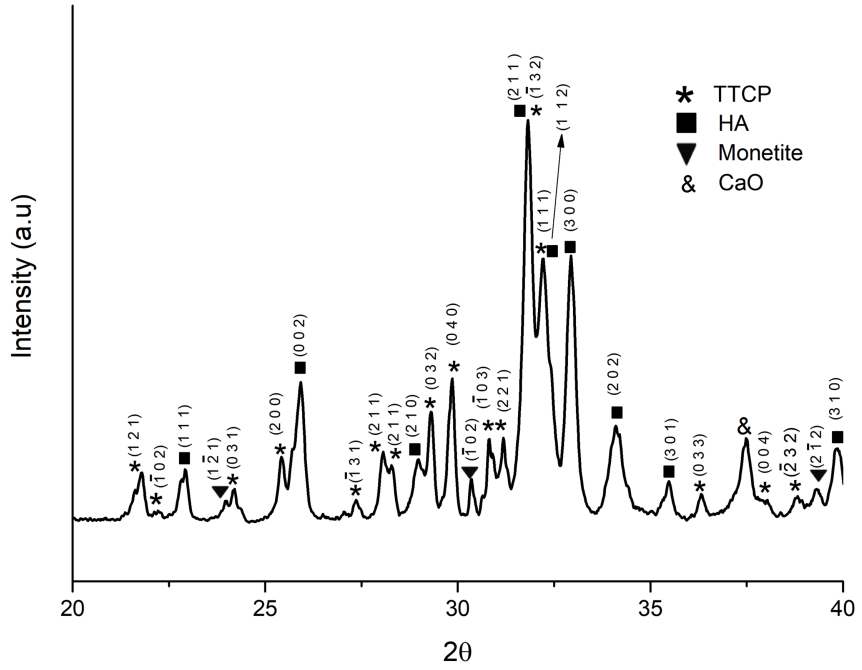

Figure 3.1 XRD pattern of synthesized TTCP powder.

Figure 3.2 shows the FTIR spectrum of synthesized powder. In FTIR spectrum, absorption peaks were found at 452, 471, 502, 567, 600, 628, 958, 987, 1044, 1091, 1625, 1922, 2001, 2077, 3435, 3570 and 3643 cm^{-1}. As labelled in Figure 3.2, PO_4^{3-} bands of TTCP were detected in the spectrum which were found similar with that of literature [136, 137, 138]. OH^- stretching bands located at 628 and 3570 cm^{-1} indicated the presence of HA [135, 139]. Absorption bands between 3000-3600 cm^{-1} indicated H_2O adsorbed. The peaks located at 1625, 1922, 2000 and 2077 cm^{-1} indicated the presence of carbonate content. These peaks were possibly found due to carbon dioxide absorption from the atmosphere [140]. Therefore, FTIR results supported the results observed from XRD spectrum which indicated synthesis of TTCP/HA-based powder [134, 137].

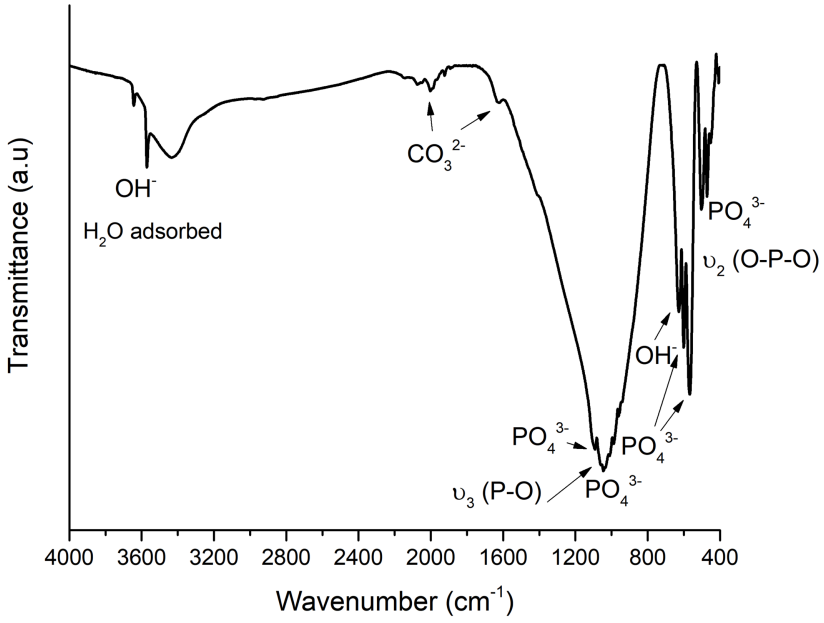

Figure 3.2 FTIR spectrum of sythesized TTCP powder.

3.2.2 Effect of MC, Gelatin and SC Concentration on Gelation Temperature and Time

The MC solution turned into a soft gel by increase of temperature. The hydrogen bonds among polymer chains of MC and water molecules makes MC soluble at low temperatures. At higher temperatures, the hydrogen bonding was broken due to presence of methoxy group [141]. As a result of this hydrophobic interactions, gel network of MC was formed. Figure 3.3 shows the transformation of MC solution to a soft gel at 37 °C. Figure 3.3 also indicates how test tube inversion technique was performed to determine gelation temperature and time.

Figure 3.4 shows the change of gelation temperature and time by the blending of different weight fractions gelatin and SC to the MC solution. Accordingly, the gelation temperature decreased with addition of gelatin solution although without the addition of SC. The gelation temperature decreased with an increase in SC concentration in the blend [48]. Bain et al. [142] indicated that heating destroys the cage-like structure

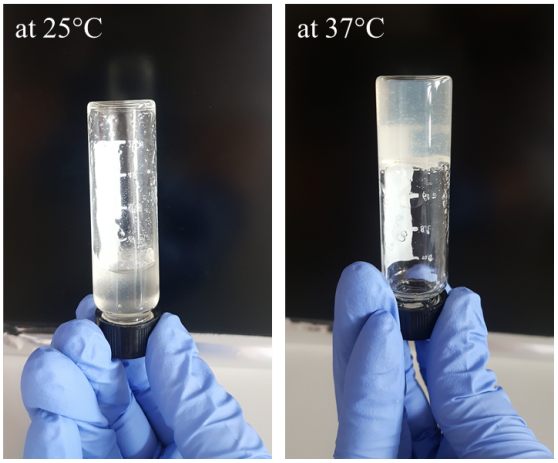

Figure 3.3 The gelation of MC solution; photographs of sol and gel state at 25 °C and 37 °C, respectively.(Sample contains 8.0 % MC solution containing 2.5 % gelatin solution).

between MC chains and water molecules therefore, aggregates form due to hydrophobic interactions. This is called salt-out effect and it leads to gelation of hydrogel at around 30 °C. Incorporation of SC interferes with the structure between MC and water molecules and therefore forms the hydrophobic aggregates at a lower temperature [142, 143].

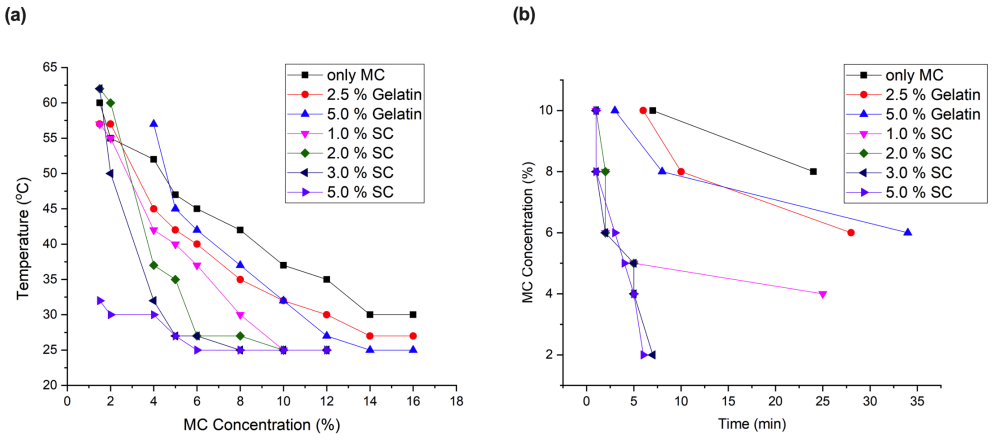

Figure 3.4 Effect of different weight fraction MC, gelatin, and SC blends on (a) gelation temperature and (b) time (SC incorporated liquid component also included 2.5 % gelatin).

When SC salts are added to the MC solution, the water molecules are attracted to the citrate ions which suppresses intermolecular hydrogen bond formation between water and hydroxyl group of MC. This depletion of water layer around hydroxyl groups of MC causes enhancement of hydrophobic-hydrophobic interaction between MC ions

which leads to gelation at a lower temperature [48, 142, 144, 145]. Sol-gel transition temperature which means gelation temperature of hydrogel samples containing 8 % MC, 2.5 % gelatin and 0.5, 1, 1.5, 2 and 3 % SC was measured with rheometer at 2 °C/min heating rate, 5Pa shear stress and 10rad/s angular frequency. Gelation time of same samples was measured at 37 °C, 5 Pa shear stress, and 10rad/s angular frequency. Sol-gel transition temperature was determined at the slope change of complex viscosity (Pa.s) graph. Similarly, gelation time values of these samples were obtained at the slope change of complex viscosity (Pa.s) graph. Figure 3.5 shows the effect of SC concentration on sol-gel transition temperature and gelation time. According to the results, sol-gel transition temperature and gelation time decreased with the increasing SC concentration [143, 144, 146]. Both analyses showed that there is no significant effect of adding SC more than 2 (w/v)% on 8 (w/v)% MC and 2.5 (w/v)% gelatin solution.

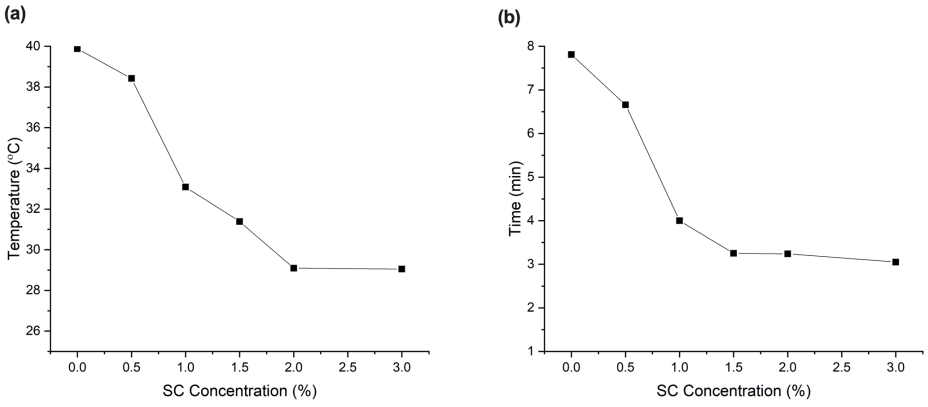

Figure 3.5 (a) Sol-gel transition temperature and (b) gelation time graphs of 8 (w/v) % MC and 2.5 (w/v) % gelatin hydrogels as a function of SC concentration.

3.2.3 Cohesive Stability Test of IBS Samples

To further optimize the suitable weight fraction of the IBS, cohesive stability experiments were evaluated in PBS at 37 °C. Briefly, prepared IBS samples were injected by using a 10 mL disposable syringe with or without a 18G needle tip in PBS solution at 37 °C. It also enabled determination of the experimental groups based on the workability of the IBS samples. The criterion was to observe whether the injected samples

retained their shape. Therefore, the outcomes of adding different amount of SC into the blend solution and various weight fraction of powder component on stability of IBS samples in PBS were evaluated at 37 °C. The stability results of various IBS samples in PBS were given in Table 3.1. Figure 3.6 shows the actual images of samples injected in PBS. Accordingly, rising the SC concentration led to decrease stability of injected paste in PBS at 37 °C. As the MC10SC5 samples were injected in PBS, the injected materials started to disintegrate. On the other hand, other IBS samples indicated in Table 3.1 and Figure 3.6 showed cohesive stability in PBS in contrast with MC10SC5 and MC10SC2 samples.

Table 3.1
Contents and stability results of IBS samples in PBS at 37 °C.

Abbreviation*	MC	SC	P/L ratio	Stability in PBS at 37 °C
	w/v %	w/v %	g/g	
MC10SC1	10	1	0.43	Stable
MC10SC2	10	2	0.43	Stable
MC10SC3	10	3	0.43	Stable
MC10SC5	10	5	0.43	Stable but tear apart
MC10SC10	10	10	0.43	Not stable
MC8SC2	8	2	0.43	Stable but tear apart
MC8SC3	8	3	0.43	Stable

*All samples included 2.5 (w/v) % gelatin solution.

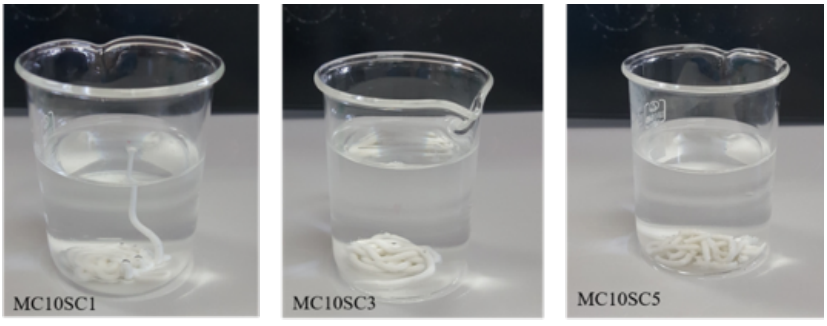

Figure 3.6 Stability images of various IBS samples in PBS at 37 °C.

This stability method was also used to adjust the weight fraction of powder component within IBS samples. While the weight fraction increased further, the powder component started to dissolve immediately and the PBS solution became blurry.

Therefore, the maximum weight fraction of powder was chosen as 50 wt% to prepare IBS samples, meaning that P/L ratio (g/g) is 1. By comparing and evaluating all of the optimization experiment results, the liquid components to prepare cement paste were finalized as 8 (w/v) % MC, 2.5 (w/v) % gelatin and 3.0 (w/v) % SC solutions.

4. EFFECT OF POWDER TO LIQUID RATIO ON THE PHYSICOCHEMICAL AND IN VITRO PROPERTIES OF THE INJECTABLE BONE SUBSTITUTES

In preliminary studies, the concentrations of liquid component mixture were decided and then the maximum P/L ratio were found as 1 (g/g). In this regard, three different P/L ratio were chosen to evaluate the effects of P/L ratio on the phase, injectability, morphology, rheology, mechanical and in vitro properties.

4.1 Preparation of IBS Samples

MC was dissolved as 6 g of MC powder in 50 ml distilled water at 90 °C until MC′s complete dispersion. The dispersed MC solution was placed at 4 °C until a clear MC solution was obtained [132]. 1.875 g of gelatin was added in 12.5 ml of distilled water at 50 °C and left for cool down before use [133]. 2.25 g of SC salts was dissolved in 12.5 ml distilled water [142]. Then all solutions were mixed together to a final concentration of 8.0, 2.5, and 3.0 (w/v) % of MC, gelatin, and SC, respectively. Powder component of IBS samples compose of TTCP powder, DCPD, and CSD. TTCP powder was synthesized by solid-state reaction, heating equi-molar mixture of dicalcium phosphate anhydrous ($CaHPO_4$) and calcium carbonate ($CaCO_3$) at 1500 °C for 6h, using a 5 °C/min heating rate and 10 °C/min cooling rate [13]. Bioceramic component was prepared by blending equi-molar mixture of DCPD and TTCP/HA-based powder and then this mixture was added to the CSD with a 4 to 1 mass ratio [131]. After this, different wt% of the powder phase was added to the polymeric component. The experimental groups and the compositions of the IBS samples are given Table 4.1.

Table 4.1
Composition of the IBS samples.

Abbreviation	MC	Gelatin	SC	Powder component
	w/v %	w/v %	w/v %	wt %
P0	8	2.5	3	0 (P/L=0.00)
P20	8	2.5	3	20 (P/L=0.25)
P30	8	2.5	3	30 (P/L=0.43)
P50	8	2.4	3	50 (P/L=1.00)

4.2 Characterization of the IBS Samples

4.2.1 Injectability Measurements

Injectability was qualitatively assessed and evaluated by extruding the IBS samples through a disposable syringe using 18-gauge needle. Each syringe and needle were filled with approximately 2 g of IBS samples, which was then extruded from the syringe manually within few seconds at relatively constant speed [146, 147]. Then the injectability was calculated by considering the percentage mass of the IBS samples extruded from the syringe divided by the original mass of the IBS inside the syringe as seen in Eq. 4.1.

$$\text{Injectability} = \frac{\text{Mass of extruded IBS}}{\text{Original mass of IBS inside the syringe}} \times 100\% \tag{4.1}$$

4.2.2 XRD Analysis

XRD (Rigaku D/MAX-Ultima+/PC) analysis was conducted to examine the setting reaction of synthesized powder and lyophilized IBS samples at 40kV and 30mA with a step size of 0.01 °C between 20 °C - 40 °C in a fixed time mode at Boğaziçi University, Istanbul, Turkey [131].

4.2.3 Morphology of the IBS Samples

The internal porous structure of the lyophilized IBS samples were examined by using Scanning Electron Microscopy (SEM) (Zeiss, Evo LS10) with 10kV accelerating voltage at Yıldız Technical University, Istanbul, Turkey [148]. Samples were coated with gold-palladium before the experiment.

4.2.4 Rheological Measurements

Rheological properties of IBS samples were performed by using a stress-controlled rheometer with a parallel plate geometry (diameter: 15 mm) (Anton Paar, MCR302, Graz, Austria) at Boğaziçi University, Istanbul, Turkey. The oscillation amplitude and frequency sweep were carried out at 37 °C. A temperature sweep was performed from 15 to 45 °C at a heating rate of 2 °C/min and at 0.1 % strain and 10 rad/s frequency within the linear viscoelastic region of IBS to determine the gelation and setting temperatures. A time sweep was carried out at 37 °C at 0.1 % strain and 10 rad/s frequency within the linear viscoelastic region of IBS to evaluate the gelation kinetics. Finally, the shear thinning properties of IBS samples were analyzed both at 25 and 37 °C [146, 149].

4.2.5 Compressive Strength Measurements

IBS samples were molded into columns of 7.0 mm of diameter and 10.0 mm length. The compressive strength of the samples was measured using a Geratech SH-500 (Geratech, Taiwan) and SH-20 testing device (Geratech, Taiwan) at Boğaziçi University, Istanbul, Turkey. The compressive strength of IBS samples was taken at 15 % strain. Measurements were taken on days 1, 3, 5 and 7 and 14 in an atmosphere of 100 % humidity at 37 °C (n = 5) [150].

4.2.6 In Vitro Degradation and pH Variation Measurements

IBS samples were molded into columns of 7.0 mm of diameter and 10.0 mm of lengths and after setting of the cement phase, they were immersed in PBS solution at 37 °C. At pre-determined times, the IBS samples were lyophilized and weighed. The remaining weight was calculated using Eq. 4.2 where W_0 is the initial weight of the lyophilized IBS samples and W_t is the lyophilized weight of the IBS samples after t days of incubation [146].

$$\text{Remaining weight} = \frac{W_t}{W_0} \times 100\% \tag{4.2}$$

Meanwhile, pH values of the PBS solution in which samples were incubated were measured at different time intervals including 5,10, 20, 30, 60, and 120 min, 1,3, 5, 7, 14, 21 and 28 days (n=3) [150].

4.3 Results

4.3.1 Injectability of IBS Samples

Figure 4.1 shows that the mixture of powder and liquid components have a chewing gum-like consistency after mixing. Since the IBS had a chewing gum-like consistency, it can be molded into the desired shape of the complex bone defects.

P0, P20, P30 and P50 samples were also extruded by using 18-gauge needle into PBS solution at 37 °C. Figure 4.2 (a), (b), (c), and (d) shows their images after extruded into PBS, respectively. Accordingly, P30 and P50 samples had a higher stability than P20, as P20 pastes tended to disintegrate during the extrusion process. Figure 4.2 (e) shows that all IBS samples had high degree of injectability. All samples had high

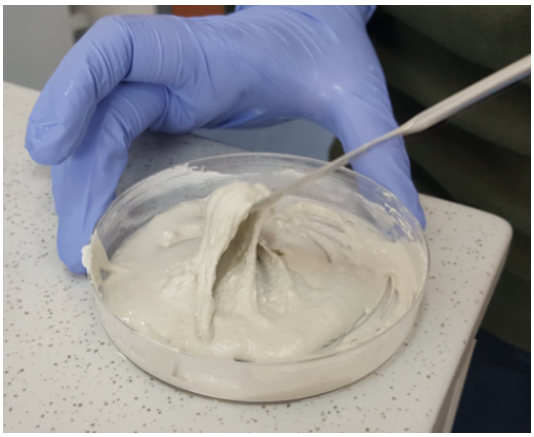

Figure 4.1 Chewing gum-like consistency of P50 samples.

degree of injectability, ranging from 94.53 to 91.73 %. As the wt % of bioceramic powder component increased, injectability was slightly decreased; however, there is no statistically significant difference between the injectability of the P20, P30 and P50 samples compared to P0.

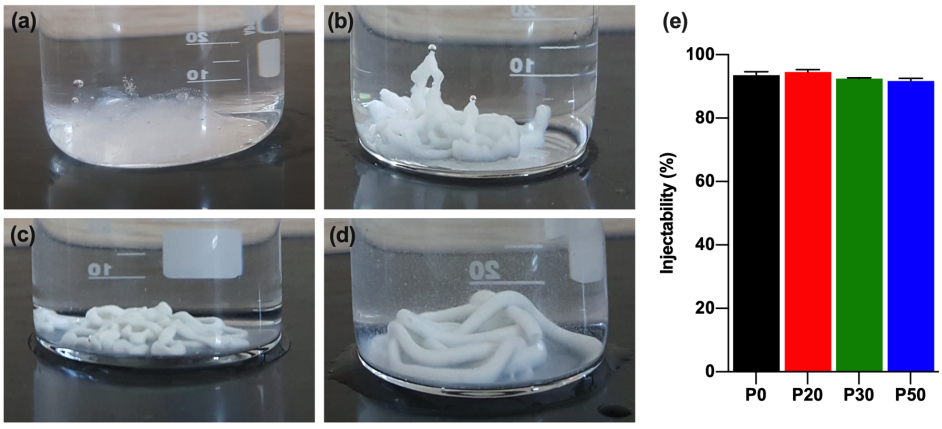

Figure 4.2 Extruded IBS samples in PBS at 37°C (a)P0, (b)P20, (c)P30, (d)P50, and (e) Injectability % of the IBS Samples (results expressed as mean ± standard deviation, n=3).

4.3.2 Morphology of the IBS Samples

Figure 4.3 shows the cross-sectional morphologies of lyophilized samples examined by SEM. Accordingly, all of the IBS samples had highly porous microstructure. When the wt % of the bioceramic component increased, the pore size decreased. P0 revealed that hydrogel scaffolds had a porous structure. SEM images also revealed that

bioceramics were well-adhered on the polymeric phase.

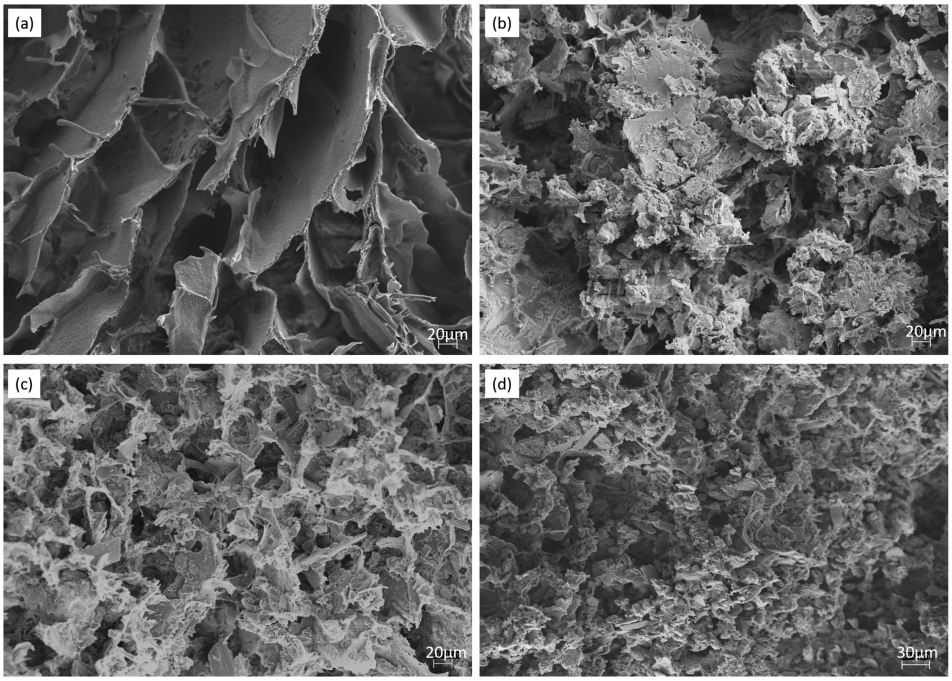

Figure 4.3 SEM images of (a) P0, (b) P20, (c) P30, (d) P50 IBS samples at a magnification of 500.

4.3.3 Rheological Measurements

Rheological measurements of IBS samples containing different wt % of the bioceramic component were evaluated. Figure 4.4 (a) shows the amplitude sweep measurement of IBS samples. Compared with P0 samples, other IBS samples present a wider linear viscoelastic region at 37 °C; as the strain required to destroy the network structure of IBS samples slightly increased. Figure 4.4 (b) shows the frequency-dependent rheological results performed under 0.1 % strain. In the measured frequency range, all of the IBS samples had a higher storage modulus (G′) than the loss modulus(G″) at 37 °C.

Temperature and time sweep measurements were taken to examine the impact of bioceramic powder phase on the gelation and hardening mechanism. Figure 4.5 (a) shows the temperature-dependent changes of G′ and G″ of IBS samples. The exponential increase of storage modulus and the interference of G′ and G″ with temperature

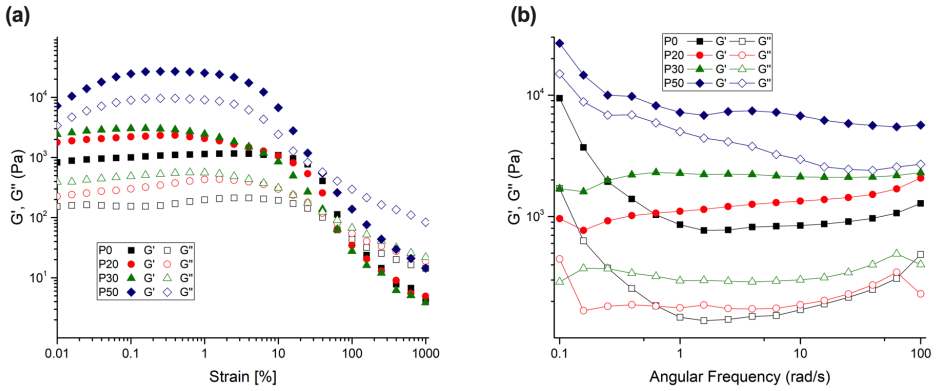

Figure 4.4 (a) Amplitude-dependent variation of G′ and G″ of P0, P20, P30 and P50 IBS samples at a frequency of 10 rad/s at 37 °C) and (b) Frequency-dependent variation of G′ and G″ of P0, P20, P30 and P50 IBS samples at a 0.1 % strain at 37 °C (results expressed as mean ± standard error, n = 3).

implies the phase transition of the samples. This phase transition temperature of the IBS samples moved to a higher temperature with the addition of 30 and 50 % of bioceramic mixture. Figure 4.5 (b) shows the gelation time at 37 °C. Similar to the temperature sweep test, the exponential increase of the storage modulus with time at 37 °C suggests the hardening of IBS samples. The plateau point indicates the curing of the polymeric chains which began less than 5 minutes for all the samples.

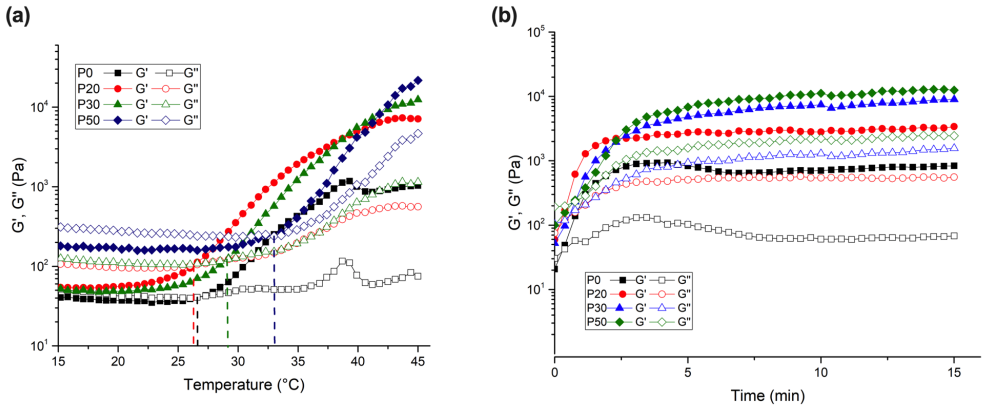

Figure 4.5 (a)Temperature-dependent variation of G′ and G″ of IBS samples at 0.1 % strain and 10 rad/s angular frequency (b) Time-dependent variation of G′ and G″ of IBS samples measured at 37 °C, 0.1 % strain, and 10 rad/s frequency (results expressed as mean ± standard error, n = 3).

Figure 4.6 shows the shear-rate dependent variation of viscosity for IBS samples both at 25 °C and 37 °C to observe whether IBS samples keep their injectability with respect to the increase of wt % of the bioceramic component. The results reveal that

both at 25 °C and 37 °C, all of the samples had shear thinning properties and P0 had a considerably lower viscosity when compared to P20, P30 and P50 [146, 150]. When the wt % of bioceramic component increased, viscosity also increased.

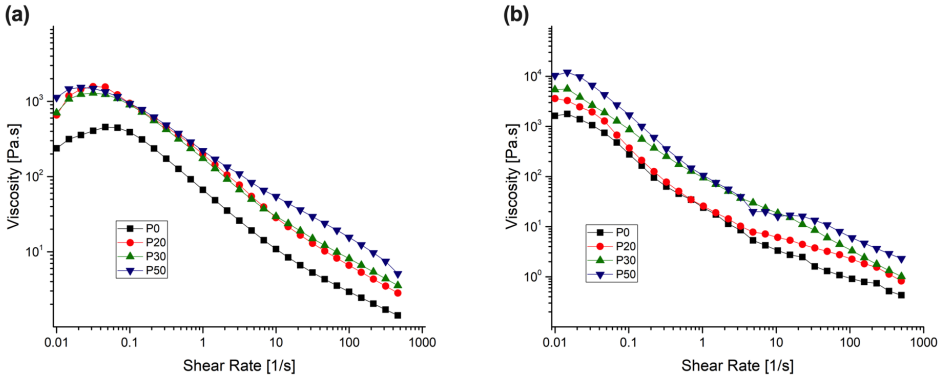

Figure 4.6 Shear-rate dependent variation of viscosity for IBS samples measured at (a) 25 °C and (b) 37 °C, respectively (results expressed as mean ± standard error, n = 3).

4.3.4 In Vitro Degradation and pH Variation Measurements

The pH profile of biomaterials in PBS is an important indicator of some of their possible biological responses. While the Figure 4.7 (a) shows the initial pH response of the samples, Figure 4.7 (b) shows the long-term pH change of the samples during their incubation.

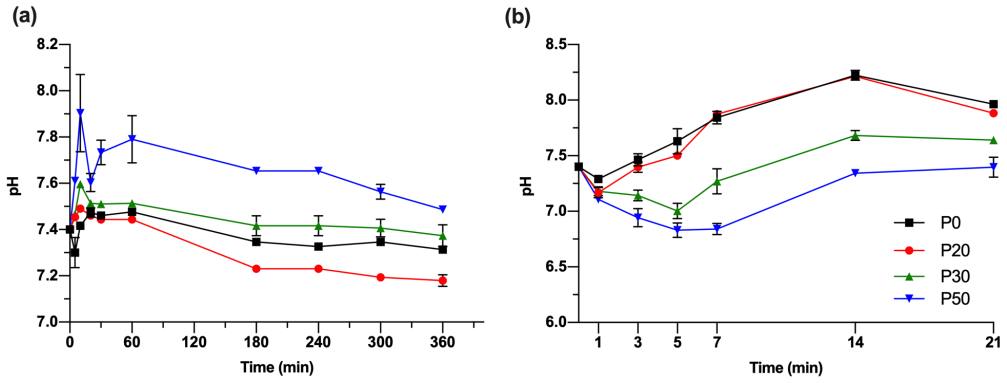

Figure 4.7 pH change of the PBS solution that IBS samples incubated at 37 °C. (a) pH changes of IBS samples until 360 min and (b) pH changes of IBS samples until 21st day (results expressed as mean ± standard error, n = 3).

IBS samples had pH values between 7.89 and 7.39 at the end of day 21. The pH of P50 samples was found to be higher than the other IBS samples at the beginning of incubation. P50 samples had the highest pH value until 60 min after which pH was gradually decreased. For P0, P20 and P30 IBS samples, the pH value reached a plateau 3 h later until the end of the first day incubation. After day 1, pH values of P0, P20, and P30 started to increase slightly.

Figure 4.8 shows % remaining weights of all IBS samples. The in vitro degradation of IBS samples was examined by the measurement of remaining weight % in PBS at 37 °C after the setting of the cement phase. After one week, P0 samples lost 60 % of their weight while the IBS samples mostly preserved their weights. When the wt % of bioceramic powder component increased, the weight loss decreased.

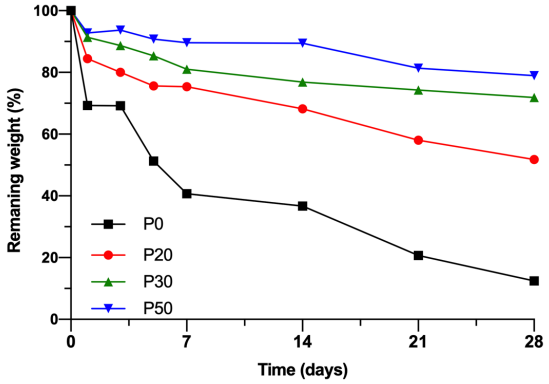

Figure 4.8 Remaining weights of IBS samples in PBS at 37 °C (results expressed as mean ± standard error, n = 3).

4.3.5 XRD Analysis

After the cement phase of the IBS samples was allowed to set, XRD analysis was conducted. Figure 4.9 shows the XRD patterns of the IBS samples. As a result of these analyses, the peaks of powder components, TTCP, HA, DCPD, and CSD were observed from the XRD spectrum of P20, P30, and P50. The peak intensity of each IBS sample was increased as the wt % of the bioceramic powder increased. As Thai and Lee [133] concluded, initial XRD data in Figure 4.9 did not reveal the setting mechanism of P20, P30, and P50 samples. Therefore, the XRD analysis was also performed after PBS

studies to interpret the setting mechanism and mechanical behavior after incubation for 14 days. Figure 4.9 (b) shows the XRD analysis after the incubation of IBS samples in PBS at 37 °C. The XRD results of the incubated IBS samples showed HA peaks which indicated the formation of an apatite layer on the samples. CSD peaks were also observed for P50.

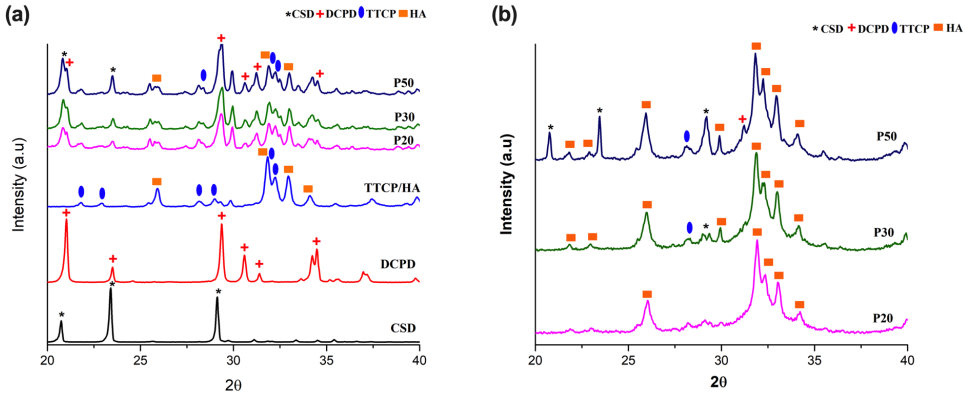

Figure 4.9 XRD analysis results of P20, P30 and P50 samples after (a) setting and (b) incubation in PBS at 37 °C for 14 day

4.3.6 Compressive Strength Measurement

Figure 4.10 shows the compressive strength results of IBS samples in 100 % humidity at 37 °C for 14 days.According to the results, P0 and P20 had almost the same compressive strength values. Until day 7, the compressive strength of P30 samples had a similar trend with P0 and P20. However, P30 had a significant increase in compressive strength on day 7. P50 samples had a much earlier rise in compressive strength than P30 samples; however, both P30 and P50 reached a plateau on day 7. On day 14, P50 samples had approximately 7 times higher compressive strength when compared to P0, P20, and P30 samples.

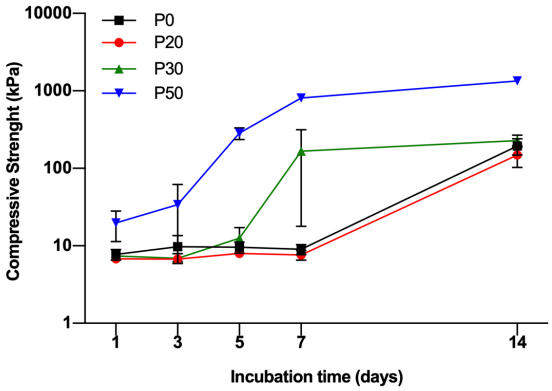

Figure 4.10 Log compressive strength of IBS samples vs. incubation time in 100 % humidity at 37 °C mean ± standard error, n = 3).

4.4 Discussion

This part of the thesis evaluates the effect of incorporation of different wt % of CaP/CSD-based bioceramic powder into an MC-based solution by investigating the physicochemical and in vitro properties. First of all, the chewing gum-like consistency of IBS samples was achieved as a result of the presence of the liquid phase [11] as shown in Figure 4.1. Higher wt % of bioceramic components were also introduced into the polymeric component; however, these samples could not be extruded through 18-gauge needle. Therefore, the maximum wt % of bioceramic component was set at 50 % as mentioned in Section 3.2.3. As the wt % of bioceramic powder component increased, injectability was slightly decreased. Alves et al. [147] indicated that the injectability was proportional with the rheology of the paste. Therefore, a higher viscosity led to more difficulty of injection of the pastes. Morphological features of IBS samples (P20, P30 and P50) revealed that the denser configuration detected by increasing the wt % of the powder component. Moreover, the bioceramic powder component was found to be homogenously distributed in the polymeric component [135, 151].

The rheological properties of the IBS samples were evaluated by the oscillatory rheometer as a temperature and time sweep after computing the amplitude and the frequency dependent variation of G′ and G″ to determine the strain % and angular frequency (rad/s) value. The amplitude sweep test showed to preserve the structural

integrity of IBS samples, 0.1 % strain was applied for frequency, temperature, and time sweep measurements. IBS samples had higher G′ than G″ at amplitude and frequency sweep, confirming the gelation and stabilization of their structure after setting at 37 °C [147, 149]. The cross-over point of G′ and G″ at temperature sweep measurement implies the incipient phase transition temperature of the samples [147]. The gelation transition temperature of the IBS samples moved to a higher value with the addition of 30 and 50 wt % of bioceramic powder mixture. The shifting of gelation temperature might be because of the change of the intra- and inter-molecular interactions of MC chains [152]. The strong hydrogen bond between MC chains and CPC causes a change in the temperature sensitivity of the MC chains [153]. Similarly, the exponential increase of the G″ with time at 37 °C and then reaching the plateau point indicates the building-up of cement network [62]. The duration of curing decreases effectively with the increase of wt % of the bioceramic powder component [154, 155, 46, 156]. For the produced IBS samples, the setting takes place in two stages. In the first stage, hardening occurs by a chelate reaction between MC and citric acid. The cross-over point of G′ and G″ refers this incipient hardening/setting reaction. In the second stage of cement setting, the hardening occurs via the transformation of the bioceramic component to HA [131]. The exponential increase of G″ with time refers to this second stage. The shear-rate dependent variation of viscosity revealed that all of the samples had shear thinning properties; hence, they had a high degree of injectability. When the wt % of bioceramic powder component increased, viscosity also increased. This is due to the increase of resistance to flow as the amount of the cement particles per unit volume increases [153].

The pH response of the samples was measured for 21 days to monitor the pH changes after setting of IBS samples during the dissolution and re-precipitation. The increase of pH after the 1st day of incubation was possibly due to the rapid dissolution and transformation of TTCP into HA as indicated by Yokoyama et al. [150]. For P30 and P50 samples, the reduction of pH value until day 5 results in PO_4^{3-} consumption which leads to formation of an apatite-like phase [153]. Overall, IBS samples had pH values between 7.89 and 7.39 at the end of day 21. Hence, it can be concluded that the prepared IBS samples may not cause any inflammatory reaction under biological

conditions due to acidity. The in vitro degradation of IBS samples showed that the P0 samples lost most of their weight due to the erosion of MC as Gupta et al. [156] and Tate et al. [157] reported. In vitro degradation studies were conducted without utilizing any enzymes. Therefore, a faster degradation rate of the IBS system is expected under dynamic or in vivo conditions [158, 159, 160]. Therefore, the degradation rate of the IBS system may be further decreased with use of additives. The deposition of an apatite layer on bone substitutes in the biological environment is an essential phenomenon as it indicates the osseointegration ability of implants [159]. So that, samples were also evaluated for their bioactivity by analyzing their phase composition. IBS samples showed HA peaks which indicated the formation of an apatite layer on the samples. CSD peaks were also observed for P50 which is possibly due to a higher wt % of CSD present in P50 samples. The compressive strength measurement revealed that their strength increased with the incubation period. The compressive strength of the IBS samples also strongly related to their setting mechanism. This increase was correlated with XRD results which indicated the phase transformation of TTCP into HA [150][. P50 samples had a much earlier rise in compressive strength than P30 samples; however, both P30 and P50 reached a plateau on day 7 indicating the completion of their phase transformation into HA. The compressive strength of cancellous bone varies between 0.22 to 10.44 MPa [161, 162, 163, 164]. Compared to human cancellous bone, the compressive strength of IBS was found to be lower. One way to improve the mechanical properties of IBS is to increase the wt % of the bioceramic component. In this study, wt % of the bioceramic component could not be increased further due to the inability to inject IBS with higher wt % of the bioceramic component. The mechanical properties of IBS may be improved with the addition of carbon-based nanomaterials as a reinforcing agent, such as GO [95, 164, 165].

This study showed that the incorporation of the bioceramic powder into MC-based polymeric matrices may improve the rheological, mechanical and degradation properties of IBS. Evaluating the same IBS by using reinforcing agent to improve rheological, mechanical and in vitro properties of IBS is important step to determine promising candidates for the treatment of bone defects for non-load bearing applications.

5. EFFECT OF GRAPHENE OXIDE REINFORCED INJECTABLE BONE SUBSTITUTES ON THEIR PHYSICAL AND IN VITRO PROPERTIES

To improve the mechanical properties of IBS samples, GO was incorporated to the polymeric phase. Primarily, the effect of GO addition on gelation time were examined by using test tube inversion technique at 37 °C. Figure 5.1 shows the sol and gel state of prepared sample with 1 wt% GO. The sol form of GO-MC solution got gelled in 5 minutes.

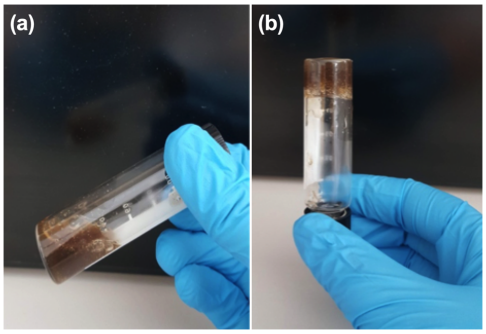

Figure 5.1 The gelation of MC-GO solution; photographs of (a) sol at 25°C and (b) gel at 37 °C state. (8.0 (w/v) % MC solution containing its 1 wt% GO, 2.5 (w/v) % gelatin and 3.0 (w/v) % SC solution).

Based on the results of the previous chapters, we decided to use commercially available TTCP powder due to low phase purity of synthesized TTCP powder. Phase pure TTCP could not be quenched from 1500 °C to room temperature. By eliminating this step, our synthesized TTCP ended up including different phases, as mentioned in Section 3.2.1. Therefore, TTCP powder used in this Chapter was purchased from Hitemco Medical (Old Bethpage, Newyork, USA). The data sheet of purchased TTCP was presented at Appendix B. This part of the thesis exhibits the effect of uniformly dispersed GO on mechanical and structural properties of synthesized injectable bone substitutes (IBS). Four different amounts of GO, 0.5 %, 1 %, 1.5 % and 2 % in mass of methylcellulose, were used. The effect of GO incorporation on the setting time

and injectability was initially investigated. The qualitative crystal and microstructural analysis were performed. Thereafter, in vitro properties of GO reinforced IBS samples were evaluated.

5.1 Preparation of GO Reinforced IBS Samples

GO reinforced IBS samples were prepared by mixing GO added liquid phase and the powder phase. 6g of MC powder was dissolved in 50 ml of 2.5 (w/v)% Na_2HPO_4 solution at 90 °C until MC′s complete dissolution. The prepared solution was placed at 4 °C overnight to obtain a clear MC solution [132]. 1.875 g of gelatin was dissolved in 6.25 ml of 2.5 % w/v Na_2HPO_4 solution at 50 °C and was allowed to cool down before use [133]. SC solution was prepared by dissolving 2.25 g of SC salts in 12.5 ml of 2.5 (w/v)% Na_2HPO_4 solution at room temperature. Different weight fractions of GO powders were dispersed in 6.25 ml of 2.5 (w/v)% Na_2HPO_4 solution by using homogenizer for 1h [166]. After this, different wt % of the GO solution was added to the polymeric component. Powder component of IBS samples compose of analytical grade TTCP, DCPD, and CSD. Bioceramic component was prepared by blending equimolar mixture of DCPD and TTCP powder and then this mixture was added to the CSD with a 4 to 1 mass ratio [131]. Table 1 shows the compositions of prepared GO reinforced IBS samples.

Table 5.1
Composition of the GO reinforced IBS samples.

Abbreviation	GO	MC	Gelatin	SC	Powder component
	wt%	w/v %	w/v %	w/v %	wt %
0GO	0	8	2.5	3	50
0.5GO	0.5	8	2.5	3	50
1GO	1	8	2.5	3	50
1.5GO	1.5	8	2.4	3	50
2GO	2	8	2.4	3	50

5.2 Characterization of GO Reinforced IBS Samples

5.2.1 Setting Time and Injectability Measurements

Gilmore needles was used to assess the setting time of IBS samples according to ASTM C266-04 standard [102]. Briefly, samples were injected into the mold and placed at 37 °C and 100 % relative humidity. The needle with the dimension and mass of m=113.4 ± 0.5 g, d=2.12 ± 0.05 mm was used to assess the initial setting time and the needle with the dimension and mass of m=453.6 ± 0.5 g, d=1.06 ± 0.05 mm was used to assess the final setting time. The passing time was noted until each needle could not create a deep indentation in three separate areas on the GO reinforced IBS samples. Injectability was qualitatively measured by extruding the IBS samples through a syringe with 18G needle. Each syringe and needle were filled with approximately 2g of IBS samples. Then the filled samples were extruded from the syringe manually by applying a relatively constant speed [146, 147]. Then the injectability was investigated by using an Eq. 4.1 given in Chapter 4.

5.2.2 Phase Composition and Morphology

GO reinforced IBS were molded into columns of 10.0 mm of diameter and 5.0 mm of length and incubated at 37 °C with a 100 % relative humidity for overnight. Then, samples were removed from the molds and lyophilized. The surface of the samples was coated with gold and examined with SEM (Philips-FEI XL30). Phase analysis of the samples was performed by using the XRD (Rigaku D/MAX-Ultima+/PC) operated at 30 kV and 30 mA at a scanning speed of 1 °/min. FTIR measurements were performed to detect the functional groups and to determine the interaction of GO and other phases (Nicolet FTIR Instruments, Thermofischer). Phase composition and morphology analysis were carried out at Boğaziçi University, Istanbul Turkey.

5.2.3 Mechanical Analysis

Rheological measurements of GO-reinforced IBS samples were performed by using a stress-controlled rheometer with a parallel plate geometry (15 mm) (Anton Paar, MCR302) at Boğaziçi University, Istanbul Turkey. The viscoelastic properties of the samples were obtained at 1 % strain and between 0.1 and 10 Hz frequency within the linear viscoelastic region [167]. Measurements were carried out at 25 and 37 °C.

GO reinforced IBS samples were molded into columns of 10.0 mm of diameter and 5.0 mm of lengths to measure the elastic modulus using compression mode of Dynamic Mechanical Analysis (DMA, TA, DMAQ800) using static force ranging from 2N to 18N, at Istanbul Technical University, Istanbul, Turkey. Measurements were taken on day 1, 7, 14 and 21 in an atmosphere of 97 % humidity at 37 °C (n=3) [98].

5.2.4 In vitro Degradation and Swelling Studies

For the in vitro degradation and swelling studies, preset samples were incubated in 5 ml of PBS at 37 °C, and the measurements were done at predetermined time intervals [146]. The weight was measured both before and after soaking for degradation studies using Eq. 4.2 given in Chapter 4. The swelling studies were carried out for 1 and 24 h after their incubation in PBS at 37 °C. The swelling ratio was evaluated using the Eq. 5.1 where W_0 is the initial weight of the sample, and W_t is the wet weight of the sample after t hour of the immersion.

$$\text{Swelling ratio} = \frac{W_t - W_0}{W_0} \times 100\% \tag{5.1}$$

5.2.5 In Vitro Biocompatibility

The hBMMSCs (ATCC) were used to examine the biocompatibility of the prepared IBS samples. Cells were cultured using low Dulbecco′s Modified Eagle′s Medium-low glucose (DMEM-low glucose; Sigma) supplemented with 10 % fetal bovine serum (Biowest) and 1 % gentamicin sulfate (50 mg/ml) solution (Biowest).

For the indirect cytocompatibility test, 0GO, 0.5GO, 1GO and 2GO IBS samples were soaked in 1.6 ml of DMEM-low glucose supplemented with 10 % fetal bovine serum (FBS; Biowest), 1 % gentamicin sulfate (50mg/ml) solution (Biowest). The medium was collected after 1^{st}, 3^{rd} and 7^{th} days of incubation. The extract medium from samples was not filtered prior to use (directly used). The 3-(4, 5 dimethylthiazol-2yl)-2, 5 diphenyltetrazolium bromide (MTT, Sigma) assay was utilized to evaluate the cytotoxicity according to ISO 10993-5 standard. When the cells reached confluency, they were seeded in 96-well culture plates with complete medium, at a density of 10^4 cells/well. Then, cells were incubated overnight. After cells attached to the bottom of 96-well plate, extracted medium was placed in the complete medium and incubated at 37 °C for 24 h (n=12). MTT was dissolved in PBS (0.5 mg/ml) and added to each and the plates as 100 microliter and then incubated at 37 °C for 4 h. After 4h, MTT solution was discarded and dimethylsulphoxide (DMSO, Sigma) was added to each well. Culture plate was gently shaken for 10 min, and the absorbance was measured with a microplate reader (Bio-rad, iMark^{TM}) using a test wavelength of 570 nm and a reference wavelength of 595 nm.

For direct biocompatibility, the GO reinforced IBS samples (n = 6) were placed in a 24-well plate and incubated at 37 °C with 5 % CO_2 and 95 % relative humidity for 1 day. Before the cell seeding, samples were sterilized by soaking in a 70 % ethanol solution for 1 h and then by exposing to ultraviolet (UV) light for 30 min for both sides of the prepared samples. When the cells reached confluency, hBMMSC suspensions at densities of 5000 cell/cm^2 were directly seeded over sterilized samples and incubated at 37 °C in a 5 % CO_2 atmosphere. After 1, 4, 7, and 14 days, cell viability was examined by using the AlamarBlue assay (Bio-rad, UK). Briefly, the present medium

was discarded, and then each sample group was incubated in medium containing 4 % alamarBlue reagent at 37 °C in a 5 % CO_2 atmosphere for 3h. After 3 h, the absorbance was measured at 570 and 595 nm with a microplate reader (Bio-rad, iMark^{TM}).

The morphology of cells cultured on IBS samples were also examined by SEM. After 7 days of cell culture, IBS samples were rinsed with PBS twice and then fixed with 2.5 % glutaraldehyde/PBS solution for 60 min at 4 °C. After fixation, samples were dehydrated by using graded ethanol followed by further dehydration in hexamethyldisilazane (HMDS). IBS samples were coated with platinum before examination.

5.2.6 Statistical Analysis

Based on the normality test results, two-way analysis of variance (ANOVA) was used to evaluate significant differences between the experimental groups. Then, Dunnett′s multiple comparison test was used. For non-parametric test, Kruskal-Wallis test and Dunn′s multiple comparisons test were performed. All results were assessed for statistically significance with a p value which is less than 0.05. GraphPad Prism 8 software was used for statistical analysis.

5.3 Results

5.3.1 Setting Time and Injectability Measurements

The setting time and injectability measurements of the samples are presented in Figure 5.2 (a). The initial and the final setting time was recorded when the specimen could bear the initial and final needles without appreciable indentation. Depending on the amount of GO, the setting time of the cement phase varied and decreased accordingly. There are statistically significant differences between the initial and final setting time of 2GO samples compared to 0GO. This analysis revealed that the prepared injectable bone fillers should be handled according to the initial and the final setting

time which are 19.93 and 76.33 min for 2GO samples, respectively.

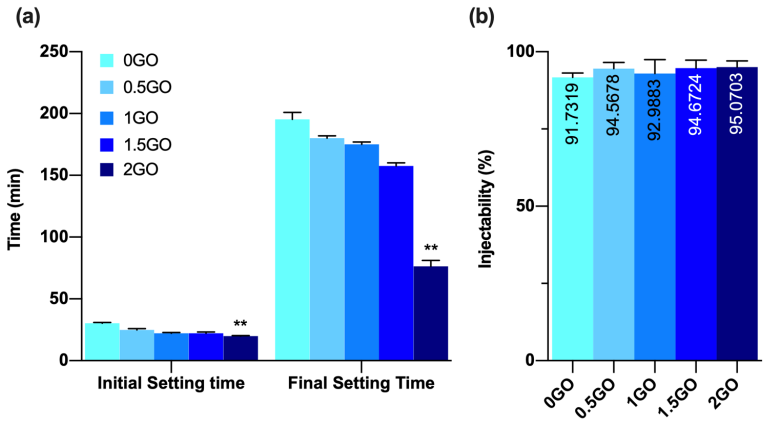

Figure 5.2 (a) Setting time and (b) injectability results (n=4). Values are mean ± standard deviationn. Asterisk means that there is statistically significant difference between the groups (** means $p < 0.01$) according to ANOVA and Dunnett's multiple comparison test

According to Figure 5.2 (b), all samples showed a high degree of injectability. There is no statistically significant difference between 0GO and GO added IBS samples. The incorporation of GO slightly increased the injectability. Visual observation of the injected samples showed that the addition of GO did not cause any segregation or phase separation during the injection. Overall, the setting time of GO-reinforced IBS samples was significantly shortened for 2GO and the fluidity of samples increased.

5.3.2 Structural Analysis

Figure 5.3 shows the XRD pattern of 0GO and 2GO samples after 24 h of setting. Samples possessed the same XRD pattern independent of incorporation of GO because of the small content of GO. Depending on the qualitative analysis, no new crystal structure was obtained after setting of the samples, only the added raw powders were detected which matched with JCPDS files no. 72-1240, 70-1379, and 74-1905, respectively.

Figure 5.4 shows the FTIR spectrum of GO, MC, polymer phase with 2 wt% GO,

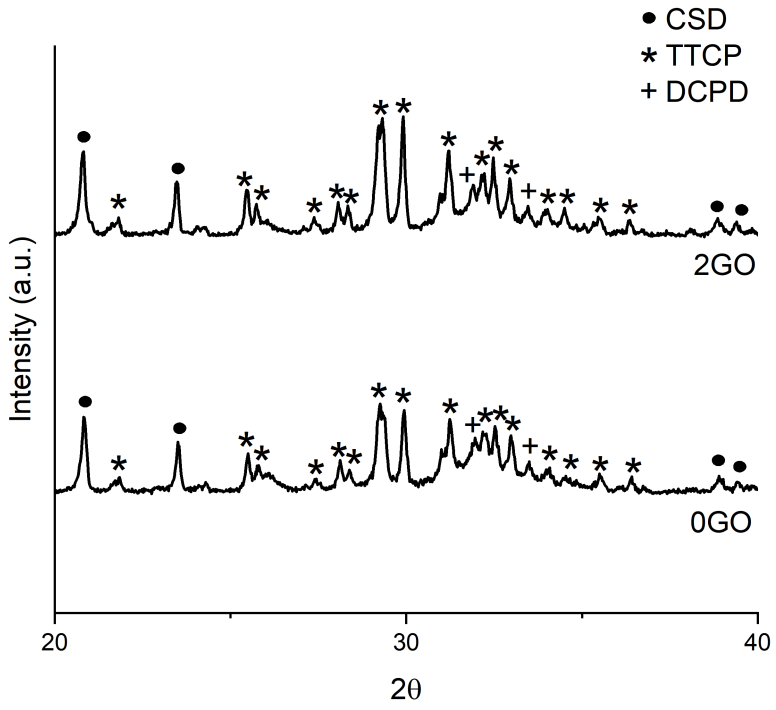

Figure 5.3 XRD pattern of 0GO and 2GO samples after setting.

0GO, and 2GO. According to the results, there were only small shifts since the materials in the samples had non-covalent interactions. In FTIR spectra of GO, there were carboxyl C=O stretching bands at 1729 and 1616 cm^{-1}, O-H deformation vibration at 1404 cm^{-1}, and also C-O stretching vibration at 1032 cm^{-1} [168, 169]. FTIR spectrum of MC had bands at around 1451, 1367 and 936 cm^{-1} due to C-H stretching of CH_2 and CH_3 group [170]. Also, the intense band around 1103-1030 cm^{-1} was related with the C-O-C stretching bond from glucosidic units [171]. In the spectrum of 0GO and 2GO samples, the broad band at around 1636 cm^{-1} was associated with H-O-H bending [172]. Another broad band at 1416 cm^{-1} was belonged to C-O-H plane bending [172]. In all spectra, the bands of PO_4^{3-} were detected at around 1086-1085, 1016-1014 and 960 cm^{-1}. While the band at 960 cm^{-1} was associated with the symmetric stretching mode ν_1 of PO_4^{3-} bands at 1019-1015 and 1086-1085 cm^{-1} were corresponding to the vibration mode ν_3 of PO_4^{3-}. Bands between 598 and 559 cm^{-1} were corresponding to bending modes of PO_4^{3-} [173]. There was a shift of the peak to lower wavenumbers at around 1014 cm^{-1} from 1016 cm^{-1} with the addition of GO.

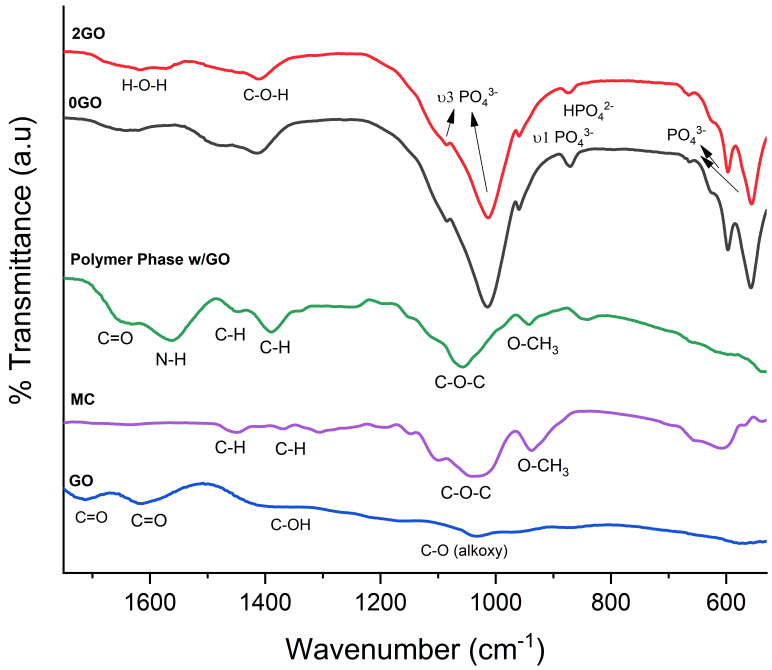

Figure 5.4 FTIR patterns of GO, MC, polymer phase with 2wt% GO, 0GO and 2GO.

Figures 5.5 (a) and 5.5 (b) show the cross-sectional morphology of lyophilized liquid phase of IBS samples. It was observed that these samples had a rough microporous structure. In Figure 5.5 (c) and 5.5 (d), 0GO samples had a flower-like morphology which disappeared with the incorporation of GO. With the addition of GO, the samples appeared less porous and denser when Figure 5.5 (d) and 5.5 (f) were compared. GO particles were indicated with a red arrow in the SEM images; however, most of the GO particles were possibly covered inside the powder phase and filled the pores between the powder/liquid matrix.

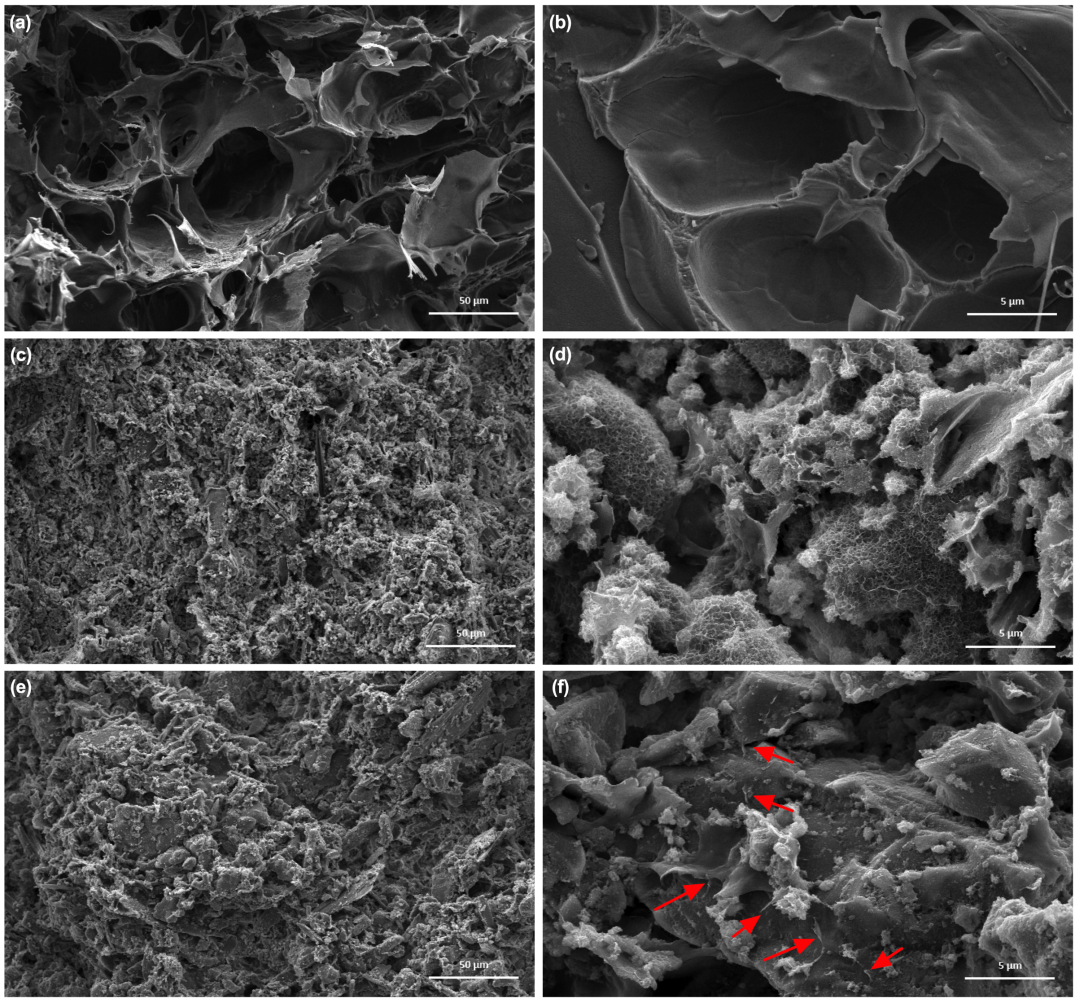

Figure 5.5 (a-f) Cross sectional SEM images of without GO and GO added lyophilized IBS samples.(a and b) Liquid phase of IBS samples without GO; (c and d) 0GO samples; (e and f) 2GO samples; (a, c, and e) with 1000× magnification; and (b, d, and f) 10.000× magnification.

5.3.3 Mechanical Analysis

Figures 5.6 (a) and 5.6 (b) shows the frequency-dependent G′ and G″ of GO-reinforced IBS samples at 25 and 37 °C using 1 % strain. All samples revealed linear viscoelastic properties both at 25 and 37 °C. Also, they preserved their linear viscoelastic properties between 0.1 and 10 Hz frequency. IBS samples without GO incorporation had the highest G′ value at 25 °C and the lowest G′ value at 37 °C. All samples revealed gel-like behavior with their G′ being rather constant and much higher than their G″ [174]. 1.5GO samples showed a higher G′ value than the other samples at 37 °C, while it had the lowest G′ value at 25 °C. G′ of 1.5GO was dramatically increased with the increase of temperature from 25 to 37 °C. However, 2GO samples had a similar G′

value with 0.5GO samples. Overall, the results demonstrated that the addition of GO up to 1.5 wt% improved G′ at 37 °C.

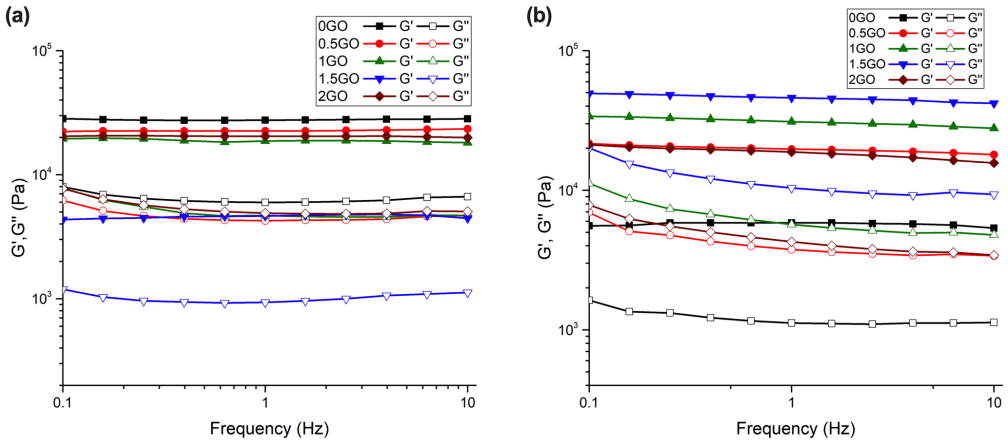

Figure 5.6 Frequency-dependent loss (G″) and storage (G′) modulus changes of all samples group by using 1 % strain at (a) 25 °C and (b) 37 °C.

Figure 5.7 shows the compressive modulus of GO reinforced samples which were calculated by using the slope of the stress-strain curves on the 1st day and after 14 days of incubation. After setting of the cement phase, incorporation of GO to the injectable bone filler samples increase the compressive modulus. On day 14, compressive modulus of 2GO reached its maximum value which was 6.89 ± 2.25 MPa. Overall, the elastic modulus increases with increasing GO content.

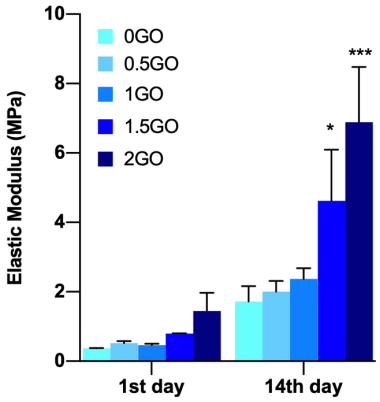

Figure 5.7 Elastic modulus of the GO reinforced IBS samples after 1 and 14 day of incubation.

5.3.4 In vitro Degradation and Swelling Measurements

Figure 5.8(a) shows in vitro degradation behavior of GO added IBS samples by the measurement of remaining weight (%) in PBS at 37 °C after setting of the cement phase. Until day 7, 0GO, 1.5GO, and 2GO samples lost ∼20 % of their weight, whereas 0.5GO and 1GO samples lost ∼30 % of their weight. 2GO and 1.5GO revealed nearly the same degradation pathway during the incubation period. 0GO samples also showed similar degradation profiles with 1.5GO and 2GO samples until day 14. After 28 days, 0GO samples lost 50 % of their weight. Overall, it could be concluded from these results that the GO incorporation reduced the % mass loss of the samples on day 28.

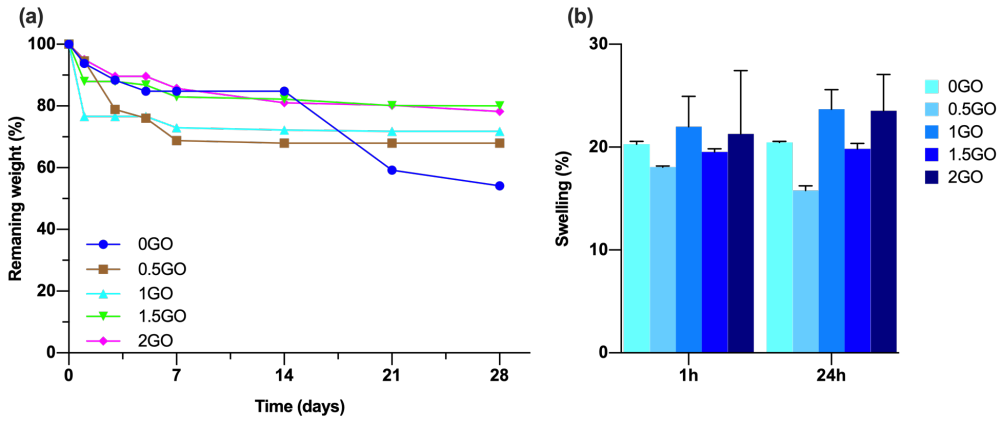

Figure 5.8 (a) In vitro degradation (n=4), (b) swelling (%) of the GO reinforced IBS samples in the PBS solution at 37 °C (n=4), Values are mean ± standard deviation

Figure 5.8 (b) shows % of swelling of the GO added IBS samples which were incubated in PBS for 1 and 24 h at 37 °C. Their dry weights and wet weights were recorded, and % of swelling was calculated. The results indicated that GO incorporation did not significantly affect the swelling of the samples.

5.3.5 In vitro Biocompatibility Results

Figure 5.9 (a) shows the MTT assay results of indirect cytotoxicity test by using extracted solution that the samples incubated for 1, 3 and 7 days. The viability increasing for 0.5, 1 and 1.5 wt% GO for 3^{rd} day extract may be explained by the dissolution and re-precipitation of the CPC phases. Cell viability was declined for the 7^{th} day extract. In literature, it is stated that GO shows dose-dependent toxicity to various types of cells. Therefore, hBMMSCs were seeded on IBS samples, and the cytotoxicity of prepared GO added IBS samples were tested by using the AlamarBlue viability assay. The results of cell proliferation during the incubation period are shown in Figure 5.9(b).

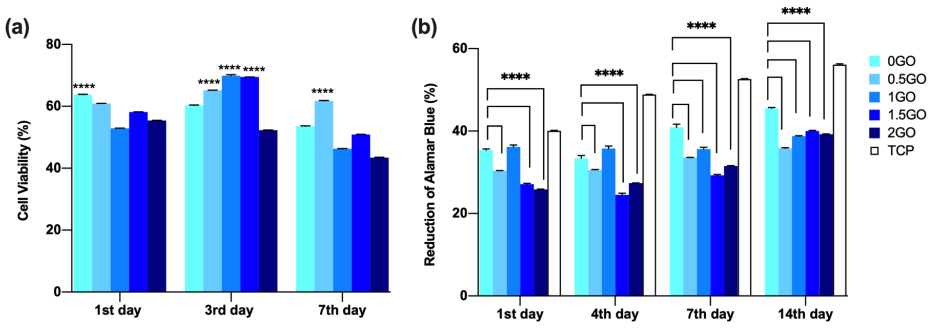

Figure 5.9 (a) Results of MTT indirect cytotoxicity test and (b) alamarBlueassay results performed with human mesenchymal stem cells. The graph includes the mean, standard error of the mean, ANOVA results with respect to mean, **** $p<0.0001$ means that there is statistically significant different between groups according to the two-way ANOVA and Dunnett′s multiple comparison test

On days 1 and 4, 0GO and 1GO samples showed significantly higher cell viability compared to the other study groups, except tissue culture plate (TCP). On days 7 and 14, the proliferation rate of 0GO was increased, and it became significantly higher than 1GO and the other GO added IBS samples. On day 7, the viability of 1GO was significantly higher than the other GO added IBS samples. When wt% of GO was increased above 1, the % cell viability did not significantly increase or decrease on day 14. There were no direct dose-dependent viability results of GO added IBS samples; however, there was an upward trend of cell viability with the time of incubation supporting that cells were growing on or in the samples. The % cell viability did not

significantly increase or decrease on day 14 when GO concentration was above 1 wt%.

Figure 5.10 shows the morphology of hBMMSCs cultured with GO incorporated IBS samples after cultured for 7 days. Although the porous morphology of IBS samples makes hard to detect the cells on the surface, extension of filopodia and overlapping cells were detected on all samples.

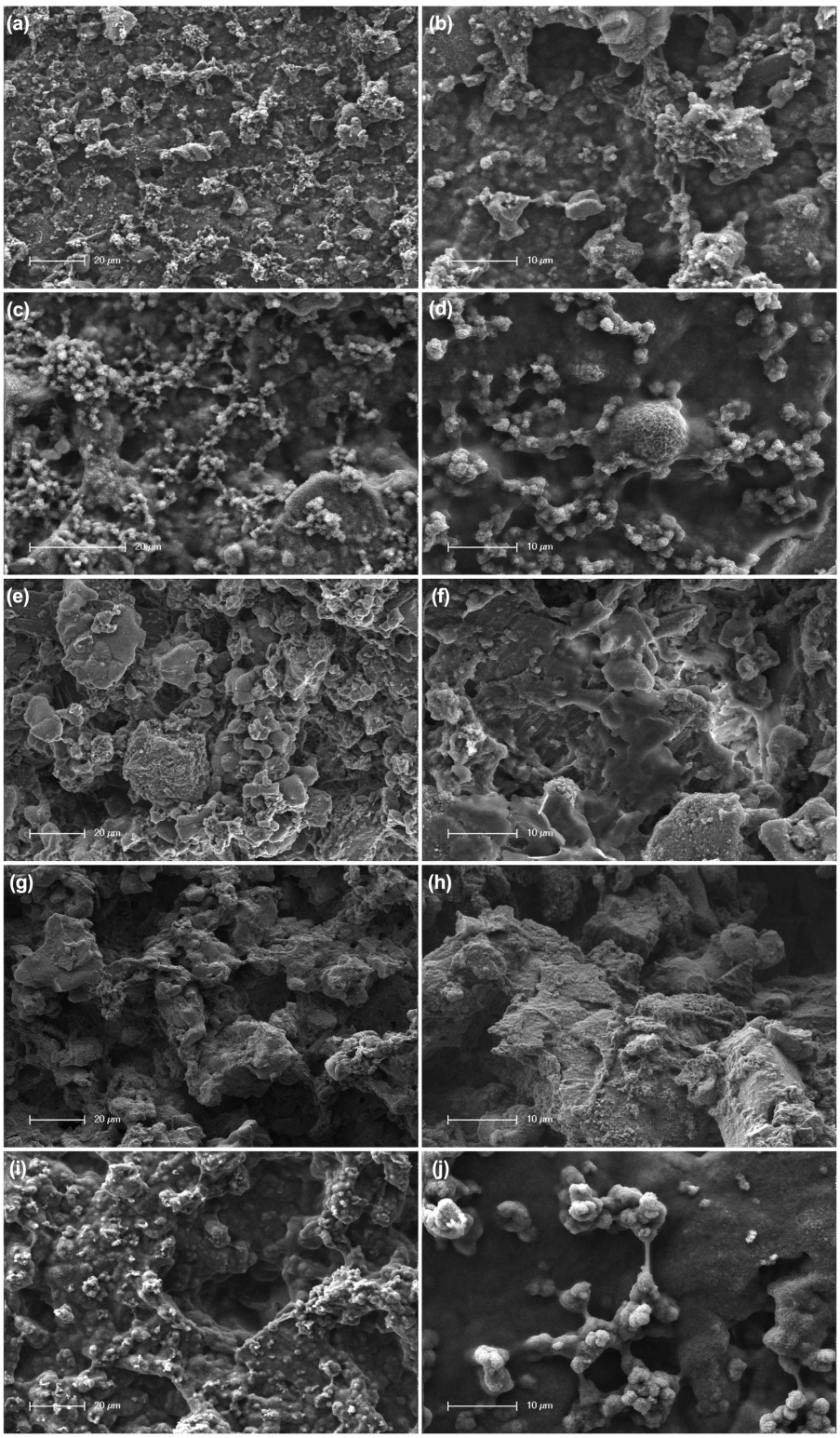

Figure 5.10 Morphology of hBMMSCs cultured with GO incorporated IBS samples after 7 days of incubation. (a-b) 0GO, (c-d) 0.5GO, (e-f) 1GO, (g-h) 1.5GO and (i-j) 2GO samples. (a, c, e, g and i with 2000× magnification and b, d, f, h and j with 5000× magnification).

5.4 Discussion

This chapter examines the enhancement effect of different mass fraction of GO in IBS samples. First of all, the handling properties of GO reinforced IBS samples were examined. Depending on the weight fraction of GO, the setting time of the cement phase varied and decreased accordingly. In literature, it is stated that the setting time is the critical factor during clinical application, and the initial setting time may be approximately 20 min for IBS [102, 161, 175]. For the 2 wt% GO incorporated samples, the clinically critical timing was achieved. All samples showed a high degree of injectability without causing any segregation or phase separation during the injection. The addition of GO did not change the crystal structure of IBS samples as presented at Figure 5.3. FTIR spectrum of the GO/polymeric phase had very similar peaks with MC′s FTIR spectrum. This is due to higher wt% of MC being present in the polymer phase in comparison with gelatin. Despite that, there were additional peaks at 1649 and 1566 cm^{-1} due to C=O and N-H bonds, respectively [176]. In the 0GO and 2GO spectra, none of the peaks of the polymeric phase was present. This is due to much more dominant signals of the powder phase and its higher weight fraction. Since a small amount of GO was added when compared to the powder phase weight percentages, the same peaks were observed after GO incorporation into the calcium phosphate cement-based composites [172, 173, 177]. There was a shift of the peak to lower wavenumbers at around 1014 cm^{-1} from 1016 cm^{-1} with the addition of GO. These could result because of the non-covalent interactions among GO and the powder phase [178]. Morphology of lyophilized IBS samples showed that the flower-like morphology of 0GO disappeared with the incorporation of GO. As Liu et al. [179] indicated, incorporated GO was cross-linked by the hydration product; therefore, it was hard to detect GO particles/flakes in the samples. After 1^{st} day of incubation, compressive modulus of GO reinforced IBS samples showed similar mechanical features with 0GO samples; however, the compressive modulus of 1.5GO and 2GO samples significantly increased after 14^{th} day of incubation at 37 °C. These mechanical test results indicated that the prepared nanocomposites may be used for substituting cancellous bone defects [162, 180]. In vitro degradation and swelling of GO reinforced IBS samples demonstrated that the GO incorporation reduced the overall % mass loss of the samples while the swelling

did not significantly change.

Calcium phosphate-based scaffolds could show high ionic reactivity by changing the ionic composition of their surrounding microenvironment, therefore extracts of synthesized IBS samples prepared according to ISO10993-5:2009 standard to test the cytotoxic effect. The viability increasing for 0.5, 1 and 1.5 wt% GO for 3rd day extract may be explained by the dissolution and re-precipitation of the CPC phases. The indirect cytotoxicity test showed that the extracted solution of the GO reinforced IBS samples did not cause any toxic effect for hBMMSCs. Therefore, the fabricated samples were non-cytotoxic upon testing in vitro. The presence of GO in the IBS samples, affect the interaction of mesenchymal stem cells with the sample surfaces. The negative charge and polarity of GO lead to its interaction with the functional groups of cellular proteins which changes the degree of biocompatibility of the samples [181]. Moreover, the addition of GO might have changed the dissolution and the re-precipitation rate of calcium phosphate phase. This might have also led to a change of the % viability of cells after GO incorporation [104]. The % cell viability did not significantly increase or decrease on day 14 when GO concentration was above 1 wt%. Therefore, probably further increase in GO concentration did not have a significant impact on the mechanism of interaction between the cells and the sample surface.

Findings of this part of the thesis confirmed that GO addition significantly reduced the setting time of the cements, improved in vitro degradation and rheological properties at 37 °C. Although the compressive modulus of different study groups did not have major difference, the found values were within the range of trabecular bone. Interestingly, 1GO and 1.5GO showed higher stability, workability, rheological properties, and biocompatibility than the other GO added IBS samples. Therefore, the optimum amount of GO that our powder and liquid phase can accommodate was found to be between 1 and 1.5 wt%. Further improvement may be achieved by the surface modification of GO to improve mechanical properties. Still, more research is needed to apply such an injectable material for bone regeneration by investigating them with other cell lines and in vivo animal tests in the future.

6. EFFECT OF ZOLEDRONIC ACID INCORPORATION ON THE PHYSICAL AND IN VITRO PROPERTIES OF INJECTABLE BONE SUBSTITUTES

In this part of the thesis, the anti-osteoporotic drug ZOL was loaded to induce anti-osteoporosis and anti-cancer properties of IBS samples. According to the mechanical and in vitro results of GO reinforced IBS samples, 1.5GO incorporated IBS samples were loaded with zoledronic acid and 0GO samples were used as a blank, control group. Two different ZOL concentrations (low as 0.5 mM and high as 5 mM) were used for investigating its effect on physicochemical and in vitro properties of IBS samples.

6.1 Preparation of ZOL loaded IBS Samples

The IBS samples comprised of a powder and a liquid phase which was prepared as described previously in Section 5.1. [182, 183]. ZOL was incorporated into the liquid phase of the IBS by dissolving the desired amount of ZOL in 2.5 wt% Na_2HPO_4 solution. After that, ZOL added liquid phase was gently mixed on magnetic stirrer overnight to obtain a homogeneous solution. Two different ZOL concentrations were used as 0.5 mM or 5.0 mM.

GO incorporated IBS samples was processed by dispersing 1.5 wt% of GO (2mg/ml, dispersion in H_2O, Sigma, Germany) in mass of MC. By adding the desired amount of Na_2HPO_4 to a dispersed GO the final concentration of Na_2HPO_4 was adjusted to 2.5 (w/v)%. Then, GO solution was sonicated by using a homogenizer (Sonopuls, Bandelin) for 1 hour to form well-dispersed GO incorporated liquid phase. Thereafter, the powder and liquid phases with a 1:1 ratio (wt:wt) were blended and stirred manually with a spatula for about 45 seconds to obtain ZOL loaded IBS samples. The ZOL loaded IBS samples were placed into teflon molds for further analysis. The cylindrical dimension of molds was 14 mm×7 mm (diameter and height) for in

vitro analysis and 10 mm×20 mm (diameter and height) for mechanical analysis. The experimental groups are presented in Table 6.1.

Table 6.1
Composition of the ZOL loaded IBS samples.

Abbveriation	ZOL	GO	MC	Gelatin	SC	Powder component
	mM	wt%	w/v %	w/v %	w/v %	wt %
0GO	0	0	8	2.5	3	50
0GO-lowZOL	0.5	0	8	2.5	3	50
0GO-highZOL	5	0	8	2.5	3	50
1.5GO	0	1.5	8	2.5	3	50
1.5GO-lowZOL	0.5	1.5	8	2.5	3	50
1.5GO-highZOL	5	1.5	8	2.5	3	50

6.2 Characterization of the ZOL loaded IBS Samples

6.2.1 FTIR Analysis

After 0GO, 0GO-highZOL and 1.5GO-highZOL IBS samples were allowed to set and freeze-dried, they were examined to detect the functional groups and to determine the interaction of ZOL and other phases. The FTIR spectrum was recorded from 4000 to 400 cm^{-1} with 32 scans by using Nicolet FTIR Instruments, Thermofischer at Boğaziçi University, İstanbul, Turkey.

6.2.2 Setting Time and Injectability Measurements

Injectability was qualitatively calculated by extruding the ZOL loaded IBS samples through a disposable syringe using 18G needle. Each syringe and needle were filled with approximately 2g of IBS samples. Then the filled samples were extruded from the syringe manually by applying a relatively constant speed [146, 147, 184]. Then the injectability was investigated by using an Eq. 4.1 given in Chapter 4.

According to ASTM C266-04 standard, setting time of the ZOL loaded IBS samples were measured by using Gilmore apparatus [102]. Briefly, samples were injected into the mold and placed at 37 °C and 100 % relative humidity. The needle with the dimension and mass of m=113.4 ± 0.5 g, d=2.12 ± 0.05 mm was used to assess the initial setting time and the needle with the dimension and mass of m=453.6 ± 0.5 g, d=1.06 ± 0.05 mm was used to assess the final setting time. The passing time was noted until each needle could not create a deep indentation in three separate areas on the ZOL loaded samples.

6.2.3 Mechanical Analysis

For the mechanical analysis, ZOL loaded IBS samples were molded with dimension of 10 mm diameter and 20 mm height. Then, the samples were incubated at 37 °C, 100 % relative humidity overnight. After samples were allowed to set, they were dried at 70 °C and then the compressive modulus were measured at a loading rate of 1mm/min by using universal testing machine (Lloyd Instruments, LF Plus, Ametek Inc.) [172].

6.2.4 Bioactivity Measurement

IBS samples were molded and after setting they were immersed in simulated body fluid (SBF) at 37 °C with 95 % relative humidity for 28 days. SBF solution was prepared with pH 7.4 at 37 °C by using the protocol given in Maçon et al. [185] All the chemicals used to prepare SBF solution were supplied from Sigma, Germany. After 28 days of incubation, the samples were washed with distilled water and then freeze-dried for SEM analysis (Philips-FEI XL30) at Boğaziçi University, İstanbul, Turkey. They were coated with platinum before the analysis.

6.2.5 In Vitro ZOL Release, Degradation, PO_4^{3-} Ions Release and pH Variation Measurements

ZOL loaded IBS samples were molded with a dimension of 0.5mm height and 10mm diameter for in vitro ZOL release, weight loss, pH and PO_4^{3-} ions release measurements. After setting, samples were incubated in 5 ml PBS (pH=7.4) at 37 °C and the measurements were done at predetermined time intervals. At these time points, the solution was taken out for analysis and PBS solution was replaced with a fresh one [189]. For the ZOL release analysis, UV-spectrophotometer (ThermoFisher^{TM} NanoDrop 2000) was used at 210 nm wavelength. Several ZOL solution ranging from 0.002 to 0.5 mg/ml concentration were prepared and their absorbances were used as a standard. For the weight loss measurement, % weight loss was calculated by using the Eq. 6.1 where W0 and Wt are the dry weights of the samples after 0 and t days of the incubation.

$$\text{Weight loss} = \frac{W_0 - W_t}{W_0} \times 100\% \tag{6.1}$$

At the predetermined times, weight of the IBS samples was measured. To examine the PO_4^{3-} release and pH variation of ZOL loaded IBS samples, same PBS solution was collected. The concentrations of PO_4^{3-} ions in the PBS were determined by using spectrophotometer (Hach DR/2010). Again, a standard solution was prepared to measure PO_4^{3-} ions in PBS solution. pH of the PBS solution was measured by using pH meter (Mettler Toledo, MP225). Three separate samples from each group were used for in vitro analysis.

6.2.6 In Vitro Cell Culture Studies

Two different cell lines which were human breast cancer cell line (MCF-7) and hFOB were used to examine the cellular response of prepared ZOL loaded IBS samples. The complete medium for MCF-7 cells was prepared as follows: high-DMEM (Sigma) supplemented with 10 % FBS (Biowest) and 1 % penicillin-streptomycin antibiotics (Biowest) . MCF-7 cells were seeded using this complete medium. After confluency, MCF-7 cells were seeded on the sterilized IBS samples with a density of 10000 cells/cm^2 in 24 well plates and then incubated in 5 % CO_2 at 37 °C with 95 % relative humidity. The complete medium for hFOBs was prepared as follows: DMEM F-12 (Sigma) supplemented with 10 % FBS (Biowest), 4 mM l-glutamine solution (Sigma) and 1 % penicillin-streptomycin antibiotics (Biowest). After confluency, hFOBs were seeded on the sterilized IBS samples with the density of 10000 cells/cm^2 in 24 well plates and then incubated in 5 % CO_2 at 37 °C with 95 % relative humidity. The medium was changed twice a week for both analysis.

6.2.6.1 Cell Viability Measurement. Alamarblue assay was used to determine the viability of the seeded cells on 1^{st}, 3^{rd}, 7^{th} days for both MCF-7 and hFOB cell lines. For this assay, the resazurin sodium salt (Sigma) reagent was used. A 440 μM resazurin sodium salts was prepared using DPBS. The solution was then filtered and sterilized before using with cells. At the predetermined time, fresh medium containing resazurin working solution (final dilution 1:10) was prepared and then added to cell culture plate. Before that, cells were washed with fresh medium. Then, cells with resazurin solution were incubated for 3h. At the end of the incubation, resazurin solution was collected and placed in 96 well-plate. The absorbance was measured at 570 nm and 595 nm with a microplate reader (Bio-rad, iMark^{TM}).

6.2.6.2 Alkaline Phosphatase Activity Measurement. Alkaline phosphates (ALP) assay kit (Biovision) was used to determine the ALP activity of hFOBs on IBS samples at day 7 and 14. At that days, hFOBs were washed twice in PBS and 0.2

% Triton X-100 were added [186]. Then, cells were frozen and thawed for 2 times to collect the lysates. Assay kit′s instructions were followed to determine ALP activity level. The color change was measured at 405 nm with a microplate reader (Bio-rad, iMark^{TM}). The standard curve was prepared according to the instruction in assay kit catalog and used to determine the ALP activity (U/L) level. ALP activity (U/L) was calculated using the equation given in assay kit catalog.

6.2.6.3 Mineralization Assay. Alizarin Red S (Sigma) staining technique was used to quantitatively determine the mineralization of hFOBs at day 14 and 21. At each time point, the cells were fixed with 4 % paraformaldehyde for 15 min at room temperature. Cells were washed 3 times with distilled water after fixative was removed. Subsequently, 40 mM alizarin red S dye was added to each well. Cell plates were incubated with gentle shaking at room temperature. 30 min later, the dye was removed and cells were washed again for 5 times with distilled water. For quantification of Alizarin dye, plates were stored at -20 °C prior to dye extraction. After thawing the cells, 800 μl 10 % acetic acid was added to each well and incubated for 30 min with gentle shaking at room temperature. Afterwards, cells were transferred to microcentrifuge tubes in 10 % acetic acid. After vortexed for 30 seconds, tubes were heated at 85 °C for 10 min and incubated on ice for 5 min. Then, tubes were centrifuged for 15 min at maximum g. After centrifugation, 500 μl supernatants were transferred to new microcentrifuge tubes. 200 μl 10 % ammonium hydroxide was added to over 500 μl supernatants to neutralize the acid [186]. For absorbance reading at 405nm with a microplate reader (Bio-rad, iMark^{TM}), each samples′ solution was transferred to 96-well plate. Alizarin Red S standard curve was prepared by dilution of 40 mM Alizarin red S solution. Standard curve was plotted as absorbance versus Alizarin red S concentration. The Alizarin red S concentration (mM) was calculated by using the standard curve′s equation.

6.2.7 Statistical Analysis

All data were processed with the software Graphpad Prism 8 and represented with their mean ± standard deviation. Differences between groups were evaluated by one-way or two-way analysis of variance and Dunnett′s multiple comparisons test based on the normality test results. For non-parametric test, Kruskal-Wallis test and Dunn′s multiple comparisons test were performed. Statistical analysis was also performed by using GraphPad Prism 8 program. Results were considered statistically significant with a P-value which is less than 0.05.

6.3 Results

6.3.1 FTIR Analysis of ZOL Loaded IBS Samples

Figure 6.1 shows the FTIR spectrum of ZOL, 0GOL, 0GO-highZOL and 1.5GO-highZOL samples. The characteristic peaks of ZOL were found at about 3440, 3149, 2819, 2620, 1580, 1550, 1450, 1399, 1300, 1090, 928, 891, 752, 703, 663 and 619 cm^{-1}. In detail, bands at around 3440 and 3149 cm^{-1} associated with -OH stretching. The band at around 2819 cm^{-1} was due to the presence of CH_2 stretching. The vibration of CH=CH group in imidazole ring was detected at around 1580 cm^{-1}. The bands at around 1550 and 1450 cm^{-1} represented the C-N stretching vibration [187]. C-H stretching vibration bands in imidazole ring was seen at around 1399, 663, 703 cm^{-1}. The bands at 928 and 891 cm^{-1} associated with the stretching vibrations of C-C bonds [187, 188]. The peaks at 1620 and 1409 cm^{-1} in 0GO spectra represented H-O-H and C-O-H plane bending, respectively. The characteristic bands of PO_4^{3-} were detected in between 1099 and 593 cm^{-1} for all the spectra. Specifically, the band at around 1099-1020 cm^{-1} were associated with the vibration mode ν_3 of PO_4^{3-}. Bands between 663 and 594 cm^{-1} represented the bending modes of PO_4^{3-} [173]. By the addition of GO, the peak at around 1099 cm^{-1} were disappeared and the peak at around 1020 cm^{-1} shifted to 1049 cm^{-1}.

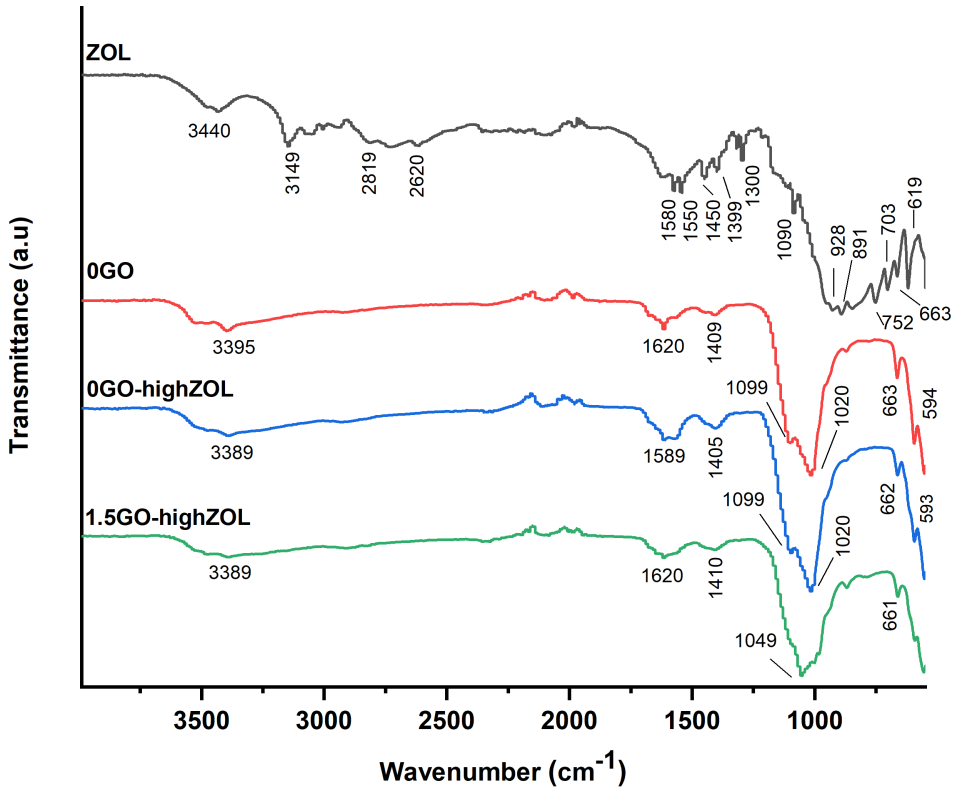

Figure 6.1 FTIR spectrum of ZOL, 0GO, 0GO-highZOL and 1.5GO-highZOL samples after setting at 37 °C.

6.3.2 Injectability and Setting Time Measurements

All samples showed similar and high degree of injectability as shown in Figure 6.2 (a). % injectability of 0GO and 0GO-highZOL were recorded as 92.98 % and 93.57 %, respectively. Similarly, % injectability of 1.5GO and 1.5GO-highZOL were recorded as 94.67 and 95.30 %, respectively. Figure 6.2 (b) shows the setting time of ZOL loaded IBS samples. The initial and final setting time were significantly prolonged by the incorporation of ZOL. For 0GO-highZOL and 1.5GO-highZOL samples, the final setting time were increased for approximately 80 and 90 min with regards to 0GO and 1.5GO, respectively. As also seen in Chapter 5, a significant decrease in setting time of the IBS samples was recorded by GO incorporation.

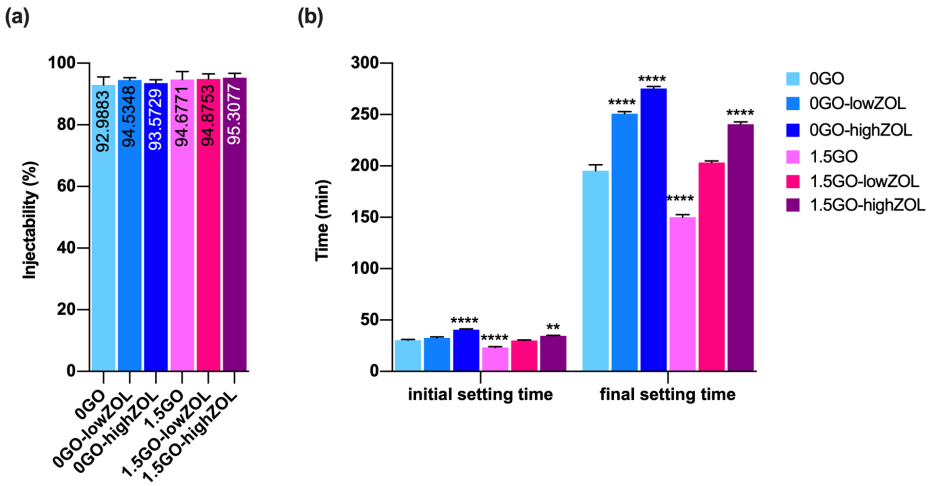

Figure 6.2 (a) Injectability and (b) setting time measurement results of ZOL loaded IBS samples (n=3).

6.3.3 Mechanical Analysis

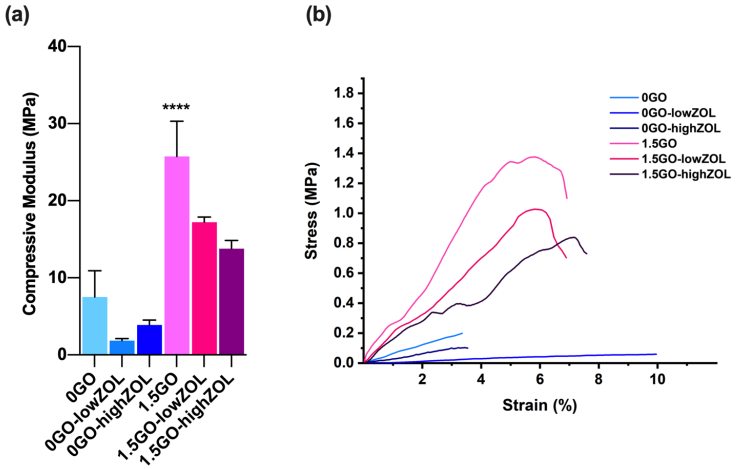

Figure 6.3 Mechanical properties of ZOL loaded IBS samples (a) compressive modulus, (b) stress-strain curves of ZOL loaded IBS samples (**** for $p<0.0001$, n=8).

Figure 6.3 shows the compressive modulus of ZOL loaded IBS samples and their stress-strain curves. Results revealed that there was no significant effect of ZOL loading on the compressive modulus of the 0GO samples. 1.5GO samples had significantly higher compressive modulus which was found as 25.73 MPa and ZOL loading to 1.5GO samples decreased the compressive modulus.

6.3.4 Bioactivity Analysis

Figure 6.4 shows the cross-sectional morphology of the ZOL loaded IBS samples after setting at 37 °C and incubating in SBF at 37 °C with 5 % CO_2 and 95 % humidity for 28 days. Apatite formation showed itself as a cauliflower-like morphology after setting of the cement phase and 28 days of incubation. A rod-like crystal structure was also observed in SEM micrographs which indicated presence of CSD crystals [189].

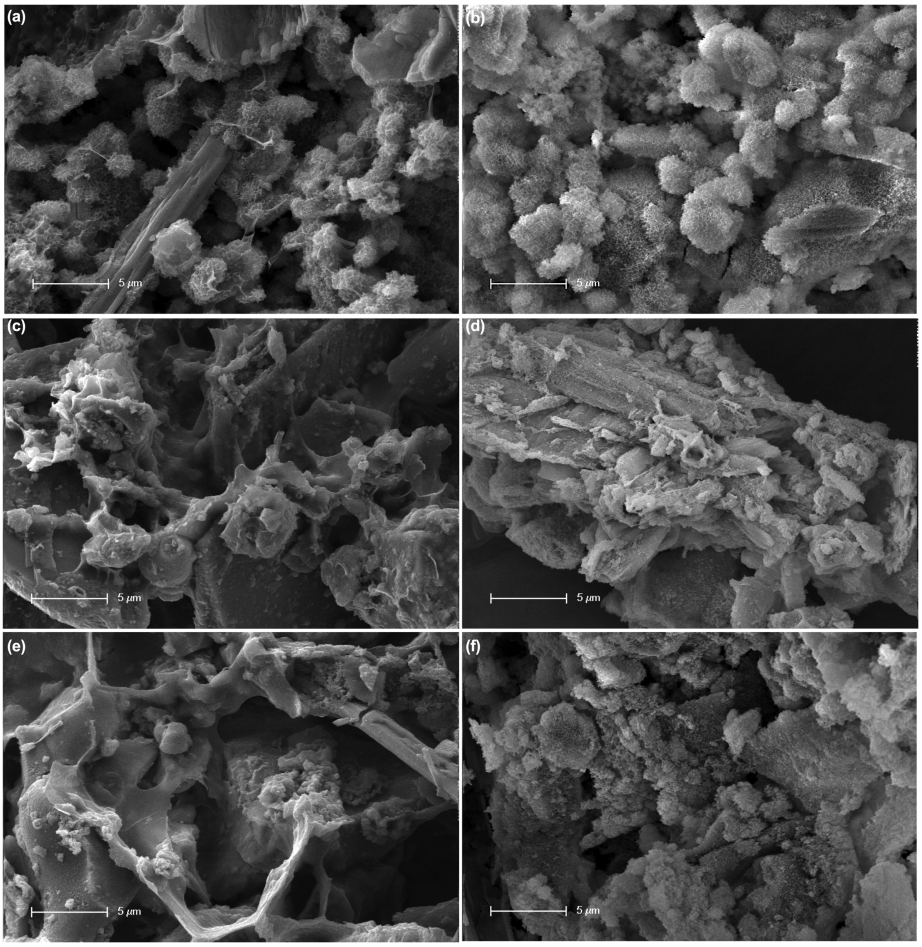

Figure 6.4 Scanning electron microscopy (SEM) images of ZOL loaded IBS samples before and after incubated in simulated body fluid (SBF) at 37 °C with 5 % CO_2 and 95 % (a) 0GO on day 0 (b)0GO on day 28 (c) 0GO-highZOL on day 0 (d) 0GO-highZOL on day 28 (e) 1.5GO-highZOL on day 0 (f) 1.5GO-highZOL on day 28.

6.3.5 In Vitro Drug Release, Degradation, PO_4^{3-} Ion Release, pH Variation Measurements

Cumulative ZOL release from IBS samples are shown in Figure 6.5 (a). The same release characteristics were detected for all ZOL loaded IBS samples. Accordingly, an initial fast release of ZOL was recorded from samples for 3 days. During the incubation period, ZOL was gradually released from the samples. At the end of day 28, 0GO-highZOL samples revealed the highest ZOL release among other groups.

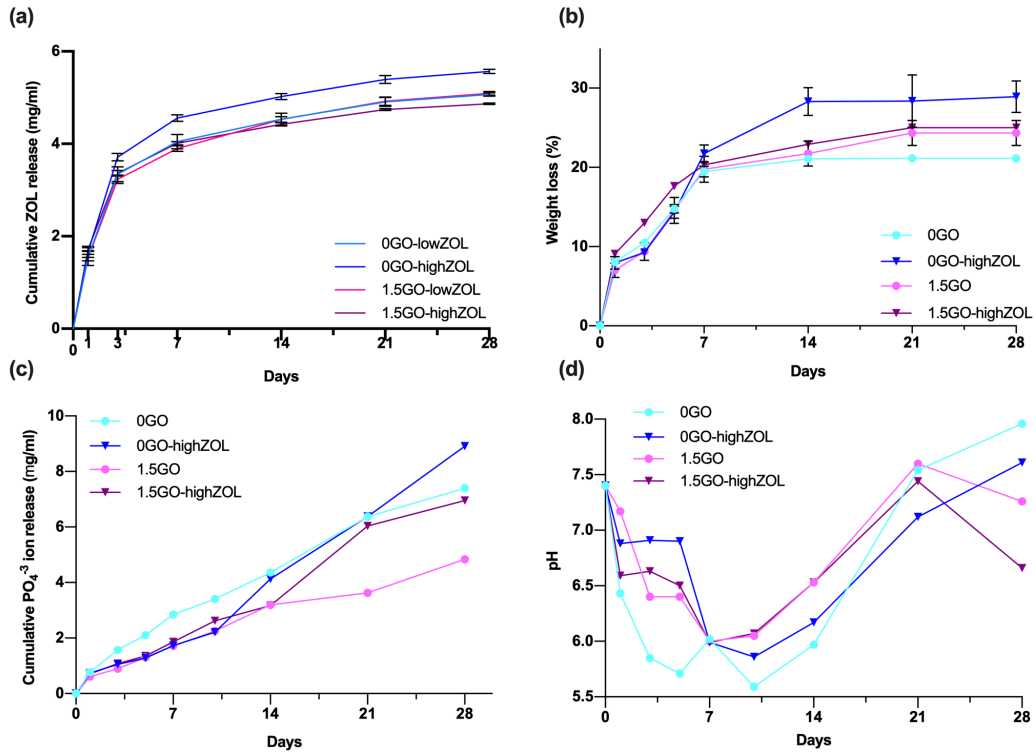

Figure 6.5 In vitro analysis results of ZOL loaded IBS samples incubated in PBS at 37 °C. (a) cumulative ZOL release (mg/ml), (b) weight loss %, (c) cumulative PO_4^{3-} ion release measurements and (d) pH variation (n=3). Error bars represent the standard deviation.

In vitro degradation behavior of 0GO, 0GO-highZOL, 1.5GO and 1.5GO-highZOL samples was measured as % weight loss in PBS at 37 °C after setting of the samples and shown in Figure 6.5 (b). The % weight loss trend of these IBS samples was almost similar to each other. All study groups lost approximately 20 % of their weight after one week. After day 7, ZOL loading into the 0GO IBS sample caused 10 % increase of the weight loss of these sample. Conversely, GO incorporation stabilized degradation

of samples. To sum up, % weight loss profile of the samples showed that the addition of ZOL increased the degradation of the samples while GO incorporation stabilized the weight loss to some extent. According to the Figure 6.5 (c), all IBS samples had a gradual release of PO_4^{3-} ions over 28 days of incubation. The results suggested that 1.5GO samples had a lower PO_4^{3-} ion release than 0GO samples. The pH profile of ZOL loaded IBS samples over was presented in Figure 6.5 (d). Initially, pH value was decreased for all the samples for 10 days. Then, the gradual increase of pH was detected. OGO samples had a lower PO_4^{3-} ion release than 1.5GO samples which led to a lower pH. On day 28, 1.5GO samples had a decrease of pH whereas 0GO samples pH continued to increase. Standard curve of ZOL and PO_4^{3-} ions were given in Appendix C.1 and Appendix C.2, respectively.

6.3.6 In Vitro Cell Culture Studies

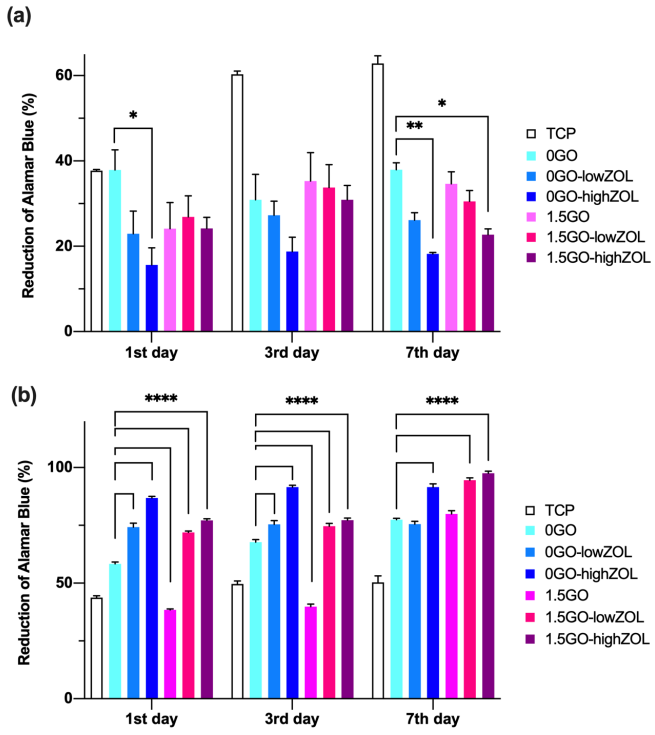

Figure 6.6 Metabolic activity of (a) MCF-7 and (b) hFOB cells cultured directly on the ZOL and GO loaded IBS samples in 24-well culture plate. Values expressed as % reduction of Alamar blue dye (results mean ± standard deviation, n=5, * for $p<0.05$, ** for $p< 0.01$ and **** for $p<0.0001$).

Figure 6.6 (a) shows the result of the inhibitory effect of developed IBS samples on cancer cell lines. This inhibitory effect was seen for 0GO-highZOL samples as the reduction of Alamar blue % was significantly decreased on day 1. The viability of MCF-7 cells decreased as the ZOL concentration increased. For the GO incorporated samples, % reduction of Alamar blue did not show a significant dose dependent decrease towards to low- or high- ZOL incorporation until day 7. On day 7, 1.5GO-highZOL samples also revealed significantly lower cell viability compared to 0GO samples.

Figure 6.6 (b) shows the effect of ZOL loading on hFOB cell culture on day 1, 3 and 7. Results revealed that low and high ZOL loaded IBS samples reached significantly higher % viability when compared to 0GO and 1.5GO samples. Hence, % cell viability coordinately increased with ZOL concentration.

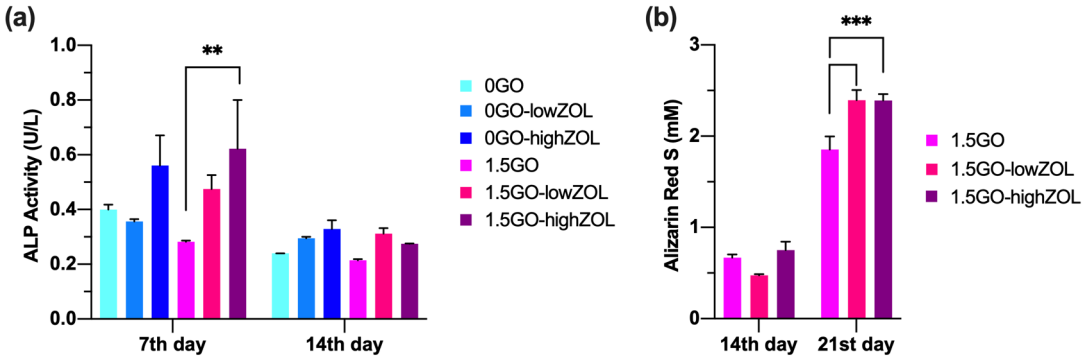

Figure 6.7 Quantitative analysis of (a) alkaline phosphatase assay on 7th and 14th day of incubation and (b) Alizarin Red S Staining on 14th and 21st day of incubation. (results mean±standard deviation, n=5, ** for $p<0.05$, *** for $p<0.001$).

Figure 6.7 shows the quantitative analysis of ALP activity and mineralization of hFOBs on prepared IBS samples. According to the results of ALP activity from hFOBs in Figure 6.7 (a), 0GO-highZOL, 1.5GO-low and -high ZOL samples enhanced the ALP activity as compared to 0GO and 1.5GO samples. The expression of ALP level was significantly higher in the hFOB cells cultured with 1.5GO-highZOL samples compared to 1.5GO samples on day 7. Overall, the ALP activity was expressed similarly from other groups with no significant differences on day 7 and 14. Figure 6.7 (b) shows the quantification of Alizarin red S staining processed by hFOBs cultured with 1.5GO, 1.5GO-lowZOL and 1.5GO-highZOL samples after 14 and 21 days.

Mineralization was started to be examined on day 14 and increased significantly on day 21. The hFOBs treated with ZOL loaded samples showed significantly the highest mineralization compared to 1.5GO samples, however low and high ZOL incorporation expressed similar mineralization independently from their concentrations for 21 days.

6.4 Discussion

In this part of the thesis, anti-osteoporotic drug ZOL was loaded into IBS samples and the effect of drug loading on the physicochemical and in vitro properties were evaluated. FTIR spectra of 0GO, 0GO-highZOL and 1.5GO-highZOL samples dominantly revealed several characteristic peaks of powder phase due to its higher weight fraction. The peaks detected at 1620 and 1409 cm^{-1} associates the H-O-H and C-O-H plane bending in the spectra of 0GO sample, respectively. Due to the ZOL loading, these two peaks were shifted and became broader in the spectra of 0GO-highZOL and 1.5GO-highZOL samples [172]. 0GO-highZOL and 1.5GO-highZOL samples had comparably similar characteristic peaks since a small amount of GO was added when compared to the powder phase weight fraction [172, 173, 177]. Main reason of this similarity could also be the result of the non-covalent interactions among GO and the powder phase [178]. While ZOL incorporation did not affect the injectability of IBS samples, setting time of IBS samples was significantly changed by the incorporation of both ZOL and GO. In previous studies, similar results were reported. The setting time was also prolonged with other types of BPs [117, 119, 120]. Interaction of bisphosphonate with calcium ions led to increase of setting time. The surface properties of CaPs were changed by BP incorporation. These changes affected the dissolution mechanism of CPC particles which was caused by a bidentate chelation of deprotonated oxygen atoms, consequently CaPs became wet and easily dispersed [120, 190]. Overall, these changes led to increase the setting time of the ZOL loaded IBS samples. Contrarily, the incorporation of GO significantly decreased the setting time. GO incorporation gave more nucleation sites to the cement phase. The deposition rate of Ca^{2+} ions and the nucleation rate of cement phase were accelerated, therefore the setting process of the cement phase was supported by GO incorporation [191, 192]. Similarly, the increase of

the compressive modulus by GO incorporation was also associated with the hydration process of the powder phase. The acceleration of the deposition rate of Ca^{2+} ions and the nucleation rate of cement phase promoted the formation of the interfacial bonding between GO and the powder phase which resulted in strengthening of the mechanical properties [193].

1.5GO-highZOL samples decreased the compressive modulus by 53.56 % and it was recorded as 13.78MPa. The weakening effect of BPs on the mechanical properties of composites were also stated in other studies [117, 119, 120, 192]. ZOL incorporation inhibits the crystal growth of CPC and this changes the binding and dissolution mechanism of the cement particles which cause a decrease in mechanical properties of the composites [183]. In spite of this weakening effect of ZOL incorporation to compressive modulus, prepared IBS samples still exhibited acceptable mechanical properties for non-load bearing applications.

Morphological observation of IBS samples by SEM analysis revealed that apatite was formed and detected with a cauli-flower like morphology after incubated in SBF at 37 °C. As mentioned above, GO incorporation increased the nucleation of the cement phase which led to a more compact and dense microstructure [191]. By examining the SEM images of ZOL loaded IBS samples, a smoother cross-sectional morphology was detected into SEM images of ZOL loaded IBS samples after incubation in SBF for 28 days. Literature also indicates that the addition of ZOL decreased apatite formation [120, 194]. Therefore, it can be concluded that ZOL loading suppressed the apatite formation.

In Figure 6.5 (a), ZOL release kinetics revealed the first initial release stage of ZOL which is defined as diffusion-control drug release occurring from the dissolution of ZOL on the outer layer of the samples [119]. Also, this fast release of ZOL could come from the free drug molecules at the beginning of the incubation in PBS. In this study, ZOL was incorporated to the liquid phase of the samples, meaning that ZOL molecules met CaP molecules after the liquid components. Therefore, some of the ZOL molecules could not succeed to chelate with CaP molecules which cause a termination of the free

ZOL molecules in PBS. Then, the loaded ZOL started to release from micropores by dissolution-controlled release process [120, 195, 196]. The affinity between Ca ions and ZOL was strong enough to prevent ZOL release. Also, 1.5GO samples released less ZOL than the 0GO samples. This could be due to banding of GO nanoparticles which had a tight bond with drug and CaP particles. Also, the compact microstructure of GO loaded IBS samples delayed the dissolution-controlled release process. The initial weight loss in Figure 6.5(b) was due to wash-out of the cement phase and degradation of MC and gelatin [157, 197, 198]. All samples lost approximately 20 % of their weights in the first 7 days. Due to the compact structure of GO added IBS samples, the weight loss from these samples was relatively slow. Due to the affinity between Ca ions and ZOL molecules, the PO_4^{3-} ion release increased with the incorporation of ZOL as seen in Figure 6.5(c). This is in vitro results in agreement with each other. In Figure 6.5(d), the initial decrease of the pH can be attributed to dissolution of Ca^{2+} ions from the powder phase of the IBS samples [199]. After 10 days of incubation, pH was started to increase because of the PO_4^{3-} ion release. This also affected to bonding of PO_4^{3-} with H+ ions which increased of alkalinity of the buffering solution. On day 28, there was a reverse relation of pH between GO incorporated samples and 0GO samples. This could be explained with the increase of CaP deposition on 1.5GO samples compared to 0GO samples. This was in accordance with SEM images of day 28 which illustrated apatite formation on 1.5GO samples whereas 0GO-highZOL samples had minimal apatite formation. In literature, the inhibitory effect of CaP nanoparticles on cancer cell lines were examined [200, 201, 202]. Released CaP nanoparticles from IBS samples could cause these inhibitory effects since MCF-7 cells were directly seeded on the IBS samples. This could clarify the decrease of cell viability of 0GO samples compared to the TCP. The viability of MCF-7 cells decreased as the ZOL concentration increased. Different cell types were used to evaluate effects of BPs with different doses during time [109, 121, 203, 204]. Therefore, we also examined the biocompatibility of ZOL loaded IBS samples by using hFOBs. Both low and high concentration of ZOL used in this study were non-cytotoxic and supported cell proliferation with regards to the result of reduction of Alamar blue dye. In accordance to the results of these two in vitro cell studies, both the inhibitory effect of ZOL loaded IBS samples on MCF-7 cells and proliferative effect of ZOL loaded IBS samples on osteoblast cells were

determined. Hence, produced IBS samples showed promising results for both cancer and osteoporosis treatment. Osteoblast differentiation in vitro can be characterized in three stages which are cell proliferation, matrix maturation, and matrix mineralization [205]. ALP activity is used to show the matrix maturation stage. So that, an increase in the ALP activity level of osteoblasts means that cells are at differentiated state [206]. In this study, ALP expression decreased from day 7 to day 14 meaning that the mineralization stage was initiated [175]. ALP activity was increased with ZOL incorporation; however, this increase was not significant compared to 0GO samples. This early osteoblastic differentiation in contact with ZOL loaded IBS samples could be beneficial for the first phases of bone healing [207]. Alizarin Red S staining shows the matrix mineralization stage. According to the results, 1.5GO-low and -highZOL loaded IBS samples showed significantly higher tendency to support mineralization of hFOBs. Taken all together, hFOBs were able to proliferate and differentiate with the prepared IBS samples.

7. CONCLUSION

This thesis was aimed to obtain an understanding of some strategies that can be applied to enhance the properties of injectable CaP-based bone grafts by adjusting some physicochemical properties with the addition of natural polymers and GO. Also, an anti-osteoporotic drug ZOL was loaded to improve the in vitro biological response of IBS samples. The effect on handling properties, in vitro degradation and the response of relevant cell types was evaluated. Firstly, the incorporation of the bioceramic powder into MC and gelatin-based polymeric phase improved the handling, rheological, mechanical and degradation properties of IBS. GO incorporation did not cause any phase separation or any reverse effect on handling properties of the IBS samples. GO addition significantly reduced the setting time of the cements, improved in vitro degradation and rheological properties at 37 °C. Specifically, 1 and 1.5 wt % GO incorporated samples showed higher stability, workability, rheological properties and biocompatibility than the other GO added IBS samples. The incorporation of ZOL into IBS led to increase of the setting time; however, it did not affect % injectability. As a result, ZOL and GO loaded IBS samples also showed acceptable handling and suitable mechanical properties for non-load bearing bone regions. Meanwhile, findings of in vitro cellular response with MCF-7 cells revealed that % viability decreased as the ZOL concentration increased. Also, another outcome of in vitro cellular response confirmed that GO and ZOL loaded IBS samples could promote osteoblast proliferation and activity. Overall, preparation of IBS samples with ZOL and GO would be beneficial since ZOL shows anti-cancer and anti-osteoporotic properties and GO would improve the physical properties which were dropped down by the addition of ZOL. To conclude that future clinical application of prepared IBS could be beneficial for medically-compromised conditions of bone.

APPENDIX A. XRD Analysis of Synthesized TTCP with JCPDS Files

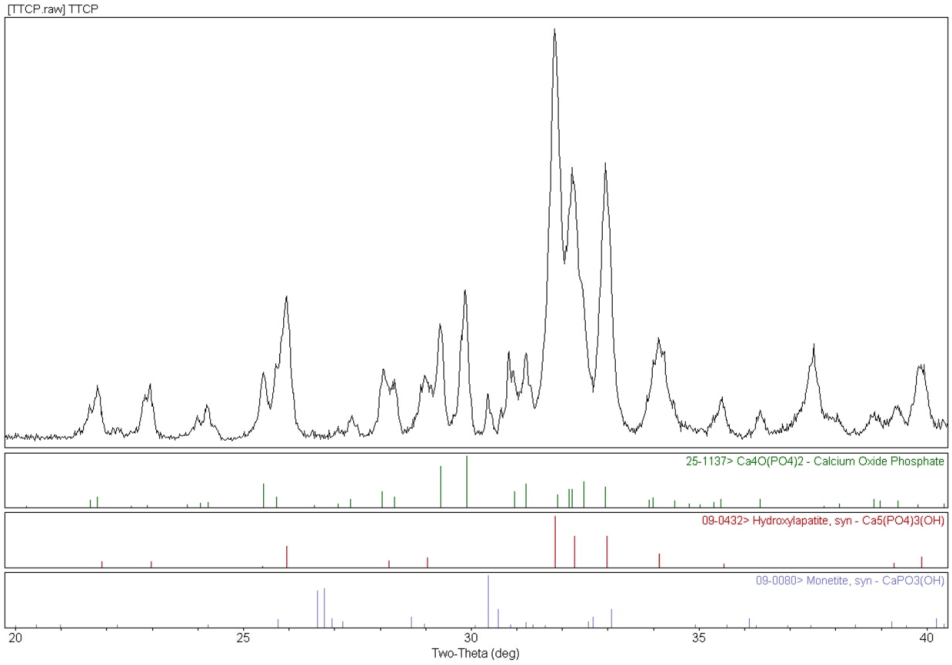

Figure A.1 Synthesized TTCP phase identified by XRD with JCPDS No. 25-1137, No. 09-0432 and No. 09-0080 files.

APPENDIX B. XRD Analysis of Purchased TTCP Powder

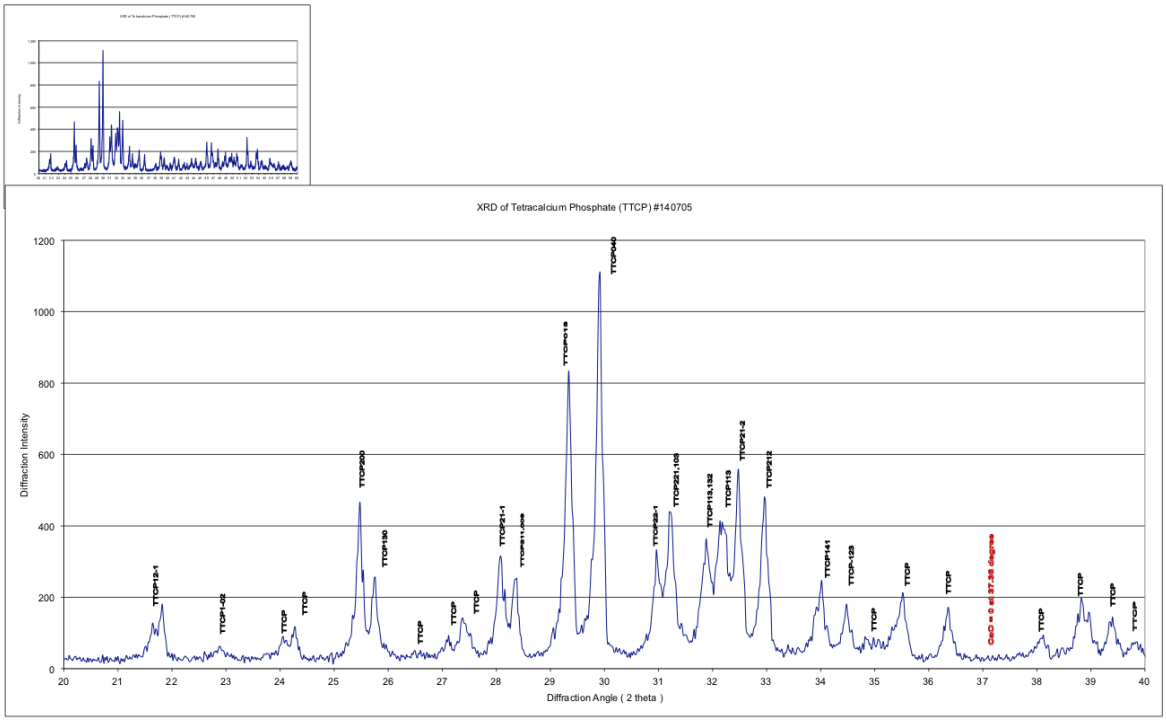

Figure B.1 XRD diagram of purchased TTCP.

APPENDIX C. Standard Curves

C.1 Standard Curve of ZOL.

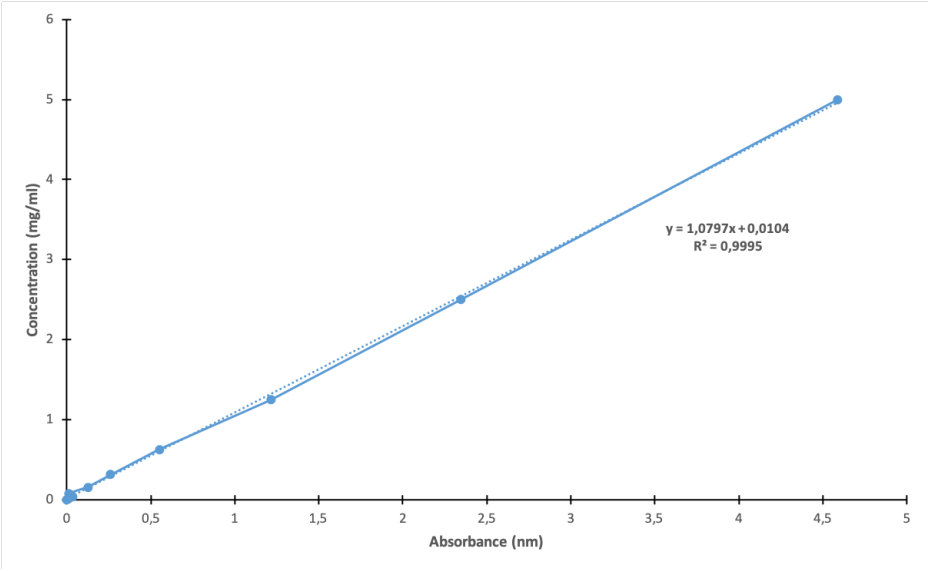

Figure C.1 Standard curve of ZOL.

C.2 Standard Curve of Phosphate Ions

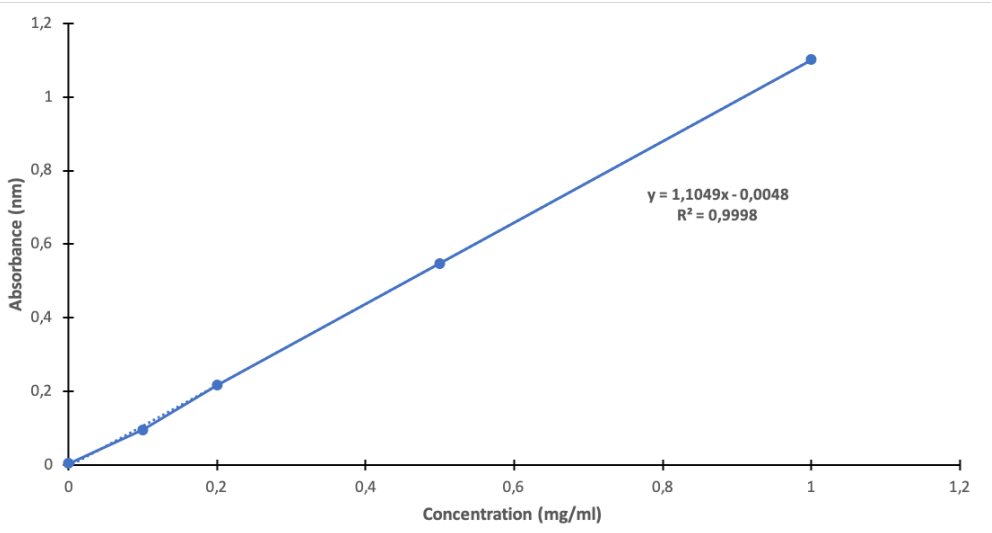

Figure C.2 Standard curve of PO_4^{3-} ion.

C.3 Standard Curve of ALP

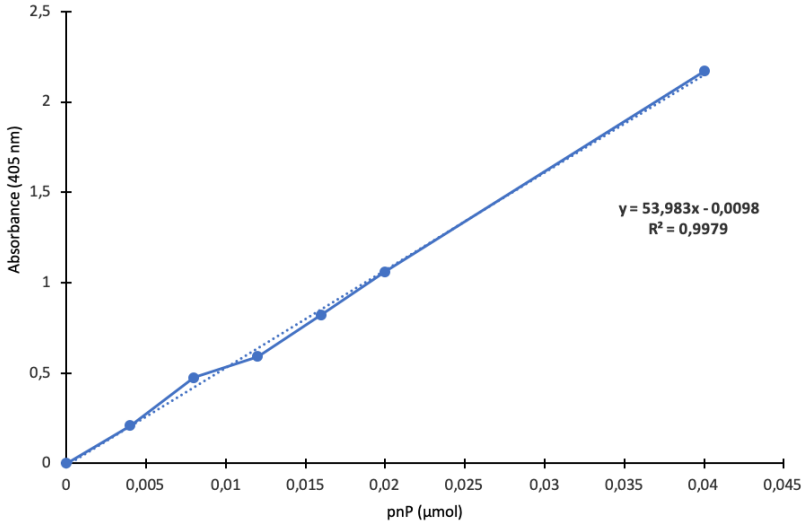

Figure C.3 Standard curve of ALP.

C.4 Standard Curve of Alizarin Red Dye

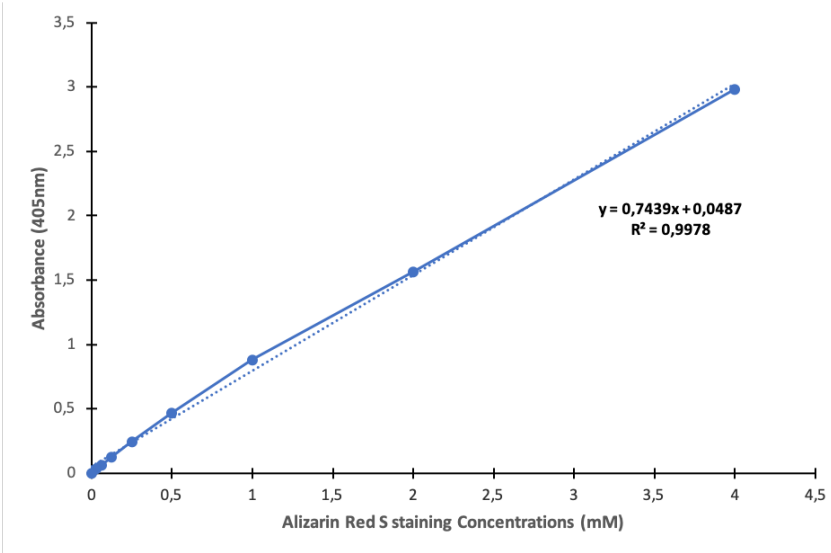

Figure C.4 Standard curve of Alizarin red dye.

REFERENCES

1. Wegst, U. G., H. Bai, E. Saiz, A. P. Tomsia, and R. O. Ritchie, "Bioinspired structural materials," *Nature Materials*, Vol. 14, no. 1, pp. 23–36, 2015.

2. Le, C., M. Bao, E. Y. Teo, M. S. K. Chong, Y. Liu, M. Choolani, and J. K. Y. Chan, "Advances in Bone Tissue Engineering," in *Regenerative Medicine and Tissue Engineering*, pp. 599–614, IntechOpen, 2013.

3. Kini, U., and B. N. Nandeesh, "Physiology of Bone Formation, Remodeling, and Metabolism," in *Radionuclide and Hybrid Bone Imaging*, pp. 29–57, Berlin, Heidelberg: Springer Berlin Heidelberg, 2012.

4. Einhorn, T. A., and L. C. Gerstenfeld, "Fracture healing: mechanisms and interventions," *Nature Reviews Rheumatology*, Vol. 11, no. 1, pp. 45–54, 2014.

5. Maas, M., U. Hess, and K. Rezwan, "The contribution of rheology for designing hydroxyapatite biomaterials," *Current Opinion in Colloid and Interface Science*, Vol. 19, no. 6, pp. 585–593, 2014.

6. Giger, E. V., B. Castagner, and J. C. Leroux, "Biomedical applications of bisphosphonates," *Journal of Controlled Release*, Vol. 167, no. 2, pp. 175–188, 2013.

7. Clézardin, P., "Bisphosphonates' antitumor activity: An unravelled side of a multifaceted drug class," *Bone*, Vol. 48, no. 1, pp. 71–79, 2011.

8. Ratner, B. D., A. S. Hoffman, F. J. Schoen, and J. E. Lemons, "Biomaterials Science: An Evolving, Multidisciplinary Endeavor," in *Biomaterials Science*, pp. 1–1573, Academic Press, 3rd ed., 2013.

9. Khan, F., and M. Tanaka, "Designing smart biomaterials for tissue engineering," *International Journal of Molecular Sciences*, Vol. 19, no. 1, pp. 1–14, 2018.

10. Wagoner Johnson, A. J., and B. A. Herschler, "A review of the mechanical behavior of CaP and CaP/polymer composites for applications in bone replacement and repair," *Acta Biomaterialia*, Vol. 7, no. 1, pp. 16–30, 2011.

11. Perez, R. A., S.-H. Shin, C.-M. Han, and H.-W. Kim, "Bioactive injectables based on calcium phosphates for hard tissues: A recent update," *Tissue Engineering and Regenerative Medicine*, Vol. 12, no. 3, pp. 143–153, 2015.

12. Fong, E. L. S., B. M. Watson, F. K. Kasper, and A. G. Mikos, "Building bridges: Leveraging interdisciplinary collaborations in the development of biomaterials to meet clinical needs," *Advanced Materials*, Vol. 24, no. 36, pp. 4995–5013, 2012.

13. Hou, Q., P. A. De Bank, and K. M. Shakesheff, "Injectable scaffolds for tissue regeneration," *Journal of Materials Chemistry*, Vol. 14, no. 13, pp. 1915–1923, 2004.

14. Chen, Z., X. Zhang, L. Kang, F. Xu, Z. Wang, F.-Z. Cui, and Z. Guo, "Recent progress in injectable bone repair materials research," *Frontiers of Materials Science*, Vol. 9, no. 4, pp. 332–345, 2015.

15. Sivashanmugam, A., R. Arun Kumar, M. Vishnu Priya, S. V. Nair, and R. Jayakumar, "An overview of injectable polymeric hydrogels for tissue engineering," *European Polymer Journal*, Vol. 72, pp. 543–565, 5 2015.

16. "Prevention and management of osteoporosis : report of a WHO scientific group," 2003.

17. Ezra, A., and G. Golomb, "Administration routes and delivery systems of bisphosphonates for the treatment of bone resorption," *Advanced Drug Delivery Reviews*, Vol. 42, no. 3, pp. 175–195, 2000.

18. Lin, J. H., "Bisphosphonates: A review of their pharmacokinetic properties," *Bone*, Vol. 18, no. 2, pp. 75–85, 1996.

19. Gomez, V., and S.-Y. Xiao, "Alendronate-induced esophagitis in an elderly woman.," *International Journal of Clinical and Experimental Pathology*, Vol. 2, no. 2, pp. 200–203, 2009.

20. Saunders, R. L. J., "Appearance of a gastric ulcer during diphosphonate therapy in a woman with CRST syndrome.," *Southern Medical Journal*, Vol. 70, pp. 1327–1329, 11 1977.

21. Yu, N. Y. C., A. Schindeler, L. Peacock, K. Mikulec, J. Fitzpatrick, A. J. Ruys, J. J. Cooper-White, and D. G. Little, "Modulation of anabolic and catabolic responses via a porous polymer scaffold manufactured using thermally induced phase separation," *European Cells and Materials*, Vol. 25, pp. 190–203, 2012.

22. Peter, B., D. P. Pioletti, S. Laïb, B. Bujoli, P. Pilet, P. Janvier, J. Guicheux, P. Y. Zambelli, J. M. Bouler, and O. Gauthier, "Calcium phosphate drug delivery system: Influence of local zoledronate release on bone implant osteointegration," *Bone*, Vol. 36, no. 1, pp. 52–60, 2005.

23. Link, D. P., J. van den Dolder, J. J. van den Beucken, J. G. Wolke, A. G. Mikos, and J. A. Jansen, "Bone response and mechanical strength of rabbit femoral defects filled with injectable CaP cements containing TGF-β1 loaded gelatin microparticles," *Biomaterials*, Vol. 29, no. 6, pp. 675–682, 2008.

24. Habraken, W. J. E. M., L. T. De Jonge, J. G. C. Wolke, L. Yubao, A. G. Mikos, and J. A. Jansen, "Introduction of gelatin microspheres into an injectable calcium phosphate cement," *Journal of Biomedical Materials Research - Part A*, Vol. 87, no. 3, pp. 643–655, 2008.

25. Low, K. L., S. H. Tan, S. H. S. Zein, J. A. Roether, V. Mouriño, and A. R. Boccaccini, "Calcium phosphate-based composites as injectable bone substitute materials," *Journal of Biomedical Materials Research - Part B Applied Biomaterials*, Vol. 94, no. 1, pp. 273–286, 2010.

26. Porter, J. R., T. T. Ruckh, and K. C. Popat, "Bone tissue engineering: a review in bone biomimetics and drug delivery strategies.," *Biotechnology Progress*, Vol. 25, no. 6, pp. 1539–60, 2009.

27. Feng, X., "Chemical and Biochemical Basis of Bone Cell," *NIH Public Access*, Vol. 3, no. 2, pp. 975–990, 2010.

28. Liu, M., X. Zeng, C. Ma, H. Yi, Z. Ali, X. Mou, S. Li, Y. Deng, and N. He, "Injectable hydrogels for cartilage and bone tissue engineering," *Bone Research*, Vol. 5, no. November 2016, 2017.

29. Le Meng Bao, C., E. Y. Teo, M. S. K. Chong, Y. Liu, M. Choolani, and J. K. Y. Chan, "Advances in Bone Tissue Engineering," in *Regenerative Medicine and Tissue Engineering*, pp. 599–614, IntechOpen, 5 2013.

30. Rho, J.-Y., L. Kuhn-Spearing, and P. Zioupos, "Mechanical properties and the hierarchical structure of bone," *Medical Engineering & Physics*, Vol. 20, no. 2, pp. 92–102, 1998.

31. Pilitsis, J. G., D. R. Lucas, and S. S. Rengachary, "Bone healing and spinal fusion.," *Neurosurgical focus*, Vol. 13, p. e1, 12 2002.

32. Capulli, M., R. Paone, and N. Rucci, "Osteoblast and osteocyte: Games without frontiers," *Archives of Biochemistry and Biophysics*, Vol. 561, pp. 3–12, 2014.

33. Soysa, N. S., N. Alles, K. Aoki, and K. Ohya, "Osteoclast formation and differentiation: an overview.," *Journal of Medical and Dental Sciences*, Vol. 59, pp. 65–74, 11 2012.

34. Vaananen, H. K., H. Zhao, M. Mulari, and J. M. Halleen, "The cell biology of osteoclast function," *Journal of Cell Science*, Vol. 113, pp. 377 LP – 381, 2 2000.

35. Hadjidakis, D. J., and I. I. Androulakis, "Bone remodeling," *Annals of the New York Academy of Sciences*, Vol. 1092, pp. 385–396, 2006.

36. Marsell, R., and T. A. Einhorn, "The Biology of Fructure Healing," *Injury*, Vol. 42, no. 6, pp. 551–555, 2012.

37. Schlickewei, C. W., G. Laaff, A. Andresen, T. O. Klatte, J. M. Rueger, J. Ruesing, M. Epple, and W. Lehmann, "Bone augmentation using a new injectable bone graft substitute by combining calcium phosphate and bisphosphonate as composite–an animal model.," *Journal of Orthopaedic Surgery and Research*, Vol. 10, no. 1, p. 116, 2015.

38. Xia, Y., F. Mei, Y. Duan, Y. Gao, Z. Xiong, T. Zhang, and H. Zhang, "Bone tissue engineering using bone marrow stromal cells and an injectable sodium alginate/gelatin scaffold," *Journal of Biomedical Materials Research - Part A*, Vol. 100 A, no. 4, pp. 1044–1050, 2012.

39. Burg, K. J., S. Porter, and J. F. Kellam, "Biomaterial developments for bone tissue engineering.," *Biomaterials*, Vol. 21, pp. 2347–59, 12 2000.

40. Śmiga-Matuszowicz, M., J. Łukaszczyk, R. Pilawka, M. Basiaga, M. Bilewicz, and D. Kusz, "Novel crosslinkable polyester resinâbased composites as injectable bioactive scaffolds," *International Journal of Polymeric Materials and Polymeric Biomaterials*, Vol. 66, no. 1, pp. 1–11, 2017.

41. Sharifi, S., M. Imani, H. Mirzadeh, M. Atai, F. Ziaee, and R. Bakhshi, "Synthesis, characterization, and biocompatibility of novel injectable, biodegradable, and in situ crosslinkable polycarbonate-based macromers," *Journal of Biomedical Materials Research Part A*, Vol. 90, no. 3, pp. 830–843, 2009.

42. Kondiah, P. J., Y. E. Choonara, P. P. D. Kondiah, T. Marimuthu, P. Kumar, L. C. Du Toit, and V. Pillay, "A review of injectable polymeric hydrogel systems for application in bone tissue engineering," *Molecules*, Vol. 21, no. 11, 2016.

43. Gyles, D. A., L. D. Castro, J. O. C. SilvaJr., and R. M. Ribeiro-Costa, "A review of the designs and prominent biomedical advances of natural and synthetic hydrogel formulations," *European Polymer Journal*, Vol. 88, pp. 373–392, 2017.

44. Tan, H., C. M. Ramirez, N. Miljkovic, H. Li, J. P. Rubin, and K. G. Marra, "Thermosensitive injectable hyaluronic acid hydrogel for adipose tissue engineering," *Biomaterials*, Vol. 30, no. 36, pp. 6844–6853, 2009.

45. Jung, Y.-s., W. Park, H. Park, D.-K. Lee, and K. Na, "Thermo-sensitive injectable hydrogel based on the physical mixing of hyaluronic acid and Pluronic F-127 for sustained NSAID delivery," *Carbohydrate Polymers*, Vol. 156, pp. 403–408, 2017.

46. Wu, J., J. Liu, Y. Shi, and Y. Wan, "Rheological, mechanical and degradable properties of injectable chitosan/silk fibroin/hydroxyapatite/glycerophosphate hydrogels," *Journal of the Mechanical Behavior of Biomedical Materials*, Vol. 64, pp. 161–172, 2016.

47. Chang, C., and L. Zhang, "Cellulose-based hydrogels: Present status and application prospects," *Carbohydrate Polymers*, Vol. 84, pp. 40–53, 2 2011.

48. Shimokawa, K., K. Saegusa, and F. Ishii, "Rheological properties of reversible thermosetting in situ gelling solutions with the methylcellulose-polyethylene glycol-citric acid ternary system (2): Effects of various water-soluble polymers and salts on the gelling temperature," *Colloids and Surfaces B: Biointerfaces.*, Vol. 74, no. 1, pp. 56–58, 2009.

49. Ghanaati, S., M. Barbeck, U. Hilbig, C. Hoffmann, R. E. Unger, R. A. Sader, F. Peters, and C. J. Kirkpatrick, "An injectable bone substitute composed of beta-tricalcium phosphate granules, methylcellulose and hyaluronic acid inhibits connective tissue influx into its implantation bed in vivo.," *Acta biomaterialia*, Vol. 7, pp. 4018–28, 11 2011.

50. Daculsi, G., A. P. Uzel, P. Weiss, E. Goyenvalle, and E. Aguado, "Developments in injectable multiphasic biomaterials. the performance of microporous biphasic calcium phosphate granules and hydrogels," *Journal of Materials Science: Materials in Medicine*, Vol. 21, no. 3, pp. 855–861, 2010.

51. Krause, M., R. Oheim, P. Catala-Lehnen, J. M. Pestka, C. Hoffmann, W. Huebner, F. Peters, F. Barvencik, and M. Amling, "Metaphyseal bone formation induced by a new injectable beta-TCP-based bone substitute: a controlled study in rabbits," *J Biomater Appl*, Vol. 28, no. 6, pp. 859–868, 2014.

52. Patenaude, M., and T. Hoare, "Injectable, mixed natural-synthetic polymer hydrogels with modular properties," *Biomacromolecules*, Vol. 13, no. 2, pp. 369–378, 2012.

53. Rangabhatla, A. S. L., V. Tantishaiyakul, K. Oungbho, and O. Boonrat, "Fabrication of pluronic and methylcellulose for etidronate delivery and their application for osteogenesis," *International Journal of Pharmaceutics*, Vol. 499, no. 1-2, pp. 110–118, 2016.

54. Caicco, M. J., T. Zahir, A. J. Mothe, B. G. Ballios, A. J. Kihm, C. H. Tator, and M. S. Shoichet, "Characterization of hyaluronan-methylcellulose hydrogels for cell delivery to the injured spinal cord," *Journal of Biomedical Materials Research - Part A*, Vol. 101 A, no. 5, pp. 1472–1477, 2013.

55. Wang, H., S. C. Leeuwenburgh, Y. Li, and J. a. Jansen, "The Use of Micro- and Nanospheres as Functional Components for Bone Tissue Regeneration," *Tissue Engineering Part B: Reviews*, Vol. 18, no. 1, pp. 24–39, 2012.

56. Zou, Y., J. L. Brooks, V. Talwalkar, T. A. Milbrandt, and D. A. Puleo, "Development of an injectable two-phase drug delivery system for sequential release of antiresorptive and osteogenic drugs," *Journal of Biomedical Materials Research - Part B Applied Biomaterials*, Vol. 100 B, no. 1, pp. 155–162, 2012.

57. Cheng, F., Y. B. Choy, H. Choi, and K. Kim, "Modeling of small-molecule release from crosslinked hydrogel microspheres: Effect of crosslinking and enzymatic degradation of hydrogel matrix," *International Journal of Pharmaceutics*, Vol. 403, no. 1-2, pp. 90–95, 2011.

58. Wang, H., O. C. Boerman, K. Sariibrahimoglu, Y. Li, J. A. Jansen, and S. C. Leeuwenburgh, "Comparison of micro- vs. nanostructured colloidal gelatin gels for sustained delivery of osteogenic proteins: Bone morphogenetic protein-2 and alkaline phosphatase," *Biomaterials*, Vol. 33, no. 33, pp. 8695–8703, 2012.

59. Ren, Z., Y. Wang, S. Ma, S. Duan, X. Yang, P. Gao, X. Zhang, and Q. Cai, "Effective Bone Regeneration Using Thermosensitive Poly(N-Isopropylacrylamide) Grafted Gelatin as Injectable Carrier for Bone Mesenchymal Stem Cells," *ACS Applied Materials and Interfaces*, Vol. 7, no. 34, pp. 19006–19015, 2015.

60. Félix Lanao, R. P., K. Sariibrahimoglu, H. Wang, J. G. C. Wolke, J. A. Jansen, and S. C. G. Leeuwenburgh, "Accelerated calcium phosphate cement degradation due to incorporation of glucono-delta-lactone microparticles.," *Tissue engineering. Part A*, Vol. 20, no. 1-2, pp. 378–88, 2014.

61. Bongio, M., M. R. Nejadnik, F. K. Kasper, A. G. Mikos, J. A. Jansen, S. C. Leeuwenburgh, and J. J. van den Beucken, "Development of an inÂ vitro confinement test to predict the clinical handling of polymer-based injectable bone substitutes," *Polymer Testing*, Vol. 32, pp. 1379–1384, 12 2013.

62. Dessi, M., M. A. Alvarez-Perez, R. De Santis, M. P. Ginebra, J. A. Planell, and L. Ambrosio, "Bioactivation of calcium deficient hydroxyapatite with foamed gelatin gel. A new injectable self-setting bone analogue," *Journal of Materials Science: Materials in Medicine*, Vol. 25, no. 2, pp. 283–295, 2014.

63. Babu, V. R., V. R. Kanth, J. M. Mukund, and T. M. Aminabhavi, "Novel methyl cellulose- grafted -acrylamide/gelatin microspheres for controlled release of nifedipine," *Journal of Applied Polymer Science*, Vol. 115, pp. 3542–3549, 3 2010.

64. Iturriaga, L., I. Olabarrieta, and I. M. de Marañón, "Antimicrobial assays of natural extracts and their inhibitory effect against Listeria innocua and fish spoilage bacteria, after incorporation into biopolymer edible films," *International Journal of Food Microbiology*, Vol. 158, no. 1, pp. 58–64, 2012.

65. Sanzana, E., M. Navarro, F. Macule, S. Suso, J. Planell, and M. Ginebra, "Of the in vivo behavior of calcium phosphate cements and glasses as bone substitutes," *Acta Biomaterialia*, Vol. 4, no. 6, pp. 1924–1933, 2008.

66. Ginebra, M. P., T. Traykova, and J. A. Planell, "Calcium phosphate cements as bone drug delivery systems: a review.," *Journal of Controlled Release*, Vol. 113, no. 2, pp. 102–10, 2006.

67. Sadiasa, A., S. K. Sarkar, R. A. Franco, Y. K. Min, and B. T. Lee, "Bioactive glass incorporation in calcium phosphate cement-based injectable bone substitute for improved in vitro biocompatibility and in vivo bone regeneration.," *Journal of Biomaterials Applications*, Vol. 28, no. 5, pp. 739–56, 2014.

68. Brown, W. E., and L. C. Chow, "A New Calcium-Phosphate Setting Cement," *Journal of Dental Research*, Vol. 62, no. SI, p. 672, 1983.

69. Gruninger, S. E., C. Siew, L. Chow, A. Oyoung, N. K. Tsao, and W. Brown, "Evaluation of the Biocompatibility of a New Calcium-Phosphate Setting Cement," *Journal of Dental Research*, Vol. 63, no. SI, p. 200, 1984.

70. Hoelscher-Doht, S., M. C. Jordan, C. Bonhoff, S. Frey, T. Blunk, and R. H. Meffert, "Bone substitute first or screws first? A biomechanical comparison of two operative techniques for tibial-head depression fractures.," *Journal of Orthopaedic Science*, Vol. 19, pp. 978–83, 11 2014.

71. Lord, B. R., T. C. B. Pollard, and A. R. McAndrew, "Injection of calcium phosphate cement in the percutaneous treatment of fractures of the lateral tibial plateau," *Acta Orthopaedica Belgica*, Vol. 77, no. 4, pp. 539–540, 2011.

72. Niwa, S., K. Morikawa, W. Zhang, Y. Aizawa, T. Hattori, and K. Sato, "Clinical significance of calcium phosphate cement in repairing of bone fracture," in *Structural Biomaterials for the 21st Century*, pp. 195–202, Minarals, Metals and Materials Society, 2001.

73. Stankewich, C. J., M. F. Swiontkowski, A. F. Tencer, D. N. Yetkinler, and R. D. Poser, "Augmentation of femoral neck fracture fixation with an injectable calcium-phosphate bone mineral cement," *Journal of Orthopaedic Research*, Vol. 14, no. 5, pp. 786–793, 1996.

74. Goff, T., N. K. Kanakaris, and P. V. Giannoudis, "Use of bone graft substitutes in the management of tibial plateau fractures," *Injury*, Vol. 44, pp. S86–S94, 4 2016.

75. J.W., G., C. T., M. C., and S. D., "Open reduction internal fixation of midshaft clavicle fractures augmented with autogenous bone graft versus bioresorbable calcium phosphate: A comparative study," *European Journal of Orthopaedic Surgery and Traumatology*, Vol. 21, no. 7, pp. 479–483, 2011.

76. Xiao, Y., Q. Yin, L. Wang, and C. Bao, "Macro-porous calcium phosphate scaffold with collagen and growth factors for periodontal bone regeneration in dogs," *Ceramics International*, Vol. 41, pp. 995–1003, 1 2015.

77. Aral, A., S. Yalcin, Z. C. Karabuda, A. Anl, J. A. Jansen, and Z. Mutlu, "Injectable calcium phosphate cement as a graft material for maxillary sinus augmentation: An experimental pilot study," *Clinical Oral Implants Research*, Vol. 19, no. 6, pp. 612–617, 2008.

78. Friedmann, A., K. Gissel, A. Konermann, and W. Götz, "Tissue reactions after simultaneous alveolar ridge augmentation with biphasic calcium phosphate and implant insertion-histological and immunohistochemical evaluation in humans," *Clinical Oral Investigations*, pp. 1595–1603, 2014.

79. Friberg, J., E. Fernandez, S. Sarda, M. Nilsson, M. P. Ginebra, S. Martinez, and J. A. Planell, "An experimental approach to the study of the rheology behaviour of synthetic bone calcium phosphate cements," in *Bioceramics*, Vol. 192-1 of *Key Engineering Materials*, (Brandrain, Switzerland), pp. 777–780, 2000.

80. Hesaraki, S., A. Zamanian, and F. Moztarzadeh, "The influence of the acidic component of the gas-foaming porogen used in preparing an injectable porous calcium phosphate cement on its properties: Acetic acid versus citric acid," *Journal of Biomedical Materials Research - Part B Applied Biomaterials*, Vol. 86, no. 1, pp. 208–216, 2008.

81. Burguera, E. F., H. H. K. Xu, and M. D. Weir, "Injectable and rapid-setting calcium phosphate bone cement with dicalcium phosphate dihydrate," *Journal of Biomedical Materials Research Part B: Applied Biomaterials*, Vol. 77B, no. 1, pp. 126–134, 2006.

82. Ooms, E. M., N. Verdonschot, J. G. C. Wolke, W. Van De Wijdeven, M. M. M. Willems, M. F. T. Schoenmaker, and J. A. Jansen, "Enhancement of initial stability of press-fit femoral stems using injectable calcium phosphate cement: An in vitro study in dog bones," *Biomaterials*, Vol. 25, no. 17, pp. 3887–3894, 2004.

83. Rodriguez, L. C., J. Chari, S. Aghyarian, I. M. Gindri, V. Kosmopoulos, and D. C. Rodrigues, "Preparation and characterization of injectable brushite filled-poly (methyl methacrylate) bone cement," *Materials*, Vol. 6, no. 9, pp. 6779–6795, 2014.

84. Verma, N. P., and A. Sinha, "Effect of solid to liquid ratio on the physical properties of injectable nanohydroxyapatite," *Journal of Materials Science: Materials in Medicine*, Vol. 24, no. 1, pp. 53–59, 2013.

85. Xu, H. H. K., M. D. Weir, and C. G. Simon, "Injectable and strong nano-apatite scaffolds for cell/growth factor delivery and bone regeneration," *Dental Materials*, Vol. 24, no. 9, pp. 1212–1222, 2008.

86. Gong, T., Z. Wang, Y. Zhang, Y. Zhang, M. Hou, X. Liu, Y. Wang, L. Zhao, N. D. Ruse, T. Troczynski, and U. O. Häfeli, "A Comprehensive Study of Osteogenic Calcium Phosphate Silicate Cement: Material Characterization and In Vitro/In Vivo Testing," *Advanced Healthcare Materials*, Vol. 5, no. 4, pp. 457–466, 2016.

87. Otsuka, M., A. Oshinbe, R. Z. Legeros, Y. Tokudome, A. Ito, K. Otsuka, and W. I. Higuchi, "Efficacy of the injectable calcium phosphate ceramics suspensions containing magnesium, zinc and fluoride on the bone mineral deficiency in ovariectomized rats," *Journal of Pharmaceutical Sciences*, Vol. 97, no. 1, pp. 421–432, 2008.

88. Chen, F., Z. Song, and C. Liu, "Fast setting and anti-washout injectable calcium-magnesium phosphate cement for minimally invasive treatment of bone defects," *Journal of Materials Chemistry B*, Vol. 3, no. 47, pp. 9173–9181, 2015.

89. Iooss, P., A.-M. Le Ray, G. Grimandi, G. Daculsi, and C. Merle, "A new injectable bone substitute combining poly(ϵ-caprolactone) microparticles with biphasic calcium phosphate granules," *Biomaterials*, Vol. 22, no. 20, pp. 2785–2794, 2001.

90. Rodriguez-Lorenzo, L. M., M. Fernandez, J. Parra, B. Vazquez, A. Lopez-Bravo, and J. S. Roman, "Acrylic injectable and self-curing formulations for the local release of bisphosphonates in bone tissue.," *Journal of Biomedical Materials Research Part B, Applied Biomaterials*, Vol. 83, pp. 596–608, 11 2007.

91. Suwandi, J. S., R. E. M. Toes, T. Nikolic, and B. O. Roep, "Inducing tissue specific tolerance in autoimmune disease with tolerogenic dendritic cells," *Clinical and Experimental Rheumatology*, Vol. 33, pp. 97–103, 2015.

92. Debeaufort, F., and A. Voilley, "Methylcellulose-Based Edible Films and Coatings:Â 2. Mechanical and Thermal Properties as a Function of Plasticizer Content," *Journal of Agricultural and Food Chemistry*, Vol. 45, no. 3, pp. 685–689, 1997.

93. Francis, L., J. Venugopal, M. P. Prabhakaran, V. Thavasi, E. Marsano, and S. Ramakrishna, "Simultaneous electrospin-electrosprayed biocomposite nanofibrous scaffolds for bone tissue regeneration," *Acta Biomaterialia*, Vol. 6, no. 10, pp. 4100–4109, 2010.

94. Baumann, M. D., C. E. Kang, J. C. Stanwick, Y. Wang, H. Kim, Y. Lapitsky, and M. S. Shoichet, "An injectable drug delivery platform for sustained combination therapy," *Journal of Controlled Release*, Vol. 138, no. 3, pp. 205–213, 2009.

95. Ege, D., A. R. Kamali, and A. R. Boccaccini, "Graphene Oxide/Polymer-Based Biomaterials," *Advanced Engineering Materials*, Vol. 19, no. 12, pp. 1700627–n/a, 2017.

96. Baudín, C., T. Benet, and P. Pena, "Effect of graphene on setting and mechanical behaviour of tricalcium phosphate bioactive cements," *Journal of the Mechanical Behavior of Biomedical Materials*, Vol. 89, no. July 2018, pp. 33–47, 2019.

97. Zhenkun, X., Y. Haoran, W. Tao, W. Ruizhen, P. Zhang, L. Xiaoying, and W. Jie, "Effects of Adding Reduced-graphene Oxide/Polypyrrole Composites on the Structure and Properties of Calcium Phosphate Cement," *Chemical Journal Of Chinese Universities*, Vol. 36, no. 12, pp. 2598–2603, 2015.

98. Wu, C., L. Xia, P. Han, M. Xu, B. Fang, J. Wang, J. Chang, and Y. Xiao, "Graphene-oxide-modified β-tricalcium phosphate bioceramics stimulate in vitro and in vivo osteogenesis," *Carbon*, Vol. 93, pp. 116–129, 2015.

99. Birenboim, M., R. Nadiv, A. Alatawna, M. Buzaglo, G. Schahar, J. Lee, G. Kim, A. Peled, and O. Regev, "Reinforcement and workability aspects of graphene-oxide-reinforced cement nanocomposites," *Composites Part B: Engineering*, Vol. 161, no. October 2018, pp. 68–76, 2019.

100. Wang, B., R. Jiang, and Z. Wu, "Investigation of the mechanical properties and microstructure of graphene nanoplatelet-cement composite," *Nanomaterials*, Vol. 6, no. 11, 2016.

101. Wang, S., X. Sun, Y. Wang, K. Sun, and J. Bi, "Properties of reduced graphene/carbon nanotubes reinforced calcium phosphate bone cement in a microwave environment," *Journal of Materials Science: Materials in Medicine*, Vol. 30, no. 3, 2019.

102. Wang, S., S. Zhang, Y. Wang, X. Sun, and K. Sun, "Reduced graphene oxide / carbon nanotubes reinforced calcium phosphate cement," *Ceramics International*, Vol. 43, no. 16, pp. 13083–13088, 2017.

103. Shie, M. Y., W. H. Chiang, I. W. P. Chen, W. Y. Liu, and Y. W. Chen, "Synergistic acceleration in the osteogenic and angiogenic differentiation of human mesenchymal stem cells by calcium silicateâgraphene composites," *Materials Science and Engineering C*, Vol. 73, pp. 726–735, 2017.

104. Gurunathan, S., M.-H. Kang, M. Jeyaraj, and J.-H. Kim, "Differential Cytotoxicity of Different Sizes of Graphene Oxide Nanoparticles in Leydig (TM3) and Sertoli (TM4) Cells," *Nanomaterials (Basel, Switzerland)*, Vol. 9, p. 139, 1 2019.

105. Zhang, W., Q. Chang, L. Xu, G. Li, G. Yang, X. Ding, X. Wang, D. Cui, and X. Jiang, "Graphene Oxide-Copper Nanocomposite-Coated Porous CaP Scaffold for Vascularized Bone Regeneration via Activation of Hif-1α," *Advanced Healthcare Materials*, Vol. 5, no. 11, pp. 1299–1309, 2016.

106. Nie, W., C. Peng, X. Zhou, L. Chen, W. Wang, Y. Zhang, P. X. Ma, and C. He, "Three-dimensional porous scaffold by self-assembly of reduced graphene oxide and nano-hydroxyapatite composites for bone tissue engineering," *Carbon*, Vol. 116, pp. 325–337, 2017.

107. Gao, C., P. Feng, S. Peng, and C. Shuai, "Carbon nanotube, graphene and boron nitride nanotube reinforced bioactive ceramics for bone repair," *Acta Biomaterialia*, Vol. 61, pp. 1–20, 2017.

108. Shen, S. C., W. K. Ng, Y. C. Dong, J. Ng, and R. B. H. Tan, "Nanostructured material formulated acrylic bone cements with enhanced drug release," *Materials Science and Engineering C*, Vol. 58, pp. 233–241, 2016.

109. Lu, Y., M. Li, L. Li, S. Wei, X. Hu, X. Wang, G. Shan, Y. Zhang, H. Xia, and Q. Yin, "High-activity chitosan / nano hydroxyapatite / zoledronic acid scaffolds for simultaneous tumor inhibition, bone repair and infection eradication," *Materials Science and Engineering C*, Vol. 82, pp. 225–233, 2018.

110. Teotia, A. K., A. Gupta, D. B. Raina, L. Lidgren, and A. Kumar, "Gelatin Modified Bone Substitute with Bioactive Molecules Enhance Cellular Interactions and Bone Regeneration," *ACS Applied Materials and Interfaces*, Vol. 8, pp. 10775–10787, 2016.

111. Gong, T., Z. Wang, Y. Zhang, C. Sun, Q. Yang, T. Troczynski, and U. O. Hafeli, "Preparation, characterization, release kinetics, and in vitro cytotoxicity of calcium silicate cement as a risedronate delivery system," *Journal of Biomedical Materials Research - Part A*, Vol. 102, no. 7, pp. 2295–2304, 2014.

112. Sorensen, T. C., J. Arnoldi, P. Procter, B. Robioneck, and H. Steckel, "Bone substitute materials delivering zoledronic acid: physicochemical characterization, drug load, and release properties.," *Journal of Biomaterials Applications*, Vol. 27, pp. 727–738, 2 2013.

113. Capra, P., R. Dorati, C. Colonna, G. Bruni, F. Pavanetto, I. Genta, and B. Conti, "A preliminary study on the morphological and release properties of hydroxyapatite-alendronate composite materials.," *Journal of Microencapsulation*, Vol. 28, no. 5, pp. 395–405, 2011.

114. Denissen, H., E. van Beek, C. Löwik, S. Papapoulos, and A. van den Hooff, "Ceramic hydroxyapatite implants for the release of bisphosphonate," *Bone and Mineral*, Vol. 25, no. 2, pp. 123–134, 1994.

115. Pascaud, P., F. Errassifi, F. Brouillet, S. Sarda, A. Barroug, A. Legrouri, and C. Rey, "Adsorption on apatitic calcium phosphates for drug delivery: interaction with bisphosphonate molecules," *Journal of Materials Science: Materials in Medicine*, Vol. 25, no. 10, pp. 2373–2381, 2014.

116. Errassifi, F., S. Sarda, A. Barroug, A. Legrouri, H. Sfihi, and C. Rey, "Infrared, Raman and NMR investigations of risedronate adsorption on nanocrystalline apatites," *Journal of Colloid and Interface Science*, Vol. 420, pp. 101–111, 2014.

117. Houdt, C. I. A. V., P. R. Gabbai-armelin, P. M. Lopez-pe, D. J. O. Ulrich, J. A. Jansen, A. C. M. Renno, and J. J. J. P. V. Den, "Alendronate release from calcium phosphate cement for bone regeneration in osteoporotic conditions," *Scientific Reports*, Vol. 8, pp. 1–13, 2018.

118. Verron, E., O. Gauthier, P. Janvier, P. Pilet, J. Lesoeur, B. Bujoli, J. Guicheux, and J.-M. Bouler, "In vivo bone augmentation in an osteoporotic environment using bisphosphonate-loaded calcium deficient apatite.," *Biomaterials*, Vol. 31, pp. 7776–84, 10 2010.

119. Panzavolta, S., P. Torricelli, B. Bracci, M. Fini, and A. Bigi, "Alendronate and Pamidronate calcium phosphate bone cements: Setting properties and in vitro response of osteoblast and osteoclast cells," *Journal of Inorganic Biochemistry*, Vol. 103, no. 1, pp. 101–106, 2009.

120. Shen, Z., T. Yu, and J. Ye, "Microstructure and properties of alendronate-loaded calcium phosphate cement," *Materials Science and Engineering C*, Vol. 42, pp. 303–311, 2014.

121. Boanini, E., P. Torricelli, M. Gazzano, M. Fini, and A. Bigi, "The effect of zoledronate-hydroxyapatite nanocomposites on osteoclasts and osteoblast-like cells in vitro," *Biomaterials*, Vol. 33, pp. 722–730, 2012.

122. Rau, J. V., V. M. Wu, V. Graziani, I. V. Fadeeva, A. S. Fomin, M. Fosca, and V. Uskoković, "The Bone Building Blues: Self-hardening copper-doped calcium phosphate cement and its in vitro assessment against mammalian cells and bacteria," *Materials Science and Engineering: C*, Vol. 79, pp. 270–279, 2017.

123. Cai, Y., T. Gao, S. Fu, and P. Sun, "Development of zoledronic acid functionalized hydroxyapatite loaded polymeric nanoparticles for the treatment of osteoporosis," *Experimental and Therapeutic Medicine*, Vol. 16, pp. 704–710, 8 2018.

124. Schnitzler, V., F. Fayon, C. Despas, I. Khairoun, C. Mellier, T. Rouillon, D. Massiot, A. Walcarius, P. Janvier, O. Gauthier, G. Montavon, J.-M. Bouler, and B. Bujoli, "Investigation of alendronate-doped apatitic cements as a potential technology for the prevention of osteoporotic hip fractures: critical influence of the drug introduction mode on the in vitro cement properties.," *Acta Biomaterialia*, Vol. 7, pp. 759–770, 2 2011.

125. Shi, X., Y. Wang, L. Ren, Y. Gong, and D. A. Wang, "Enhancing alendronate release from a novel PLGA/hydroxyapatite microspheric system for bone repairing applications," *Pharmaceutical Research*, Vol. 26, no. 2, pp. 422–430, 2009.

126. Verron, E., M. L. Pissonnier, J. Lesoeur, V. Schnitzler, B. H. Fellah, H. Pascal-Moussellard, P. Pilet, O. Gauthier, and J. M. Bouler, "Vertebroplasty using bisphosphonate-loaded calcium phosphate cement in a standardized vertebral body bone defect in an osteoporotic sheep model," *Acta Biomaterialia*, Vol. 10, no. 11, pp. 4887–4895, 2014.

127. Cheng, T. L., C. M. Murphy, R. Ravarian, F. Dehghani, D. G. Little, and A. Schindeler, "Bisphosphonate-adsorbed ceramic nanoparticles increase bone formation in an injectable carrier for bone tissue engineering," *Journal of Tissue Engineering*, Vol. 6, 2015.

128. Josse, S., C. Faucheux, A. Soueidan, G. Grimandi, D. Massiot, B. Alonso, P. Janvier, S. Laib, P. Pilet, O. Gauthier, G. Daculsi, J. J. Guicheux, B. Bujoli, and J.-M. Bouler, "Novel biomaterials for bisphosphonate delivery.," *Biomaterials*, Vol. 26, pp. 2073–2080, 5 2005.

129. Nejadnik, M. R., X. Yang, M. Bongio, H. S. Alghamdi, J. J. J. P. Van den Beucken, M. C. Huysmans, J. A. Jansen, J. Hilborn, D. Ossipov, and S. C. G. Leeuwenburgh, "Self-healing hybrid nanocomposites consisting of bisphosphonated hyaluronan and calcium phosphate nanoparticles," *Biomaterials*, Vol. 35, no. 25, pp. 6918–6929, 2014.

130. Zhang, Y., C. Gao, X. Li, C. Xu, Y. Zhang, Z. Sun, Y. Liu, and J. Gao, "Thermosensitive methyl cellulose-based injectable hydrogels for post-operation anti-adhesion," *Carbohydrate Polymers*, Vol. 101, no. 1, pp. 171–178, 2014.

131. Thai, V. V., and B. T. Lee, "Fabrication of calcium phosphate-calcium sulfate injectable bone substitute using hydroxy-propyl-methyl-cellulose and citric acid," *Journal of Materials Science: Materials in Medicine*, Vol. 21, no. 6, pp. 1867–1874, 2010.

132. Thirumala, S., J. Gimble, and R. Devireddy, "Methylcellulose Based Thermally Reversible Hydrogel System for Tissue Engineering Applications," *Cells*, Vol. 2, pp. 460–475, 2013.

133. Fang, J., Z. Yang, S. Tan, C. Tayag, M. E. Nimni, M. Urata, and B. Han, "Injectable gel graft for bone defect repair.," *Regenerative Medicine*, Vol. 9, no. 1, pp. 41–51, 2014.

134. Guo, D., K. Xu, and Y. Han, "Influence of cooling modes on purity of solid-state synthesized tetracalcium phosphate," *Materials Science and Engineering B: Solid-State Materials for Advanced Technology*, Vol. 116, no. 2, pp. 175–181, 2005.

135. Huang, Z., Q. Feng, B. Yu, and S. Li, "Biomimetic properties of an injectable chitosan/nano-hydroxyapatite/ collagen composite," *Materials Science and Engineering C*, Vol. 31, no. 3, pp. 683–687, 2011.

136. Radwan, M. M., H. K. Abd El-Hamid, and S. M. Nagi, "Synthesis, properties and hydration characteristics of novel nano-size mineral trioxide and tetracalcium phosphate for dental applications," *Oriental Journal of Chemistry*, Vol. 32, no. 5, pp. 2459–2472, 2016.

137. Jayasree, R., T. S. Kumar, K. P. S. Kavya, P. R. Nankar, and D. Mukesh, "Self Setting Bone Cement Formulations Based on Egg shell Derived TetraCalcium Phosphate BioCeramics," *Bioceramics Development and Applications*, Vol. 05, no. 01, pp. 1–6, 2015.

138. Liao, J., X. Duan, Y. Li, C. Zheng, Z. Yang, A. Zhou, and D. Zou, "Synthesis and mechanism of tetracalcium phosphate from nanocrystalline precursor," *Journal of Nanomaterials*, Vol. 2014, 2014.

139. Kim, H., R. P. Camata, Y. K. Vohra, and W. R. Lacefield, "Control of phase composition in hydroxyapatite/tetracalcium phosphate biphasic thin coatings for biomedical applications," *Journal of Materials Science: Materials in Medicine*, Vol. 16, pp. 961–966, 10 2005.

140. Eslami, H., M. Solati-Hashjin, and M. Tahriri, "Synthesis and Characterization of Hydroxyapatite Nanocrystals via Chemical Precipitation Technique," *Iranian Journal of Pharmaceutical Sciences*, Vol. 4, no. 2, pp. 127–134, 2008.

141. Park, H., M. H. Kim, Y. I. Yoon, and W. H. Park, "One-pot synthesis of injectable methylcellulose hydrogel containing calcium phosphate nanoparticles," *Carbohydrate Polymers*, Vol. 157, pp. 775–783, 2017.

142. Bain, M. K., D. Maity, B. Bhowmick, D. Mondal, M. M. R. Mollick, G. Sarkar, M. Bhowmik, D. Rana, and D. Chattopadhyay, "Effect of PEG-salt mixture on the gelation temperature and morphology of MC gel for sustained delivery of drug," *Carbohydrate Polymers*, Vol. 91, no. 2, pp. 529–536, 2013.

143. Kim, M. H., H. Park, and W. H. Park, "Effect of pH and precursor salts on in situ formation of calcium phosphate nanoparticles in methylcellulose hydrogel," *Carbohydrate Polymers*, Vol. 191, pp. 176–182, 2018.

144. Kiminami, K., T. Konishi, M. Mizumoto, K. Nagata, M. Honda, H. Arimura, and M. Aizawa, "Effects of adding polysaccharides and citric acid into sodium dihydrogen phosphate mixing solution on the material properties of gelatin-hybridized calcium-phosphate cement," *Materials*, Vol. 10, no. 8, pp. 1–14, 2017.

145. Tang, Y., X. Wang, Y. Li, M. Lei, Y. Du, J. F. Kennedy, and C. J. Knill, "Production and characterisation of novel injectable chitosan/methylcellulose/salt blend hydrogels with potential application as tissue engineering scaffolds," *Carbohydrate Polymers*, Vol. 82, no. 3, pp. 833–841, 2010.

146. Liu, Z., and P. Yao, "Injectable thermo-responsive hydrogel composed of xanthan gum and methylcellulose double networks with shear-thinning property.," *Carbohydrate polymers*, Vol. 132, pp. 490–8, 11 2015.

147. Alves, H. L. R., L. A. dos Santos, and C. P. Bergmann, "Injectability evaluation of tricalcium phosphate bone cement," *Journal of Materials Science: Materials in Medicine*, Vol. 19, no. 5, pp. 2241–2246, 2008.

148. Nishinari, K., K. E. Hofmann, K. Kohyama, H. Moritaka, N. Nishinari, and M. Watase, "Polysaccharide-protein interaction: a rheological study of the gel-sol transition of a gelatin-methylcellulose-water system.," *Biorheology*, Vol. 30, no. 3-4, pp. 243–252, 1993.

149. Fan, R. R., X. H. Deng, L. X. Zhou, X. Gao, M. Fan, Y. L. Wang, and G. Guo, "Injectable thermosensitive hydrogel composite with surface-functionalized calcium phosphate as raw materials," *International Journal of Nanomedicine*, Vol. 9, no. 1, pp. 615–626, 2014.

150. Yokoyama, A., S. Yamamoto, T. Kawasaki, T. Kohgo, and M. Nakasu, "Development of calcium phosphate cement using chitosan and citric acid for bone substitute materials," *Biomaterials*, Vol. 23, no. 4, pp. 1091–1101, 2002.

151. Liu, W., J. Zhang, G. Rethore, K. Khairoun, P. Pilet, F. Tancret, J. M. Bouler, and P. Weiss, "A novel injectable, cohesive and toughened Si-HPMC (silanized-hydroxypropyl methylcellulose) composite calcium phosphate cement for bone substitution," *Acta Biomaterialia*, Vol. 10, no. 7, pp. 3335–3345, 2014.

152. Chow, L. C., "Next generation calcium phosphate-based biomaterials," *Dental Materials J.*, Vol. 28, no. 1, pp. 1–10, 2009.

153. Marefat Seyedlar, R., A. Nodehi, M. Atai, and M. Imani, "Gelation behavior of in situ forming gels based on HPMC and biphasic calcium phosphate nanoparticles," *Carbohydrate Polymers*, Vol. 99, pp. 257–263, 2014.

154. Ghorbani, M., J. Ai, M. R. Nourani, M. Azami, B. Hashemi Beni, S. Asadpour, and S. Bordbar, "Injectable natural polymer compound for tissue engineering of intervertebral disc: In vitro study," *Materials Science and Engineering C*, Vol. 80, pp. 502–508, 2017.

155. Arvidson, S. A., J. R. Lott, J. W. McAllister, J. Zhang, F. S. Bates, T. P. Lodge, R. L. Sammler, Y. Li, and M. Brackhagen, "Interplay of phase separation and thermoreversible gelation in aqueous methylcellulose solutions," *Macromolecules*, Vol. 46, no. 1, pp. 300–309, 2013.

156. Gupta, D., C. H. Tator, and M. S. Shoichet, "Fast-gelling injectable blend of hyaluronan and methylcellulose for intrathecal, localized delivery to the injured spinal cord.," *Biomaterials*, Vol. 27, pp. 2370–9, 4 2006.

157. Tate, M. C., D. A. Shear, S. W. Hoffman, D. G. Stein, and M. C. LaPlaca, "Biocompatibility of methylcellulose-based constructs designed for intracerebral gelation following experimental traumatic brain injury," *Biomaterials*, Vol. 22, no. 10, pp. 1113–1123, 2001.

158. Ma, X., L. Zhang, D. Fan, W. Xue, C. Zhu, X. Li, Y. Liu, W. Liu, P. Ma, and Y. Wang, "Physicochemical properties and biological behavior of injectable crosslinked hydrogels composed of pullulan and recombinant human-like collagen," *Journal of Materials Science*, Vol. 52, no. 7, pp. 3771–3785, 2017.

159. Ding, Y., S. Tang, B. Yu, Y. Yan, H. Li, J. Wei, and J. Su, "In vitro degradability, bioactivity and primary cell responses to bone cements containing mesoporous magnesiumâcalcium silicate and calcium sulfate for bone regeneration," *Journal of the Royal Society Interface*, Vol. 12, no. 111, p. 20150779, 2015.

160. Qasim, S. B., S. Husain, Y. Huang, M. Pogorielov, V. Deineka, M. Lyndin, A. Rawlinson, and I. U. Rehman, "In-vitro and in-vivo degradation studies of freeze gelated porous chitosan composite scaffolds for tissue engineering applications," *Polymer Degradation and Stability*, Vol. 136, pp. 31–38, 2 2017.

161. O'Neill, R., H. O. McCarthy, E. B. Montufar, M. P. Ginebra, D. I. Wilson, A. Lennon, and N. Dunne, "Critical review: Injectability of calcium phosphate pastes and cements," *Acta Biomaterialia*, Vol. 50, pp. 1–19, 2017.

162. Misch, C. E., Z. Qu, and M. W. Bidez, "Mechanical properties of trabecular bone in the human mandible: Implications for dental implant treatment planning and surgical placement," *Journal of Oral and Maxillofacial Surgery*, Vol. 57, pp. 700–706, 6 1999.

163. Baino, F., "Ceramics for bone replacement," in *Advances in Ceramic Biomaterials*, pp. 249–278, Elsevier, 2017.

164. Newman, P., A. Minett, R. Ellis-Behnke, and H. Zreiqat, "Carbon nanotubes: Their potential and pitfalls for bone tissue regeneration and engineering," *Nanomedicine: Nanotechnology, Biology and Medicine*, Vol. 9, no. 8, pp. 1139–1158, 2013.

165. Gholami, F., S. H. S. Zein, L. C. Gerhardt, K. L. Low, S. H. Tan, D. S. McPhail, L. M. Grover, and A. R. Boccaccini, "Cytocompatibility, bioactivity and mechanical strength of calcium phosphate cement reinforced with multi-walled carbon nanotubes and bovine serum albumin," *Ceramics International*, Vol. 39, no. 5, pp. 4975–4983, 2013.

166. Du, H., and S. D. Pang, "Dispersion and stability of graphene nanoplatelet in water and its influence on cement composites," *Construction and Building Materials*, Vol. 167, pp. 403–413, 2018.

167. Park, J., S. J. Lee, S. Chung, J. H. Lee, W. D. Kim, J. Y. Lee, and S. A. Park, "Cell-laden 3D bioprinting hydrogel matrix depending on different compositions for soft tissue engineering: Characterization and evaluation," *Materials Science and Engineering C*, Vol. 71, pp. 678–684, 2017.

168. Çiplak, Z., N. Yildiz, and A. Çalimli, "Investigation of graphene/Ag nanocomposites synthesis parameters for two different synthesis methods," *Fullerenes Nanotubes and Carbon Nanostructures*, Vol. 23, no. 4, pp. 361–370, 2015.

169. He, D., Z. Peng, W. Gong, Y. Luo, P. Zhao, and L. Kong, "Mechanism of a green graphene oxide reduction with reusable potassium carbonate," *RSC Advances*, Vol. 5, no. 16, pp. 11966–11972, 2015.

170. Nadour, M., F. Boukraa, A. Ouradi, and A. Benaboura, "Effects of Methylcellulose on the Properties and Morphology of Polysulfone Membranes Prepared by Phase Inversion," *Materials Research*, Vol. 20, no. 2, pp. 339–348, 2017.

171. Oliveira, R. L., J. G. Vieira, H. S. Barud, R. M. Assunção, G. R. Filho, S. J. Ribeiro, and Y. Messadeqq, "Synthesis and characterization of methylcellulose produced from bacterial cellulose under heterogeneous condition," *Journal of the Brazilian Chemical Society*, Vol. 26, no. 9, pp. 1861–1870, 2015.

172. Nasrollahi, N., A. N. Dehkordi, A. Jamshidizad, and M. Chehelgerdi, "Preparation of brushite cements with improved properties by adding graphene oxide," *International Journal of Nanomedicine*, Vol. 14, pp. 3785–3797, 2019.

173. Depan, D., T. C. Pesacreta, and R. D. Misra, "The synergistic effect of a hybrid graphene oxide-chitosan system and biomimetic mineralization on osteoblast functions," *Biomaterials Science*, Vol. 2, no. 2, pp. 264–274, 2014.

174. Lospichl, B. V., S. Hemmati-sadeghi, P. Dey, T. Dehne, R. Haag, M. Sittinger, J. Ringe, and M. Gradzielski, "Injectable hydrogels for treatment of osteoarthritis â A rheological study," *Colloids and Surfaces B: Biointerfaces*, Vol. 159, pp. 477–483, 2017.

175. Chiang, T. Y., C. C. Ho, D. C. H. Chen, M. H. Lai, and S. J. Ding, "Physicochemical properties and biocompatibility of chitosan oligosaccharide/gelatin/calcium phosphate hybrid cements," *Materials Chemistry and Physics*, Vol. 120, no. 2-3, pp. 282–288, 2010.

176. Quiroz-Reyes, C. N., E. Ronquillo-de Jesús, N. E. Duran-Caballero, and M. Ã. Aguilar-Méndez, "Development and characterization of gelatin nanoparticles loaded with a cocoa-derived polyphenolic extract," *Fruits*, Vol. 69, no. 6, pp. 481–489, 2014.

177. Yan, Y., X. Zhang, H. Mao, Y. Huang, Q. Ding, and X. Pang, "Hydroxyapatite/gelatin functionalized graphene oxide composite coatings deposited on TiO 2 nanotube by electrochemical deposition for biomedical applications," *Applied Surface Science*, Vol. 329, pp. 76–82, 2015.

178. Nair, M., D. Nancy, A. G. Krishnan, G. S. Anjusree, S. Vadukumpully, and S. V. Nair, "Graphene oxide nanoflakes incorporated gelatin-hydroxyapatite scaffolds enhance osteogenic differentiation of human mesenchymal stem cells," *Nanotechnology*, Vol. 26, no. 16, 2015.

179. Liu, J., Q. Li, and S. Xu, "Reinforcing Mechanism of Graphene and Graphene Oxide Sheets on Cement-Based Materials," *Journal of Materials in Civil Engineering*, Vol. 31, no. 4, p. 04019014, 2019.

180. Shim, V. P. W., L. M. Yang, J. F. Liu, and V. S. Lee, "Characterisation of the dynamic compressive mechanical properties of cancellous bone from the human cervical spine," Vol. 32, pp. 525–540, 2005.

181. Prasadh, S., S. Suresh, and R. Wong, "Osteogenic Potential of Graphene in Bone Tissue Engineering Scaffolds," *Materials (Basel, Switzerland)*, Vol. 11, no. 8, p. 1430, 2018.

182. Demir Oğuz, O., and D. Ege, "Rheological and mechanical properties of thermoresponsive methylcellulose/calcium phosphate-based injectable bone substitutes," *Materials*, Vol. 11, no. 4, 2018.

183. Demir Oğuz, O., and D. Ege, "Preparation of graphene oxide-reinforced calcium phosphate/calcium sulfate/methylcellulose-based injectable bone substitutes," *MRS Communications*, Vol. 9, no. 4, pp. 1–7, 2019.

184. Chew, K. K., K. L. Low, S. H. Sharif Zein, D. S. McPhail, L. C. Gerhardt, J. A. Roether, and A. R. Boccaccini, "Reinforcement of calcium phosphate cement with multi-walled carbon nanotubes and bovine serum albumin for injectable bone substitute applications," *Journal of the Mechanical Behavior of Biomedical Materials*, Vol. 4, no. 3, pp. 331–339, 2011.

185. Macon, A. L. B., T. B. Kim, E. M. Valliant, K. Goetschius, R. K. Brow, D. E. Day, A. Hoppe, A. R. Boccaccini, I. Y. Kim, C. Ohtsuki, T. Kokubo, A. Osaka, M. Vallet-Regi, D. Arcos, L. Fraile, A. J. Salinas, A. V. Teixeira, Y. Vueva, R. M. Almeida, M. Miola, C. Vitale-Brovarone, E. Verne, W. Holand, and J. R. Jones, "A unified in vitro evaluation for apatite-forming ability of bioactive glasses and their variants.," *Journal of Materials Science: Materials in Medicine*, Vol. 26, no. 2, p. 115, 2015.

186. Montazerolghaem, M., and M. Karlsson Ott, "Sustained release of simvastatin from premixed injectable calcium phosphate cement," *Journal of Biomedical Materials Research - Part A*, Vol. 102, no. 2, pp. 340–347, 2014.

187. Khajuria, D. K., R. Razdan, and D. R. Mahapatra, "Development, in vitro and in vivo characterization of zoledronic acid functionalized hydroxyapatite nanoparticle based formulation for treatment of osteoporosis in animal model," *European Journal of Pharmaceutical Sciences*, Vol. 66, pp. 173–183, 2015.

188. Prasanthi, M. M., B. A. Rao, B. V. N. Rao, Y. P. Krishna, and D. V. Ramana, "Formulation and Evaluation of Zoledronic Acid for Injection By Lyophilization Technique," *International Research Journal of Pharmacy*, Vol. 8, no. 2, pp. 50–56, 2017.

189. Chen, Z., H. Liu, X. Liu, and F. Z. Cui, "Injectable calcium sulfate/mineralized collagen-based bone repair materials with regulable self-setting properties," *Journal of Biomedical Materials Research - Part A*, Vol. 99, no. 4, pp. 554–563, 2011.

190. Nancollas, G. H., R. Tang, R. J. Phipps, Z. Henneman, S. Gulde, and W. Wu, "Novel insights into actions of bisphosphonates on bone : Differences in interactions with hydroxyapatite," *Bone*, Vol. 38, pp. 617–627, 2006.

191. Xu, C., B. Ma, J. Peng, L. Gao, Y. Xu, Z. Huan, and J. Chang, "Tricalcium silicate/graphene oxide bone cement with photothermal properties for tumor ablation," *Journal of Materials Chemistry B*, Vol. 7, no. 17, pp. 2808–2818, 2019.

192. Locs, J., W. Li, M. Sokolova, J. A. Roether, D. Loca, and A. R. Boccaccini, "Zoledronic acid impregnated and poly (L-lactic acid) coated 45S5 Bioglass®-based scaffolds," *Materials Letters*, Vol. 156, pp. 180–182, 2015.

193. Yang, H., M. Monasterio, H. Cui, and N. Han, "Experimental study of the effects of graphene oxide on microstructure and properties of cement paste composite," *Composites Part A*, Vol. 102, pp. 263–272, 2017.

194. Khajuria, D. K., R. Vasireddi, M. Trebbin, D. Karasik, and R. Razdan, "Novel therapeutic intervention for osteoporosis prepared with strontium hydroxyapatite and zoledronic acid: In vitro and pharmacodynamic evaluation.," *Materials Science and Engineering C*, Vol. 71, pp. 698–708, 2017.

195. Ginebra, M.-p., C. Canal, M. Espanol, D. Pastorino, and E. B. Montufar, "Calcium phosphate cements as drug delivery materials," *Advanced Drug Delivery Reviews*, Vol. 64, pp. 1090–1110, 2012.

196. T. Higuchi, "Mechanism of Sustained- Action Medication," *Journal of Pharmaceutical Sciences*, Vol. 52, no. 12, pp. 1145–1149, 1963.

197. Jang, J. H., S. Shin, H. J. Kim, J. Jeong, H. E. Jin, M. S. Desai, S. W. Lee, and S. Y. Kim, "Improvement of physical properties of calcium phosphate cement by elastin-like polypeptide supplementation," *Scientific Reports*, Vol. 8, no. 1, pp. 1–11, 2018.

198. Kanimozhi, K., S. Khaleel Basha, and V. Sugantha Kumari, "Processing and characterization of chitosan/PVA and methylcellulose porous scaffolds for tissue engineering," *Materials Science and Engineering C*, Vol. 61, pp. 484–491, 2016.

199. Kaur, K., K. J. Singh, V. Anand, G. Bhatia, A. P. Singh, and M. Kaur, "Elucidating the role of size of hydroxyl apatite particles toward the development of competent antiosteoporotic bioceramic materials: In vitro and in vivo studies," *Journal of Biomedical Materials Research Part A*, Vol. 107, no. 8, pp. 1723–1735, 2019.

200. Meena, R., K. K. Kesari, M. Rani, and R. Paulraj, "Effects of hydroxyapatite nanoparticles on proliferation and apoptosis of human breast cancer cells (MCF-7)," *Journal of Nanoparticle Research*, Vol. 14, no. 712, pp. 1–11, 2012.

201. Pourbaghi-Masouleh, M., and V. Hosseini, "Amorphous calcium phosphate nanoparticles could function as a novel cancer therapeutic agent by employing a suitable targeted drug delivery platform," *Nanoscale Research Letters*, Vol. 8, no. 1, p. 449, 2013.

202. Rahmanian, M., S. M. Naghib, A. Seyfoori, A. A. Zare, H. Sanati, and K. Majidzadeh-A, "Inhibitory Effect of Tricalcium Phosphate Sintered at Different Temperatures on Human Breast Cancer Cell Line MCF-7," *Multidisciplinary Cancer Investigation*, Vol. 1, no. 1, pp. 11–14, 2016.

203. Reinholz, G. G., B. Getz, L. Pederson, E. S. Sanders, M. Subramaniam, J. N. Ingle, and T. C. Spelsberg, "Bisphosphonates directly regulate cell proliferation, differentiation, and gene expression in human osteoblasts," *Cancer Research*, Vol. 60, no. 21, pp. 6001–6007, 2000.

204. Koch, F. P., S. S. Yekta, C. Merkel, T. Ziebart, and R. Smeets, "The impact of bisphosphonates on the osteoblast proliferation and Collagen gene expression in vitro," *Head and Face Medicine*, Vol. 6, no. 12, pp. 1–6, 2010.

205. Stein, G. S., and J. B. Lian, "Molecular mechanisms mediating proliferation/differentiation interrelationships during progressive development of the osteoblast phenotype.," *Endocrine Reviews*, Vol. 14, no. 4, pp. 424–442, 1993.

206. Mohammad, N. F., R. Othman, N. A. Abdullah, and F. Y. Yeoh, "In vitro Evaluation of Mesoporous Carbonated Hydroxyapatite in MC3T3-E1 Osteoblast Cells," *Procedia Chemistry*, Vol. 19, pp. 259–266, 2016.

207. Le Guehennec, L., M.-A. Lopez-Heredia, B. Enkel, P. Weiss, Y. Amouriq, and P. Layrolle, "Osteoblastic cell behaviour on different titanium implant surfaces," *Acta Biomaterialia*, Vol. 4, no. 3, pp. 535–543, 2008.